EFFECT OF LAND SURFACE-ATMOSPHERIC BOUNDARY LAYER INTERACTIONS ON RICE PRODUCTION IN WEST ARICA

GUIDIGAN, GILDAS LANDRY MÈMINVÈGNI,
BSc (Agronomy),
MTech (Climate Change and Adapted Land Use),
MET/19/3751

A Thesis of the Doctoral Research Programme of the West Africa Climate Systems, under the West Africa Science Service Centre on Climate Change and Adapted Land Use, in the Department of Meteorology and Climate Science submitted to the School of Postgraduate Studies in partial fulfilment of the requirements for the award of the degree of Doctor of Philosophy in Meteorology and Climate Science of the Federal University of Technology, Akure, Nigeria.

July, 2023

DECLARATION

I hereby declare that this Thesis was written by me and is a correct record of my own research work. It has not been presented in any previous application for any degree of this or any University. All citations and sources of information are clearly acknowledged by means of references.

Candidate's Name: GUIDIGAN, Gildas Landry Mèminvègni.

Signature:…… Date……

CERTIFICATION

We certify that this Dissertation entitled "Effect of Land Surface-Atmospheric Boundary Layer Interactions on Rice Production in West Africa" is the outcome of the research carried out by GUIDIGAN, Gildas Landry Mèminvègni under the WASCAL DRP-WACS in the Department of Meteorology and Climate Science of the Federal University of Technology, Akure.

Prof. A.A. Balogun ……..

(Major Surpervisor) Signature Date

Department of Meteorology and Climate Science,
Federal University of Technology,
Akure, Nigeria.

Prof. Stefan Kollet ……..

(Co-Surpervisor) Signature Date

Institute of Bio-Geosciences (IBG-3, Agrosphere),
Forschungszentrum Jülich / Centre for High-Performance
Scientific Computing, Geoverbund ABC/
Jülich, Germany.

Dr. Elliott Dossou-Yovo ……..

(Co-Surpervisor) Signature Date

AfricaRice,
Bouake, Cote d'Ivoire

Prof. Zachariah Debo Adeyewa ……..

(Director) Signature Date

Doctoral Research Program–West African Climate Systems
West African Science Service Center on Climate Change and
Adapted Land Use (DRP-WACS, WASCAL),
Federal University of Technology,
Akure, Nigeria.

ABSTRACT

Land cover change can influence the LCL height, which in turn affects cloud formation and consequently convective precipitation. This study compares the LCL height over three land cover types (Urban, vegetation, and crop) in West Africa and assesses their influence on convective cloud and precipitation using a new land surface model eCLM, a variant of CLM5 which has the same modelling capabilities as CLM5, but it uses much "leaner" scripts for building and running a model. The forcing provided is the Global Soil Wetness Project (GSWP) version 3. Land surface fluxes (SH, sensible heat flux; LH, latent heat flux) data were collected from eddy covariance stations at 11 sites distributed across West Africa. The simulation results from eCLM for the three land covers show a good agreement compared to both measurement and ERA5 with a correlation coefficient of above 0.75 and root mean square error lower than 30 W/m^2. LCL is higher for cropland compared to natural vegetation and urban areas. Monthly LCL trends were estimated from the three land cover types over West Africa. LCL increases more over crop area with a high reaching 4.5 km with an average change of 1.7 km compared to the vegetation and urban land cover where LCL height reaches a high of 4.2 km. The height of the LCL shows a strong relation with precipitation. The LCL decreases when the monsoon progresses in June-July-August (JJA) and increases during the dry season when the monsoon retreats in December-January-February (DJF). We also observed a strong correlation between LCL and surface fluxes over the study area. Over the three land cover types (urban, vegetation, crop), LCL and LH are negatively correlated, while LCL and SH are positively correlated. Thus, changing from one land cover to another affects land surface fluxes (sensible and latent), and then significantly modifies moisture conversion at the lifting condensation level (LCL) and hence at the cloud base height, thereby increasing or decreasing precipitation over West Africa. Rice (Oryza sativa L.) is the main staple food for millions of people in sub-Saharan Africa (SSA) and its production in the

region is threatened by climate variability and climate change. The objectives of this study were to evaluate the performance of APSIM-ORYZA for simulating rice yield under current climate conditions in irrigated systems in the derived savannah agro-ecological zone of West Africa. Data were collected on soil properties, weather, management practices, and rice yield during two years from experimental studies considering two irrigated schemes namely Mbe and Lokakpli. These data were used to calibrate and validate the APSIM-ORYZA model to represent with acceptable accuracy rice growth and yield under the conditions of production of the sites of studyOnce validated, the future bias-corrected climate data from Representation Concentration Pathways (RCPs) climate scenarios RCP 4.5 and RCP 8.5 were compiled and formatted to inform scenarios simulations with the model. Impact of climate change on rice yield was then assessed for six alternative management practices that are mostly preferred by farmers. The results showed that APSIM-ORYZA simulated satisfactorily irrigated rice with R2 values of 0.8 to 1, a root-mean-square error (RMSE) of 0.08 t/ha, and a Nash–Sutcliffe Efficiency of 0.99. Rice yield was projected to decrease of 17 and further 18% by 2070 under RCP 4.5 and 8.5, respectively compared to the reference rice yield of 2019. Rice yield was projected to be maintained with a relative increase from its baseline value in 2019 if alternative management practices such as rice straw mulching, alternate wetting, and drying, transplanting of 35 days old seedlings, organic fertiliser application at 120 kg N ha-1 and rice sowing date after 1 April were used. This study filled a gap in the literature concerning the potential of management practices to increase rice yield under future climate change conditions and highlight the importance of adoption of improved practices for the sustainability of rice production in the region of SSA.

DEDICATION

This work is dedicated to God the Author of Life and Knowledge The Great I AM that I AM, The One who Knows the End from the Beginning, The Almighty God, To You Be All the Honour, Glory and Adoration.

This work is also dedicated to my wife, Sewade Sena Glwadys, and my daughter Divine Sessi Guidigan, who endured my absence for the whole period of this study.

And in memory of Clement Comlan Guidigan, my late father, who contributed a lot to whom I'm becoming today, may his soul rest in peace.

The great price of the dedication is for Odjarado O. Celestine, my mother who saw the beginning and the end of this work, encouraged me to have the strength to finish it. Proud of you my sweet Mum.

ACKNOWLEDGMENTS

I am very grateful to God, the almighty, maker of heaven and earth, it is in him that I have had the strength and well-being that enabled me to complete this research.

I'm grateful to the German Ministry of Education and Research (BMBF), that fully sponsored this Ph.D. work through the West African Science Service Centre for Climate Change and Adapted Land-use (WASCAL).

My sincere thanks to the executive director and the staff of WASCAL Headquarter in Accra, Ghana, and the Director Prof. Z. Debo Adeyewa and staff of WASCAL-DRP-WACS, FUTA, Nigeria for their support and encouragement throughout the period of the study at FUTA. My thanks also go to the Deputy Director Prof. Balogun Ifeoluwa Adebowale, the Head and staff of the Department of Meteorology and Climate Science, FUTA, Nigeria for their cooperation.

I would like to express my sincere gratitude to Prof. Ahmed A. Balogun for the supervision of this work, for all the guidance he provided along the way of this study. My thank to Prof. Stefan Kollet for the co-supervision and by hosting me almost 6 months in his research group Institute of Bio-Geosciences (IBG-3, Agrosphere), Forschungszentrum Jülich / Centre for High-Performance Scientific Computing, Geoverbund ABC/ Jülich, Germany, and to Dr. Elliott Dossou-Yovo for his supervision and hosting me during my stay for field work and data collection at Africa Rice, Bouake, in Cote d'Ivoire.

My special thanks and gratitude to Mr. Paul Rigor for his supervision, advice, and support during my stay in the Institute of Bio-Geosciences (IBG-3, Agrosphere), Forschungszentrum Jülich. He introduced and assisted me on HPC using, models installing, models and simulations. I am so proud of you.

I would also like to express my special thanks and gratitude to Bamidele Oloruntoba (Ph.D. Student) for his candid supervision, advice, and support during my stay in the Institute of Bio-Geosciences (IBG-3, Agrosphere), Forschungszentrum Jülich. He introduced and assisted me also on HPC usage, and models simulations, and also provided to me some codes. You were more than a supervisor of my Ph.D work, but a brother and a friend.

I would like also express my gratitude and special thanks to Prof. Dr. Harrie-Jan Hendricks Franssen for his co-supervision and kind collaborations and advises before and during my stay in the Institute of Bio-Geosciences (IBG-3, Agrosphere), Forschungszentrum Jülich.

. I am also grateful to the Deutscher Akademischer Austauschdienst (DAAD) for the short grant it allocated for us. I am also grateful for the West African Research Association (WARA) for the short travel grant.

A special thanks to Mr Justin Djagba, Dr. Expedit Ago, Dr. Mayeul Quenum, Dr. Solomon Nagbo, Mr Phung Ta, for their encouragement and support for the completion of the present work, and thanks to all the colleagues from AfricaRice for their support.

My gratitude also go to all my fellow WASCAL-DRP-WACS comrades, mainly: Nimon Pouerero, Peter Odoum, Assa Tapily, Dakega Saberma RAGATOA.

Finally, I am happy to thank all my family and relations whoassisted, encouraged, and support me during these 43 months I was away from home. I would like to mention especially: Roland Guidigan, Maurice B. Guidigan, Jaures Guidigan and Eugene Guidigan, Annette Odjarado, Fidele Atakla, Mr AVOTRICAN Sylvain.

TABLE OF CONTENTS

DECLARATION **ii**

CERTIFICATION **iii**

ABSTRACT **iv**

DEDICATION **vi**

ACKNOWLEDGMENTS **vii**

TABLE OF CONTENTS **ix**

LIST OF TABLES **xiv**

LIST OF FIGURES **xvi**

ACRONYMS **xxii**

Chapter One **1**

1.0 Introduction **1**

1.1 Background 1

1.2 Statement of the problem and research question 13

1.3 Aim and Objectives 16

1.4 Innovation 17

1.5 Structure of the thesis 17

Chapter Two **19**

2.0 Literature Review **19**

2.1 Definition of some concepts 19

2.1.1 Land Surface model 19

2.1.2 Surface energy fluxes 19

2.1.3 West African climate systems 21

2.1.4 Surface Characterization and Model Input Requirements 26

2.2 Land-atmosphere interaction 27

2.3 Impact of climate change on rice production 33

2.3.1 Climate change in Cote d'Ivoire 33

2.3.2 Crop models and model simulation 34

2.3.3 Representative Concentration Pathways (RCPs) 35

2.3.4 Global and Regional Climate Models 36

2.3.5 Bias Correction procedure 38

2.3.6 Bias correction Methods 40

2.3.6.1 Linear Scaling (LS) of Precipitation and Temperature 40

2.3.6.2 Local Intensity Scaling (LOCI) of Precipitation 41

2.3.6.3 Power Transformation (PT) of precipitation 42

2.3.6.4 Variance scaling (VARI) of temperature 42

2.3.6.5 Delta-change correction of precipitation and temperature 42

2.3.6.6 Distribution Mapping (DM) of Precipitation and Temperature 43

2.3.7 Rice for food security 43

Chapter Three **48**

3.0 Materials and Methods **48**

3.1 Study area 48

3.2 Study datasets 49

3.2.1 Land surface model dataset 49

3.2.2 Observational Data 50

3.3 Methods 56

3.3.1 Couple land surface and LCL processing 56

3.3.1.1 Lifting Condensation Level (LCL) height expression 56

3.3.1.2 eCLM Model Simulation 58

3.3.1.3 LCL Height calculation 59

3.3.2 Climate change datasets and emissions scenarios 60

3.3.2.1 Future climate data and climate scenarios 60

3.3.2.2 Bias Correction procedure 61

3.3.2.3 Change analysis and extreme indices 62

3.3.2.4 Climate indices 62

3.3.2.5 Evaluation of Bias-Correction Methods 63

3.3.3 Crop simulation processing 65

3.3.3.1 APSIM-ORYZA for simulating adequately climate change impact on rice production 65

3.3.3.2 Crop phenology 68

3.3.3.3 Soil data 68

3.3.3.4 Crop management 70

3.3.3.5 Data collection 70

3.3.3.6 Model evaluation 71

3.3.4 Alternative management practices to mitigate climate change impacts on rice yield 77

3.3.4.1 Scenario 1: Crop establishment 77

3.3.4.2 Scenario 2: Soil Organic Matter (SOM) application 77

3.3.4.3 Scenario 3: Mulch amount application 78

3.3.4.4 Scenario 4: Mineral fertilizer application 78

3.3.4.5 Scenario 5: seedling age 80

3.3.4.6 Scenario 6: sowing date 80

Chapter Four **82**

4.0 Result and Discussion **82**

4.1 Coupling of land surface model fluxes and lifting condensation level (LCL) height simulations with the present climate 82

4.1.1 Model Configuration 82

4.1.2 Comparison of simulated energy fluxes 82

4.1.3 Comparison of Lifting Condensation Level (LCL) with different PFT types and current climate 88

4.1.4 Difference between the different land cover for the express LCL 96

4.1.5 Couple LCL and land surface fluxes 98

4.1.6 Relationship between LCL, precipitation and Cloud base 101

4.1.7 Relationship between LCL height, the monsoon seasonal cycle and convective cloud 106

4.1.8 Role of Plant functional type (PFTs) on LCL height and present day climate 113

4.2 Parameterisation of APSIM-ORYZA model 119

4.2.1 Model calibration output 119

4.2.2 Model validation output 119

4.2.3 Performance of Bias-Correction Methods 123

4.2.3.1 Precipitation 123

4.2.3.2 Minimum and maximum temperature 124

4.2.3.3 Projected changes in the main precipitation parameters 131

4.2.3.4 Projected changes in the main parameters for maximum and minimum temperature under scenarios RCP 4.5 and 8.5 134

4.2.3.5 Climate change impacts on rice yield under RCP 4.5 and 8.5 scenarios 139

4.2.3.6 Effect of alternative management practices to mitigate climate change impact on rice yield 140

Chapter Five **149**

5.0 Conclusion and Recommendations **149**

5.1 Conclusion and Recommendation 149

5.2 Limitation of the study 151

5.3 Recommendation 152

References **153**

LIST OF TABLES

Table 2:1. Global warming (°C) and sea level (m) increase projections with four global radiative forcing pathways from greenhouse gas emissions from human activities, with radiative forcing of 2.6, 4.5, 6.0 and 8.5 W/m² by 2100. The corresponding respective greenhouse gas concentrations in the year 2100 are equivalent to 490, 650, 850 and more than 1370 parts per million (ppm) carbon dioxide. 39

Table 2:2. Bias correction for precipitation and temperatures 45

Table 3:1. Characteristic of the selected site modify and adopted from Rahimi et al (2021) 53

Table **3:2**. Land and meteorological forcing used for the historical simulation of GSWP3 55

Table **3:3**. Temperature and Rainfall indices, definition used in this study: TX and TN are temperature daily maximum and daily minimum respectively, and RR the daily precipitation 64

Table 3:4 Validation of the robustness and accurate of eCLM Vs CLM5 66

Table **3:5**. Soil properties for experiments conducted in the two sites and used in simulation studies 67

Table **3:6**. The parameter description and variance in the APSIM-ORYZA model 72

Table **3:7**. : WITA9 rice variety phenological parameters and their values used for model calibration 73

Table 3:8 Soil organic matter scenarios: Manure application 15 days before early rice transplanting (30, 60 and 100 kg N ha-1) and nitrogen application scenarios (45, 90, 120, 150, 180 kg N ha-1). 79

Table 4:1 Statistical analysis result from simulation output and ERA5 land: DLCL= lifting condensation level calculated from default land cover; VLCL= lifting condensation level express from vegetation type; CLCL= lifting condensation level express from crop vegetation type; LCL_ERA5=lifted condensation level calculated from ERA5 land dataset 89

Table **4:2**. Model evaluation statistics after calibration and validation showing Model efficiency (ME), root-mean-square error percentage (RMSE), and percent bias (PBIAS) for yield and phenology, and the coefficient of determination R^2. 121

Table 4:3. Changes (%) in precipitation, minimum and maximum temperatures during the growing season under the future climate scenarios compared to the baseline. The difference in temperature compare to the baseline is showing in parenthesis. 136

Table **4:4**. Percentage Changes (%) in simulated projected rice yield under the future climate scenarios compared to the baseline 141

Table **4:5**. Absolute difference (t/ha) and relative (%) changes in rice yield under alternative management practices compared to the farmers practices under future climate conditions. 144

LIST OF FIGURES

Figure 1.1 Graphic representation of moist air lifting and condensation onset at LCL. (Not to scale) Source : Daidzic, (2019) 6

Figure 1.2. eCLM subgrid hierarchy configuration. A hypothetical subgrid distribution for a single grid cell is shown in the box on the top right. Remember that you will only use the acreage units if you are running the model with the acreage model enabled. Abbreviations: TBD - Tall Building District; HD - High Density; MD - Medium Density; G - Glacier; L - Lake; U - Urban; C - Crop; V - Vegetation; PFT - Plant Functional Type; Irr - Irrigated; UIrr - Unirrigated. Allowed transitions between land units are indicated by red arrows. Allowed transitions at plot level are indicated by purple arrows. 9

Figure 2.1. Land process simulation by eCLM a variance of CLM5 20

Figure 2.2. Different climatic zones in West-Africa (Source: https://eros.usgs.gov/westafrica/node/147 accessed on 20 March 2023 23

Figure 2.3. Vegetation-Rainfall-SST feedback affecting the monsoon rainfall over the West Africa monsoon region. Source (Zeng et al. 1999). 24

Figure 2.4. Production/yield quantities of rice paddy in the world (1994–2019) (FAOSTAT 2021) 46

Figure 2.5. Production share of rice paddy by region (Average 1994–2019) (FAOSTAT 2021) 47

Figure 3.1. Study area highlighting the three climatic zones 51

Figure 3.2. Long term average weather data during rice growing season (2019) and cumulated monthly rainfall and temperature in Mbe, Bouake, Côte d'Ivoire 52

Figure 3.3 Flowchart showing the crop simulation procedure, bias correction methods and rice simulation and forecast 81

Figure 4.1. Comparison of monthly latent heat (LH) between simulation output and ERA5-land reanalysis data over the 11 eddy covariance selected sites in West Africa 84

Figure 4.2. Comparison of monthly sensible heat (SH) between simulation output and ERA5-land reanalysis data over the 11 eddy covariance selected sites in West Africa 85

Figure 4.3. Variation of latent (LH) and sensible (SH) heat fluxes times series of observed, ERA5 and simulated monthly averaged diurnal cycle over (A, Kayoro; B, Nazinga; C, Sumbrumgu) for LH, and SH (D, Kayoro; E, Nazinga; F, Sumbrumgu) in 2013. DLH, VLH, CLH for latent heat flux simulated from default, vegetation and crop land vegetation types respectively; DSH, VSH, CSH are sensible heat flux simulated from default, vegetation and crop vegetation types respectively. 86

Figure 4.4. Correlation between simulation land surface fluxes, ERA5-land and observe (eddy covariance) data over the selected sites in (A) Kayoro station in Ghana and (B) Nazinga in Burkina Faso. LH, latent heat flux form EC data, DLH, VLH, CLH, latent heat flux from default, vegetated and crop land cover simulated output, LH_ERA5, latent heat from ERA5 land data. SH, sensible heat from eddy covariance station; DSH, VSH, CSH, are sensible heat from default, vegetation and crop simulated vegetation types; SH_ERA5, sensible heat from ERA5 land dataset. 87

Figure 4.5. Observed and simulated monthly averaged diurnal cycle of (A) latent heat, (B) sensible heat, and (C) Lifting condensation level (LCL) height at the Sumbrungu, in Ghana EC site (2013) 90

Figure 4.6. Comparison of monthly lifting condensation level (LCL) height between simulation output and ERA5-land reanalysis data over the 11 eddy covariance selected sites in West Africa 91

Figure 4.7. Linear correlation (coefficient of determination and root mean square error) of the mean 3 hourly in monthly sensible and latent flux from the default (DLH, DSH), vegetation (VLH, VSH) and crop PFT (CLH, CSH) with observe eddy covariance data (SH, LH) and ERA5 land (LH_ERA5, SH_ERA5) over Kayoro in Ghana and Nazinga in Burkina Faso 92

Figure 4.8. Mean maximum and minimum of lifting condensation level height for the three hourly land cover DLCL = default plant functional type (PFT), VLCL = vegetation PFT and CLCL = crop PFT 94

Figure 4.9. The climatology pattern of 14 years average of lifting condensation level (LCL) height from (A) default, (B) vegetation and (C) cropland land units over West Africa 95

Figure 4.10. Level of significance change of LCL height between the three PFTs : (A) difference (VLCL-DLCL), (B) difference (VLCL-CLCL), (C) difference (CLCL-DLCL) 97

Figure 4.11. Fourteen years average correlation coefficient between LH and LCL height, SH and LCL height, EF and LCL height for the three land cover over West Africa during 2000-2013. DLCL, default PFT; VLCL, vegetation PFT; CLCL, crop PFT; LH, latent heat, SH, sensible heat; EF, evaporative fractional; PFT, plant functional type; LCL, lifting condensation level 100

Figure 4.12. Climatology of Simulated rainfall mean monthly from 2000-2013 over West Africa 102

Figure 4.13. Fourteen years average correlation coefficient between rainfall, energy and water fluxes and LCL in West Africa during 2000-2013. DLCL, default PFT; VLCL, vegetation PFT; CLCL, crop PFT; LH, latent heat, SH, sensible heat; EF, evaporative fractional; PFT, plant functional type; LCL, lifting condensation level; PCT, rainfall. 104

Figure 4.14 : Climatology of average minimum daily LCL for wet and dry season over West Africa. JJA, June-July-August, DJF, December-January-February, DLCL, Default land cover, VLCL, vegetation land cover and CLCL, crop land cover 108

Figure 4.15 : Climatology of average maximum daily LCL for wet and dry season over West Africa. JJA, June-July-August, DJF, December-January-February, DLCL, Default land cover, VLCL, vegetation land cover and CLCL, crop land cover 109

Figure 4.16 : Difference for maximum daily average over JJA and DJF seasonal LCL between vegetation and default (Veg-Def), and between crop and default (Crop-Def) over West Africa. JJA, June-July-August; DJF, December-January-February; MaxLCL, maximum lifting condensation level height. 110

Figure 4.17 : Difference for minimum daily average over JJA and DJF seasonal LCL between vegetation and default (Veg-Def), and between crop and default (Crop-Def) over West Africa. JJA, June-July-August; DJF, December-January-February; MinLCL, minimum lifting condensation level height 111

Figure 4.18. Correlation plot of the 14 years averages surface fluxes (latent LH and sensible SH heat), net radiation (SR), relative humidity (RH), evaporative fraction (EF), and LCL height in West Africa during the periods 2000-2013 in Kayoro, Ghana characterise with cropland (Dark blue colour reveal a strong positive correlation, medium

light blue show a low positive correlation, light blue show a low positive correlation while the contrast in red colour 116

Figure 4.19. Correlation plot of the 14 years averages surface fluxes (latent LH and sensible SH heat), net radiation (SR), relative humidity (RH), evaporative fraction (EF), and LCL height in West Africa during the periods 2000-2013 in Bontioli, Burkina-Faso characterise with trees and grassland. Dark blue colour reveal a strong positive correlation, medium light blue show a low positive correlation, light blue show a low positive correlation while the contrast in red colour 117

Figure 4.20 : Evaluation metric for APSIM-Oryza model calibration and validation 120

Figure 4.21. Relationship between the ensemble of the raw simulation, observed and bias-corrected daily precipitation series, measured by the mean, standard deviation (STD) and 90th percentile (X90) for the months of March (dry season) and August (wet season). 125

Figure 4.22. Seasonal cycle of precipitation bias correction for the four models (CNRM-CM5, HadGEM2-ES, MPI and NOAA) 126

Figure 4.23. Relationship between the ensemble of raw simulation, observed and bias-corrected daily series of minimum temperature measured by mean, sta dard deviation (STD) and 90th percentile (X90) for the months of March (dry season) and August (wet season). 127

Figure 4.24. Seasonal cycle of minimum temperature bias correction for the four models (CNRM-CM5, HadGEM2-ES, MPI and NOAA) 128

Figure 4.25. Relationship between the ensemble of raw simulation, observed and bias-corrected daily series of maximum temperature measured by mean, standard deviation

(STD) and 90th percentile (X90) for the months of March (dry season) and August (wet season) 129

Figure 4.26. : Seasonal cycle of maximum temperature for the four model (CNRM-CM5, HadGEM2-ES, MPI and NOAA) 130

Figure 4.27. Mean monthly change of minimum temperature over the periods 2020s (2010–2040), 2050s (2041–2070) and 2080s (2071–2100) for the four GCMs under the RCP 4.5 (above) and RCP 8.5 (below) scenarios 133

Figure 4.28. Mean monthly change of minimum temperature over the periods 2020s (2010–2040), 2050s (2041–2070) and 2080s (2071–2100) for the four GCMs under the RCP 4.5 (above) and RCP 8.5 (below) scenarios 137

Figure 4.29. Mean monthly change of maximum temperature over the periods 2020s (2010–2040), 2050s (2041–2070) and 2080s (2071–2100) for the four GCMs under the RCP 4.5 (above) and RCP 8.5 (below) scenarios 138

ACRONYMS

Acronym	Meaning
AEJ :	African Easterly Jet
APSIM :	Agricultural Production Systems Simulator
CBH :	Cloud Base Height
CFT :	Crop Functional Types
CLM5 :	Community Land Model version 5
CORDEX :	Coordinated Regional Downscaling Experiment
DJF :	December-January-February
DM :	Distribution Mapping
eCLM :	Re-Enggening
EF :	Evaporative Fraction
FAO :	Food and Agriculture Organisation
FAOSTAT :	Food and Agriculture Organisation Statistic
GCMs :	General Circulation Models
GSWP3 :	Global Soil Wetness Project version 3
IPCC :	Intergovernmental Panel on Climate Change
ITCZ :	Intertropical Convergence Zone
JJA :	June-July-August
LCL :	Lifting Condensation Level

LH :	Latent Heat
LSM : ,	Land Surface Models
MCS :	Mesoscale convective systems
PCT_CFT :	Percentage Crop Functional Type
PCT_NAT_VEG :	Percentage Natural Vegetation
PFT:	Plant functional type
RCM :	Regional Climate Model
RCP :	Representative Concentration Pathways
SH :	Sensible Heat
SSA :	Sub-Saharan Africa
TEJ :	Tropical Easterly Jet
USDA :	United States Department of Agriculture
WA :	West Africa
WAM :	West African Monsoon
WAM :	West African Monsoonal

Chapter One

1.0 Introduction

1.1 Background

Interactions between the land surface and the atmospheric boundary layer (ABL) play a key role in the climate system. They significantly influence regional climates and have global impacts. Climate-related risks and their impacts on people are also strongly dependent on land-atmosphere interactions and their evolution with climate change. (Cheruy et al., 2020). The land and atmosphere interact through exchanges of energy, mass and momentum. These interactions regulate climate variability and influence climate change at the regional scale. Among all the factors, vegetation and crops are the key component in the land surface-atmosphere coupling (de Noblet-Ducoudré et al., 2012). Vegetation interacts with and influences the atmosphere. It controls the rate of moisture exchange from the soil to the atmosphere through evapotranspiration, regulates surface radiation and temperature through surface albedo and ratio of latent to sensible heat, and influences vertical mixing and turbulence due to roughness length. On the other hand, atmospheric fields (i.e. temperature, precipitation, cloudiness, and CO_2 concentration) feedback on vegetation distribution by modulating vegetation growth, mortality, phenology and competition (Xue, et al., 1993; Wang, et al., 2000; Cox, et al., 2000; Bonan, 2008; Swann, et al., 2010; Yu, et al., 2014; Swann, et al., 2015; Erfanian & Entezar, 2017).

Land and atmosphere interact through exchanges of energy, mass and momentum. These interactions regulate climate variability and influence climate change at the regional scale. Among all the factors, vegetation and crops are the key component in the land surface-atmosphere coupling (de Noblet-Ducoudré et al., 2012). Vegetation interacts with and affects the atmosphere. It controls the rate of soil-atmosphere moisture exchange

through evapotranspiration, regulates surface radiation and temperature through surface albedo and the ratio of latent to sensible heat, and influences vertical mixing and turbulence through roughness length.

West Africa is recognized to be one of the most drought-affected regions. This region experienced a decrease in rainfall in the second half of the 20th century (Didi et al., 2020) and a severe drought in the 1970s and 1980s, leading to widespread famine (Mortimore and Adams 2001). The climate in the region has been improving, especially since the end of the 20th century, with an increase in rainfall (Lebel and Ali 2009; Yu et al., 2016). Since agriculture in the area is primarily rain-fed, understanding the variability and future shifting of the regional climate is crucial to assess the potential impact of future changes and developing adaptation and mitigation measures (Yu et al., 2016). West Africa climate is characterize by the movement of the West African Monsoon (WAM) circulation and is sensitive to land surface conditions especially soil moisture availability and land unit type (vegetation, cropland, urban) (Erfanian and Entezar, 2017).

Charney was the first that introduced the land cover impact concept on rainfall variability over West Africa, and argue that reduction of vegetation in Sahel could lead to an increase of albedo and decrease of precipitation, which could then trigger a positive feedback with the drought in this region of Sahel during the late 20^{th} century (Charney, et al., 1975; Charney, et al., 1977). This approach has developed research on land-atmosphere interactions, including understanding vegetation dynamics, vegetation feedback to climate variability and change, and vegetation feedback to atmospheric mechanisms at different scales (Wang, et al., 2000; Cook, 1999). Atmospheric precipitation and land surface change and variability as a dominant factor in the Sahel's decade-to-decade rainfall patterns till today remain the main studies of land-atmosphere interaction over West Africa. However, no much work focus on the contribution of different land cover

on the couple land surface fluxes and lifting condensation level height and their variability in West Africa precipitation.

The study of land-atmosphere interactions in regional climate variability examines the role of land surface processes, which include plant functional types (urban/default, vegetation and cropland), soil moisture, surface albedo and evaporation in cloud base formation and thus in regional rainfall dynamics. Cloud formation, such as tropical cumulonimbus clouds, occurs during El Niño events. These deep cumulus clouds favour the transfer of heat, moisture and kinetic energy at the lifting condensation level (LCL) (Wu and Newell 1998). Change from one plant functional type to another has an effect on the climate system similar to that of El Niño events (Chase et al., 1996, 2000; Claussen 2002).

The influence of land cover on rainfall variability in West Africa (WA) was first introduced by Charney, who argued that desertification and associated albedo variations, energy and fluxes may have contributed to the intensification of drought in the Sahel during the second half of the 20th century (Charney, et al., 1975; Charney, et al., 1977). Land surface conditions, characterised by PFT (vegetation, crops Figure 1.2) cover and soil moisture, play an important role in rainfall variability over WA. The influence of ecosystem and crop development on seasonal cycles has been extensively reviewed (Schwartz, 1994, 1996; Fitzjarrald et al, 2001; Schwartz et al, 2012; Betts et al, 2013; Sultan et al, 2014). Pielke (2001) investigated the relationship between land surface heat fluxes (latent and sensible), soil moisture and cumulus convective precipitation. He found a significant decrease in the sensible heat flux to the atmosphere in both winter and spring, which may be related to the decrease in seasonal precipitation over the cropland region. The study by Mishra et al (2010) assesses the regional impacts of land cover and climate change on water and energy cycles. The results show that the total conversion of forest

to cropland reduces the annual mean net radiation and land surface fluxes, in some cases due to the significant effect of albedo in the JJA and DJF seasons. They also found that conversion of forest to cropland reduces annual evapotranspiration with an increase in JJA latent and sensible heat fluxes. The nature of the energy balance of the land surface and the hydrological cycle is determined by the type of land cover. The land surface influences the atmosphere by exchanging water, CO_2, energy, momentum and trace gases through the atmospheric boundary layer (Bounoua et al., 2002). The transition from one land cover to another can change the albedo, the surface hydrology, the length of the boundary layer roughness and consequently the surface energy distribution. In addition, different types of land cover change can lead to very different climate changes (Lu and Kueppers 2012). Changing from one PFT to another affects land surface fluxes (sensible and latent), surface albedo, and then significantly modifies moisture conversion at the lifting condensation level (LCL) and hence at the cloud base height (CBH), thereby increasing or decreasing precipitation over the region.

Most research develop the contribution of vegetation change of desertification (afforestation) on land surface component, net radiation, surface albedo convective system and rainfall. However, study need to focus on the effect of plant functional type in lifting condensation level (CLC) height and by the mean on convective system and rainfall over West Africa. The significance of this research is to provide a clear understanding of the effect of vegetation and crop ecosystem on lifting condensation level (LCL) height and precipitation event over West Africa. The land surface model process is highly interactive with the atmospheric component (humidity, temperature, radiation and precipitation) and the surface hydrological process. The atmospheric mechanism (cloud and precipitation formation, mesoscale circulation) is strongly dependent on land

surface fluxes such as latent and sensible heat fluxes. These land surface fluxes are determined by the type of vegetation and soil moisture storage.

The lifting condenser level (LCL) is defined as the height at which an air parcel becomes saturated when it is lifted adiabatically (Romps 2017, Wei et al. 2021). The LCL has been used to estimate and predict the cloud height boundary layer (Figure 1.1), to parameterise precipitation and convection in climate and weather models, and to interpret atmospheric dynamics (Romps 2017; Atreya et al. 2006). The cloud base or cloud top is the height of the lowest visible part of the cloud. The LCL height has therefore been widely used in the study of land-atmosphere coupling as it provides a good estimate of the mean cloud base height and is an indicator of the probability of precipitation (Betts, 2009). PASS research has shown that LCL height is mostly positively correlated with land surface sensible heat flux (SH) and temperature, and negatively correlated with precipitation rate, cloud albedo, soil moisture, surface relative humidity, evaporative fraction (EF), and latent heat flux (LH) (Betts 2009; Wei et al. 2021).

Many analytical but approximate expressions have been proposed for the height of the rising condensation level (LCL), including the widely used expressions of Espy, Bolton and Lawrence. Some of the earlier LCL expressions were explicit and may have uncertainties of hundreds or thousands of metres. Romps has derived the accurate, expressive analytical expression of the LCL of a parcel of air as a function of its temperature, relative humidity and surface pressure. While these studies have provided many useful insights into the effect of land surface fluxes on LCL height and precipitation event on large regional processes, there have been few studies that have assessed the capabilities of land surface models in simulating energy partitioning over different land units (vegetation, crop, urban) and comparing their respective effects on

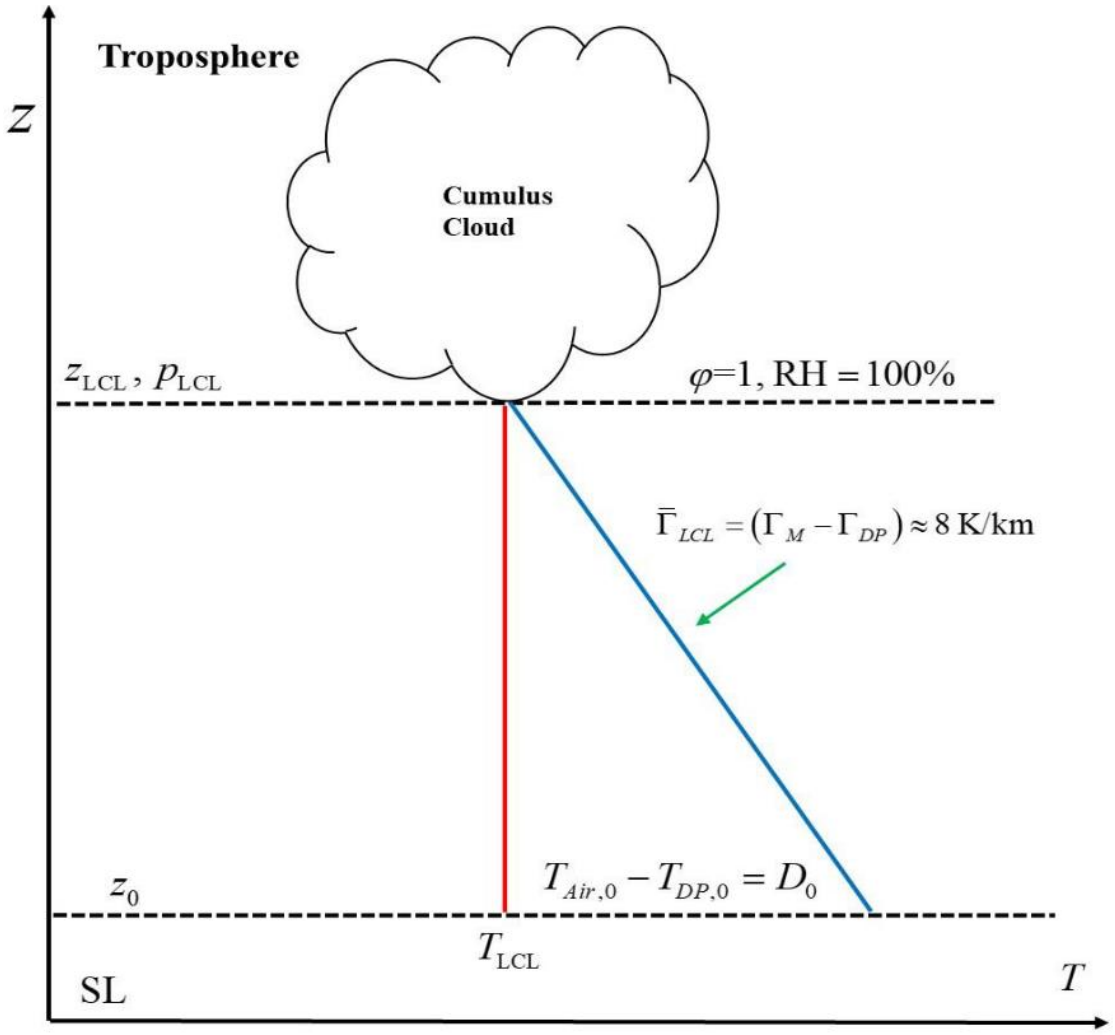

Figure 1.1 Graphic representation of moist air lifting and condensation onset at LCL. (Not to scale) Source : Daidzic, (2019)

LCL and precipitation event in West Africa. Land surface models (LSMs) are the key elements of general climate models that simulate land surface processes, including the uptake and distribution of radiation, moisture and carbon. LSMs typically receive meteorological inputs from the ABL model and generate outputs such as latent and sensible heat fluxes, CO2 fluxes, reflected solar radiation and emitted longwave radiation (Sulis et al. 2015).

The objective of the current work was to quantify the LCL at three hourly resolution between 2000 and 2014 in West Africa for three land units (vegetation, crop and urban, with urban considered as default in this study). The sub-objectives are as follows: i) express the daily and monthly LCL for the three land cover types using the land surface component and atmospheric output from model simulations; ii) assess the magnitude and significance of seasonal LCL trends in West Africa over the selected eddy covariance (EC) sites with observed and ERA5 land; iii) compare the different LCL trends and significance for the three land cover types over the selected EC sites with observed and ERA5 land; iv) analyse the relationship between LCL and land surface fluxes, cloud formation, net radiation and present day climate in WA.

Climate change and the rise in global average temperatures and associated impacts pose a significant threat to natural systems and socio-economic livelihoods around the world. The agricultural sector in particular is highly vulnerable to climate change. Even a small increase of 1° to 2°C in global average temperatures can have a significant negative impact on crop yields, particularly in sub-Saharan Africa (SSA). Climate change poses an increasing risk to agricultural productivity in different regions, even under relatively optimistic scenarios for near-term mitigation efforts (Rosenzweig et al., 2014). Climate change in the 21st century will have a significant impact on global agriculture, and the Intergovernmental Panel on Climate Change (IPCC) assessment report indicates that

most countries will experience an increase in average temperature, more frequent heat waves, increased water stress, desertification and periods of heavy precipitation (IPCC 2007, 2014). The last three decades have been the warmest on record, with each decade warmer than the last (IPCC 2014; Ochieng et al., 2016). Africa is also warmer than a century ago. The impacts are expected to worsen in the future as temperatures continue to rise and rainfall becomes more uncertain (Ochieng et al., 2016). Given the vulnerability of agricultural production to climate variability, it is difficult to improve it to meet the increasing demands of a growing population under the threat of climate change. This requires greater attention to adaptation and mitigation research, capacity building, policy reforms, national and regional cooperation, and support from national and global adaptation funds and other resources to minimise negative impacts. A reduction in food supply due to climate change could have serious socio-economic consequences, such as production patterns and food price insecurity (Stevanovi'c et al., 2016; Wiebe et al., 2015). Adaptation to climate variability and extreme events is the basis for reducing vulnerability to long-term climate change. Simple adaptation measures, such as adopting alternative management practices using modelling and simulation approaches, could help reduce the impacts of climate change.

Climatic parameters such as rainfall, temperature, solar radiation and CO_2 concentration are some of the key factors affecting crop variability and production (Li et al., 2017). Climate change and climate variability affect both crop yield (van Oort and Zwart, 2018) and land suitability (Akpoti et al., 2022) and its availability, stability of food supply, access to food and its prices globally, and food utilisation (Schmidhuber and Tubiello 2007). These climatic factors will influence crop development, growth and yield. All aspects of crop production systems are likely to be affected by future climate change at global and regional levels (Li et al., 2017). Sub-Saharan Africa is known to be the most

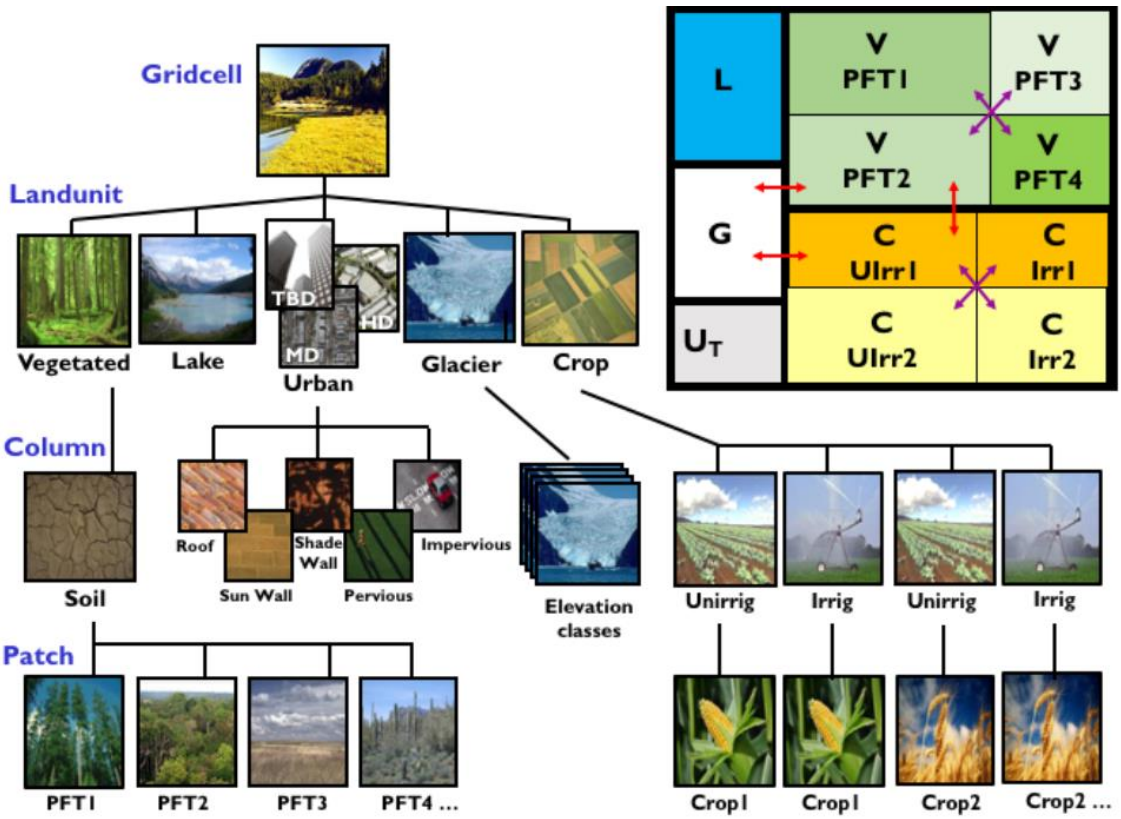

Figure 1.2. eCLM subgrid hierarchy configuration. A hypothetical subgrid distribution for a single grid cell is shown in the box on the top right. Remember that you will only use the acreage units if you are running the model with the acreage model enabled. Abbreviations: TBD - Tall Building District; HD - High Density; MD - Medium Density; G - Glacier; L - Lake; U - Urban; C - Crop; V - Vegetation; PFT - Plant Functional Type; Irr - Irrigated; UIrr - Unirrigated. Allowed transitions between land units are indicated by red arrows. Allowed transitions at plot level are indicated by purple arrows.

vulnerable to climate change due to its inherently higher rates of climate variability, high dependence on rain-fed agriculture, and limited institutional capacity to cope with and adapt to climate variability and change due to limited economic resources and, in some cases, lack of technological know-how (Challinor et al. 2014; Müller et al. 2014). Sub-Saharan Africa is currently facing frequent food crises and water scarcity, exacerbated by climate variability and extreme events such as droughts, extreme rainfall and floods, which have affected the agricultural sector and productivity, as well as the livelihoods of rural populations, and are likely to increase in the future (Sultan and Gaetani, 2016).

Rice provides food for more than half of the world's population and is an important and integral source of income for most of the population (Nawaz et al., 2022). World rice production is estimated at 508.7 million tonnes (FAO, 2020). Under flooded conditions, 75% of the world's rice is transplanted, which requires large amounts of water, while the rest is directly sown (Nawaz et al., 2022). The impacts of climate change are increasing water scarcity due to changes in agricultural practices as an adaptation strategy. The sustainability of the traditional flooded transplanted rice production system is threatened by deteriorating soil conditions, increasing methane emissions, low nutrient use efficiency, micronutrient deficiencies, emergence of new weed species, insect pests and diseases, declining yields and declining rice productivity (Nawaz et al., 2019). Africa is far from rice self-sufficiency and this is likely to worsen in the future (Van Ittersum et al., 2016; Van Oort, Saito et al., 2015). Rice production in Africa will be around 24 million tonnes in 2020/2021 and this production is expected to decline slightly to about 23 million tonnes in 2021/2022 due to climate change effect (USDA, 2022). Sub-Saharan African (SSA) countries have an urgent need to meet the high demand for rice (Arouna et al., 2021a). The increase in rice yields could be achieved by increasing the area under production and increasing yields (Tanaka et al., 2017). Rice production systems in SSA

are irrigated lowland, rainfed lowland and rainfed upland. As a result, the average rice yield in irrigated systems is higher (3.6 t/ha) than in rainfed lowland (2.8 t/ha) and rainfed upland (1.6 t/ha) (Tanaka et al., 2017; Dossou-Yovo et al., 2020). Total rice production in SSA (40%) (FAOSTAT, 2020) is irrigated on about 22% of the total rice area (Diagne et al., 2013a). West African countries, particularly Côte d′Ivoire, are experiencing increased demand for rice due to population growth (Fofana et al., 2014). Yield change has been estimated at 0.1 to 8.0 t/ha and 0.2 to 7.0 t/ha in 2000 and 2020, respectively, with the change due to low input use relative to land area tending to expand the area under cultivation (Komatsu et al., 2022). However, changes in agronomic management practices have had a limited impact on yield growth. There is a clear need to identify the drivers of low adoption of agronomic practices, such as water management practices, fertiliser use, variety types, sowing dates and soil organic matter use, and to identify yield associations with agronomic drivers. This could help identify strategies to reduce the yield gap through the diffusion of yield-enhancing agronomic practices. This could help identify potential approaches to reduce the yield gap and reduce the impact of climate change on rice yields.

Crop modelling is a tool used to assess the large-scale impacts of climate variability and change on crop yields (Challinor et al., 2010; Rötter et al., 2011) and can also help to assess the best agronomic adaptation strategies to reduce the impacts of climate change and the causes that affect crop development, growth and yield. A number of models such as DSSAT (Basso et al., 2016; Jones et al., 2003), EPIC (Wang et al., 2012), FASSET (Bassu et al., 2009), APES (Donatelli et al., 2002), APSIM (Keating et al., 2003), SPASS (Wang and Engel, 2000, 2002), STICS (Brisson et al., 2003), SWAP (Chen et al., 2010; Eitzinger et al., 2004; Ma et al., 2015), CERES (Ritchie et al., 1998), CROPGRO (Godwin and Singh, 1998), CropSyst (Rosenzweig and Parry, 1994; Willmott et al.,

1985), DAISY (Sayre et al., 1997), SOYGRO (Monsi and Saeki, 2005) and WOFOST (Eitzinger et al., 2004), HERMES (Asseng et al., 2014), RZWQM (Ma et al., 2011). have been developed to understand yield gaps and maximise yield potential. However, the application of these models over large areas is often limited by the lack of available data for model calibration and testing and by the presence of a large number of errors (Angulo et al., 2013ab; Rezaei et al., 2015). To simulate the effects of alternative management practices to reduce the impact of climate change on rice yield, scenarios have been developed. Soltani and Sinclair (2015) investigated the sensitivity and robustness of four wheat models (APSIM, DSSAT, CropSyst and SSM) and found that the most simplified models (CropSyst and SSM) were more robust in predicting yield than the more complex models (APSIM and DSSAT). O'Leary et al. (2015) evaluated the performance of six crop models (APSIM-Wheat, APSIM-Nwheat, CAT-Wheat, CROPSYST, OLEARY-CONNOR and SALUS) in response to CO2 elevation and found that the model responses to CO2 elevation were similar and that the models were able to simulate biomass, yield and water use close to experimental observations. Nevertheless, none of those studies calibrated and validated APSIM and the couple model APSIM-ORYZA over the West Africa condition. In addition, the study by van Oort and Zwart (2018) focused on the effects of climate change on potential yield, but not on farmers yields. Therefore, it is still not clear how climate change would impact rice yield, and what could be the mitigation strategies that need to be promoted under climate change.

Climate models offer opportunities to improve understanding of the impacts of climate change and variability on crop yield and production. In many cases, a combination of different General Circulation Models (GCMs) is used to assess the impact of climate change given the uncertainties in a given climate scenario. The base-corrected GCMs are integrated with crop models to simulate yield projections. APSIM (Agricultural

Production Systems sIMulator) is a crop growth simulation model that is increasingly used in related studies due to its widely accepted platform (Gaydon et al., 2017a; Holzworth et al., 2014; Radanielson et al., 2018; Liu et al., 2019). In this study, APSIM is coupled with ORYZA (APSIM-ORYZA) for rice growth simulation. The crop growth process of APSIM-ORYZA was borrowed from the Oryza2000 model (https://sites.google.com/a/irri.org/oryza2000/, Bouman and Van Laar, 2006; Li et al., 2017) and used over a single point. The APSIM-ORYZA platform provides the flexibility, primarily for model calibration, to validate the accuracy of rice growth, development and yield production using the bias-corrected dynamic downscaling of regional climate model (RCM) climate data at the finer spatial scale. A scenario approach was developed using the APSIM-ORYZA platform to simulate the effects of alternative management practices to reduce the impact of climate change on rice yield.

The present study aims to fills several of the knowledge gaps identified using APSIM-Oryza a model for rice growth simulation which is a combination of Oryza and APSIM platform (Amarasingha et al., 2015; Gaydon et al., 2009; Gaydon et al., 2017a,b; Holzworth et al., 2014; Radanielson et al., 2018; Zhang et al., 2018). We calibrate the APSIM-Oryza model for rice growth and yield, for Cote d'Ivoire, and used the calibration model to project the future yield in rice crop.

1.2 Statement of the problem and research question

According to scientists from the Intergovernmental Panel on Climate Change (IPCC), anthropogenic influences are the main cause of ongoing environmental changes and rising temperatures (IPCC, 2013). In addition, anthropogenic CO_2 is an important source of carbon for plants, and its increased concentration in the atmosphere accelerates photosynthesis and increases yields and biomass. However, its excess in the atmosphere is detrimental to plants by modulating meteorological parameters. Temperature is a key

determinant of plant growth rate. Climate change is expected to lead to higher temperatures and more extreme temperatures, which are likely to affect crop productivity. Phenological stages are sensitive to temperature extremes, all species combined, and during this stage of development extreme temperatures would significantly affect production. (Hatfield and Prueger, 2015).

Agriculture is the predominant economic sector in Sub-Saharan Africa (SSA), with 70% of rural households depending on it as a source of their livelihood. Rice is the most important staple food crop of the world's population (Vidigal et al., 2019). SSA represents 6 % and 26 % of total global rice production and area, respectively (FAOSTAT, 2022). In many SSA countries, rice is the second most important source of calories and a strategic crop in terms of food security (Seck et al., 2012). Ten SSA countries (Burkina Faso, Ethiopia, Ghana, Kenya, Mali, Niger, Nigeria, Tanzania, Uganda and Zambia) account for 37% and 19%, respectively, of total regional rice production and harvested area in SSA (FAOSTAT, 2022). Tropical climates characterise most of the rice-growing areas in SSA. Due to population growth, rising household incomes, urbanisation, and changing food consumption patterns and preferences, demand for rice in SSA is growing faster than for any other staple crop (Djurfeldt, 2015; Nigatu et al., 2017). Rice production is at the same time an important carbon dioxide sequestration from the atmosphere and in addition, an important source of greenhouse gases such as methane and nitrite oxide emission (FAO, 2007). In 2004, rice sequestered about 1.74 billion tonnes of CO2 from the atmosphere to produce about 1.16 billion tonnes of biomass at 0% moisture content.

Rice produced on flood condition field emit methane (CH4), which is in importance to CO2 as a greenhouse gases. Under anaerobic condition of submerged soils of flooded rice fields, methane is produced and a quantities of it escapes from the soil into the atmosphere through gas spaces in the rice roots and stems, and the balance of CH4

bubbles up from the soil and / or spread slowly through the soil and overlying flood water. Agriculture is highly dependent on the variations in temperature, precipitation and solar radiation and long-term climate patterns. Of the natural environmental resources that influence plant growth, development and adaptation, climate is perhaps the most important. It comes on top of land and water resources, which can be predicted and easily modified to increase rice production (Akinbile et al., 2020). The effect of carbon dioxide (CO2) and increasing in temperature significantly reduced rice yield, which was not compensated by increasing CO2 (Jagadish et al., 2010). The reduction in grain yield occurred above a critical temperature of 30°C. Combined elevated CO2 and temperature slightly increased dry season biomass and yield and slightly decreased wet season biomass and yield (Matsui et al., 2000). Thus, increased maximum and minimum temperatures can reduce rice yield through sterile spikelets and increased respiration losses (Jagadish et al., 2010; Matsui et al., 2000). A severe reduction and deterioration in the annual tonnage of rice yield was the result of continuous variation in meteorological conditions (Akinbile et al., 2020).

Although, the ways to assess the effect of the expected climate conditions on the rice growth, development and yield is the use of the crop models (Pohanková et al., 2015). This study will one hand use eCLM a variant of CLM5 to simulate the and express lifting condensation level (LCL) height over different land cover types and assess their effect on boundary layer and precipitation and another hand use of crop model to forecast rice yield under climate change impact.

The following research question have been ask:

i. Does eCLM land surface model capable to simulate the type of vegetation can influence the lifting condensation level (LCL) height which in turn influence atmospheric condition (atmospheric boundary layer, precipitation events) over

West Africa whose coupling are important for land-atmosphere interaction and system?

ii. Does calibration and validation of APSIM-ORYZA crop model in rainfed lowland and irrigated lowland production systems will improve rice yield in the context of climate change?

iii. Is evaluating the future impacts of climate change using the RCP scenarios will improve the understanding of the impacts of climate change on rice yield?

iv. Does simulating the effects of alternative management practices using model simulation approaches will help for reducing the climate change impacts on rice yield?

1.3 Aim and Objectives

This study aim to assess the effect of land-atmosphere boundary layer processes on rice production in West Africa.

Specifically to,

1. assess the lifting condensation level heigh over different land cover types and evaluate its effect atmospheric boundary layer and precipitation event in West Africa;
2. calibrated and validated APSIM crop model in rainfed lowland and irrigated lowland production systems;
3. evaluate the future impacts of climate change using the RCP scenarios to understand the impacts of climate change on the rice yield;
4. simulate the effects of alternative management practices for reducing the climate change impacts on rice yield.

1.4 Innovation

Firstly, most research develop the contribution of vegetation change and desertification (or afforestation) on land surface component, net radiation, surface albedo convective system and rainfall. However, study need to focus on the effect of plant functional type in lifting condensation level (CLC) height and by the mean on convective system and rainfall over West Africa. The innovation of this research is to use a new land surface model eCLM a variant of CLM5 to provide a clear understanding of the effect of vegetation and crop ecosystem on lifting condensation level (LCL) height and precipitation event over West Africa.

Secondly, few studies have calibrated and validated APSIM for crop simulation. However, none work done to calibrate and validate it over the West Africa condition. In addition, the study by , van Oort and Zwart (2018) evaluated the impacts of climate change on rice yield, in SSA but their study focused on the potential yield, and not on farmers' rice production and potential yields. Therefore, it is still not clear how climate change would impact rice yield on farmers', and how the use of alternative management practices could mitigate rice yield reduction due to climate change. The objectives of this study were then to evaluate the performance of APSIM-ORYZA for simulating rice yield under current and future climate conditions in irrigated systems in the derived savannah agro-ecological zone of West Africa. This will and identify the alternative management practices to mitigates its impact.

1.5 Structure of the thesis

This thesis is organized into five chapters. Chapter one provides the general introduction, the statement of the problem leading to the present study and some research questions which can derive from it. This chapter also details the objectives of the work and the innovation for the scientific community. Chapter two presents the literature relevant to

the research areas. It discusses the land surface and convective system, defines lifting condensation level height and land surface fluxes, crop model and production, exposed methods for their investigation. Chapter three enumerates the methodology used in the study. It presents the study area, the data used and methods adopted for investigation on land-atmospheric interaction and crop production. Chapter four presents and discusses the results obtained during these researches. It discusses the . The last chapter (Chapter five) is dedicated to the conclusion, the limits and perspectives for future researches related to the same field.

Chapter Two

2.0 Literature Review

2.1 Definition of some concepts

2.1.1 Land Surface model

In atmospheric models, land surface models (LSMs) play a role in partitioning the net radiative energy input into sensible and latent heat fluxes (Richardson et al., 2009). Their accurate representation in land surface models (Figure 2.1) is necessary for weather (Ingwersen et al., 2011) and climate simulations, as these partitioned energy fluxes influence boundary layer development, cloud formation, weather and climate (Pitman 2003, Prentice et al., 2015). To understand and predict the exchange of mass and energy between the terrestrial biosphere and the atmosphere, land surface models are important tools (Bonan, 1995; Foley et al., 1996; Williams et al., 1996; Sellers et al., 1997). A land surface model (LSM) is a typical and critical component of larger, globally integrated models such as global carbon cycle and global climate prediction models. These integrated models are key tools to predict likely future states of the Earth system under human-induced forcings (IPCC, 2007) and to assess feedbacks with and impacts on the biosphere (MEA, 2004). Land surface model processes, such as diurnal changes in solar radiation and seasonal changes in temperature and precipitation, are sensitive to environmental forcing over a range of timescales. Land surface processes have an impact on the climate system through their control of the energy balance and the exchange of greenhouse gases. The output from the LSM simulation help to expression the lifting condensation level, which is important for cloud level formation.

2.1.2 Surface energy fluxes

The surface energy fluxes (Figure 2.1) are an important component of Earth's global mean energy budget and are a primary determinant of surface climate. The annual energy

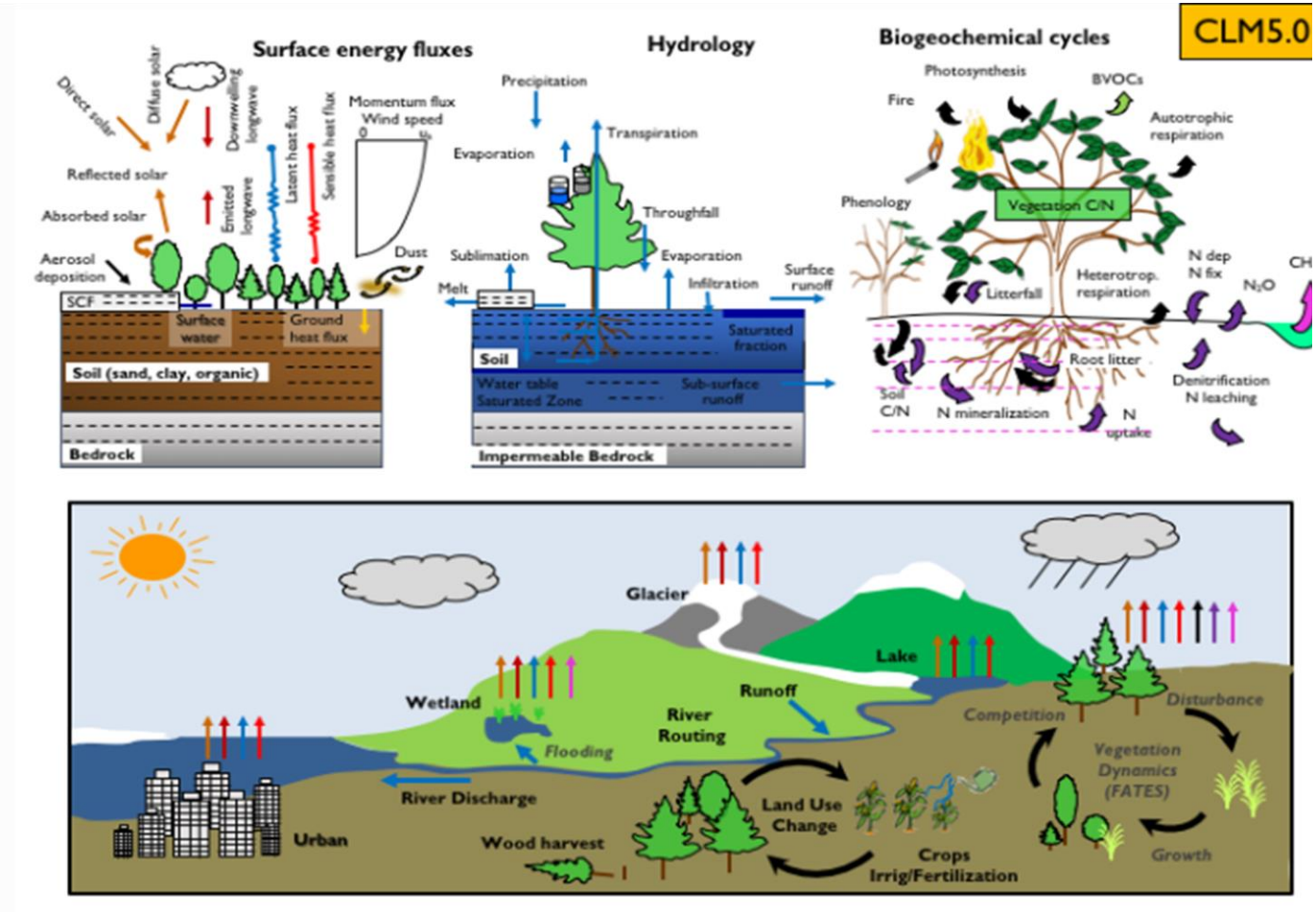

Figure 2.1. Land process simulation by eCLM a variance of CLM5 (Lawrence et al., 2019)

balance at the land surface varied geographically in relation to incoming solar radiation and soil water availability. Energy fluxes vary over the course of a day and throughout the year, and in relationship with soil water availability, and the diurnal and annual cycles of solar radiation. The various terms in the energy budget (net radiation , sensible heat flux, latent heat flux, and soil heat flux) are illustrated for different climate zones and for various vegetation types over the course of a year and over a day.

2.1.3 West African climate systems

The climate of West Africa is dominated by the monsoon, a large-scale circulation that is characterised by seasonal changes in the direction of the wind and is mainly driven by the temperature contrast between the continent and the ocean (Afiesimama et al., 2006). During the June to September rainy season of the West African monsoon (WAM) in the West African Sahel (Klutse et al., 2015), the ITCZs are accompanied by very high convective available energy (CAPE) and horizontal moisture fluxes due to the abundance of available water vapour. These conditions, with their inherent conditional instability, generate deep convection, which forms the major rain-producing systems in this region (Omotosho, 1985).

The West African Monsoonal (WAM) circulation provides over 75% of the annual precipitation in West Africa (Omotosho, 1985) and is the major precipitation producing system during the summer (Abiodun et al., 2008). Other known precipitation-producing systems in West Africa include the African easterly jet (AEJ, Figure 2.3), the tropical easterly jet (TEJ) (Cook, 1999) and the African easterly wave (AEW) (Diedhiou et al., 2001). Rainfall over West Africa is produced by several types of precipitation systems. Mesoscale convective systems (MCSs), monsoon rains and cyclones are the most important.

WA is divided into four climatical zones (Guinean, Sudanese, Sahelian, Saharan). Precipitation is relatively constant in the various zones, but decreases from southern to northern equatorial zones (Eltahir and Gong, 1996). It can be seen from Figure 2.1 that West Africa can be divided into four main climatic zones (Figure 2.2):

- Guinean zone: the annual average rainfall varies between 900-1500 mm, and could be more in some places,
- Sudanese zone: with annual average rainfall between 400-900 mm,
- Sahelian zone: average annual rainfall in the range of 150-400 mm,
- Saharan zone: mostly less than 150 mm of rainfall per year.

The WAM is sensitive to land surface conditions, including soil moisture availability and vegetation, and is driven by the strong land-ocean (meridional) contrast.

Evidence from West Africa suggests that rainfall has declined substantially since the early 1960s (for example, Nicholson 1994; Hulme 1994). Since the late 1960s, an unprecedented drought has affected the Sahel, a semi-arid region of West Africa between the Sahara Desert and the Guinean coastal rainforest. The drought was a major impetus for the establishment of the United Nations Convention to Combat Desertification and Drought, and has had a devastating impact on this ecologically fragile region (Nicholson et al., 1996). However, records for 1995 and 1996 indicate that the dry regime continues (Horton and Parker 1997). The decline in rainfall and persistence of the drought episode in WA has significantly altered the normal regional climate regime over West Africa. Many studies on rainfall, drought and climate variability over WA have been motivated by this observation. These studies fall into two groups: studies that emphasise the role of land-atmosphere interactions in regional climate, and studies that emphasise the role of

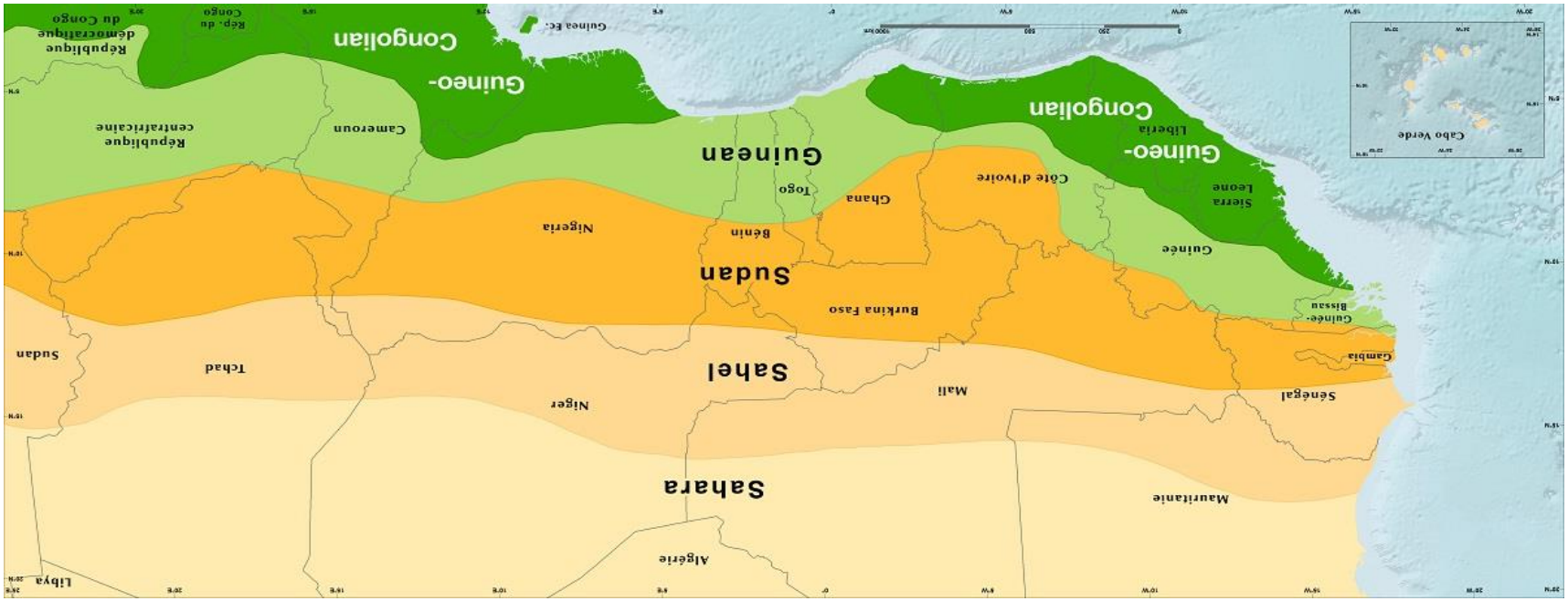

Figure 2.2. Different climatic zones in West-Africa (Source: https://eros.usgs.gov/westafrica/node/147 accessed on 20 March 2023

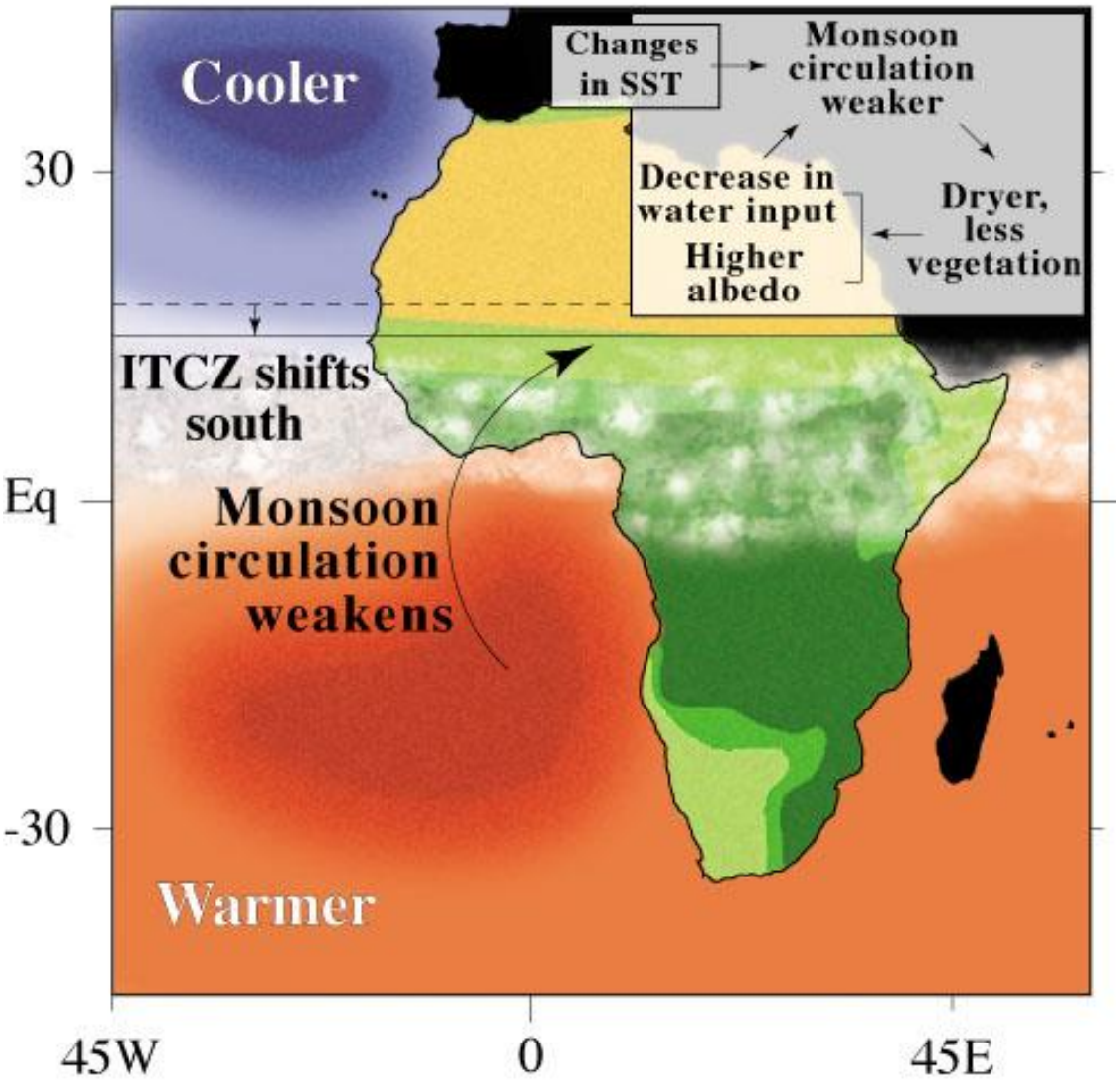

Figure 2.3. Vegetation-Rainfall-SST feedback affecting the monsoon rainfall over the West Africa monsoon region. Source (Zeng et al. 1999).

ocean-atmosphere interactions and sea surface temperature (SST) distribution in precipitation variability over WA (Figure 2.3). Zeng et al. (1999) explore the relative roles of sea surface temperature, land and vegetation feedbacks, while Zeng (2003) outlines our current understanding of the problem in a perspective article in Science. Furthermore, several papers explore the nonlinear dynamics of vegetation-atmosphere interactions in desert-forest transitions.

Land-surface processes such as vegetation, soil moisture, surface albedo and evapotranspiration have been shown to play an important role in regional precipitation dynamics (Zheng and Eltahir 1997). The role of land surface processes in the regional climate was investigated by several modelling studies: Charney et al. (1975), Charney et al. (1977), Sud and Fennessy (1984), Sud and Molod (1988), Rowell and Blondin (1990), RodriguezIturbe et al. (1991), Xue and Shukla (1993), Cook (1999), Wang, et al. (2000), Patricola, et al. (2008). Studies by Kutzbach et al. (1996) examined the role of vegetation and soil moisture in African paleoclimate. They found that replacing the Sahara with grassland and desert soils with more loamy soils could bring their model simulations and palaeo-vegetation observations into closer agreement than otherwise. Their findings suggest that land surface conditions, characterised by vegetation cover and soil moisture, are important in determining precipitation variability over West Africa. It is generally concluded that desertification near the sub-Saharan desert margin reduces rainfall within the vegetation perturbation region and increases rainfall south of the perturbation region (e.g. Charney et al. 1975; Xue and Shukla 1993). Zheng and Eltahir (1997) sudy investigate the role of vegetation in the dynamics of West Africa monsoons, and result show that West African monsoons, and hence precipitation distribution, depend crucially on where vegetation disturbances occur. The simulated monsoon circulation may be little affected by changes in vegetation cover along the Saharan-West African border

(desertification). If the monsoon circulation is disrupted, regional precipitation may be drastically affected.

2.1.4 Surface Characterization and Model Input Requirements

The heterogeneity of the land surface in space is represented in CLM as a nested subgrid hierarchy, where grid cells consist of multiple land units, snow and soil columns and PFTs. Each grid cell can contain any number of land units, each land unit can contain any number of columns, and each column can contain any number of PFTs. The first subgrid level which is the land unit glacier, lake, urban, vegetation and crop (if crop modelling enabled)) can be used to capture broadest spatial patterns. The second sub-grid level, the column, is intended to capture the potential variability of soil and snow condition variables within a single land unit. For example, vegetated land may contain several rows, and cropped vegetated land may be divided into two rows, irrigated and unirrigated. The patch level is the third subgrid level. Patches can be PFTs or bare ground on vegetated land and crop functional types (CFTs) on cultivated land. The patch level aims to capture the biogeophysical and biogeochemical differences between broad categories of plants in terms of their functional characteristics (Oleson et al. 2010b).

Up to 15 possible Plant Functional Types (PFTs) plus bare ground make up the vegetated area. An additional PFT will be added if the Irrigation model is active and an additional six PFTs will be added if the Crop model is active. The vegetation in the land surface model simulation is referring to index percentage natural vegetation (PCT_NAT_VEG) on the surface dataset while crop plant functional type refers to the index of percentage crop functional type (PCT_CFT) on the surface dataset. The actual atmospheric state is used to force the land models. This atmospheric state is obtained from a coupled atmospheric model or a land-only observational data set. The land model then initiates a full set of calculations of surface energy, constituents, momentum and radiative fluxes.

There are two steps in the land model calculations. Using the snow and soil hydrological states from the previous time step, the land model continues to calculate surface energy, constituents, momentum and radiative fluxes. Based on these fluxes, the land model then updates the soil and snow hydrology calculations.

Observational datasets provide the atmospheric forcing required by the CLM. A 110-year (1901-2010) dataset provided by the Global Soil Wetness Project (GSWP3) is the default forcing supplied with the model. The GSWP3 dataset has a spatial resolution of 0.5° X 0.5° and a temporal resolution of three hours. Here the GSWP3 dataset is modified by missing data for certain fields over oceans, lakes and Antarctica. These missing data are filled in with the 1948 data from Qian et al. (2006), which are interpolated by the Data Atmosphere model to the 0.5° grid of GSWP3. This means that the model can run across the continent, ensuring that data is available along the coast regardless of model resolution.

There is also an alternative forcing dataset, CRUNCEP, a 110 years (1901-2010) dataset (CRUNCEP; Viovy 2011) that is a combination of two existing datasets, the CRU TS3.2 0.5° × 0.5° monthly data covering 1901-2002 (Mitchell and Jones 2005) and the NCEP reanalysis 2.5° × 2.5° 6 h data covering 1948-2010. It was used for forcing CLM (eCLM) in studies on vegetation growth, transpiration and gross primary production (Mao et al. 2012, Mao et al. 2013, Shi et al. 2013) and for TRENDY (trends in net land-atmosphere carbon exchange for 1980-2010) (Piao et al. 2012). Version 7 is available here (Viovy 2011).

2.2 Land-atmosphere interaction

Land, atmosphere interact with each other through energy, mass, and momentum exchanges. These interactions regulate climate variability and influence climate changes

at the regional scale. Among all of the factors, vegetation and crop are the keys component in the land surface-atmosphere coupling (de Noblet-Ducoudré et al., 2012). Vegetation interacts with and influences the atmosphere. It controls the rate of moisture exchange from the soil to the atmosphere through evapotranspiration, regulates surface radiation and temperature through surface albedo and ratio of latent to sensible heat, and influences vertical mixing and turbulence due to roughness length. On the other hand, atmospheric fields (i.e. temperature, precipitation, cloudiness, and CO_2 concentration) feedback on vegetation distribution by modulating vegetation growth, mortality, phenology and competition (Xue, et al., 1993; Wang, et al., 2000; Cox, et al., 2000; Bonan, 2008; Swann, et al., 2010; Yu, et al., 2014; Swann, et al., 2015).

The significance of this research is to provide the analysis and contribution of vegetation and crop ecosystem and their effect on the lifting condensation level (LCL) height and precipitation event over West Africa. Land surface model process highly interactive with atmosphere component (humidity, temperature, radiation and precipitation) and surface hydrological process. The mechanism of atmosphere (formation of cloud and precipitating system, mesoscale circulation) are strongly dependence of land surface fluxes such as latent and sensible heat fluxes. These land surface fluxes are determined by the vegetation and soil moisture storage.

Land cover change (LCC) through climate model can have an impact on the regional climate simulation, changing energy available between surface fluxes (latent and sensible heat fluxes), through change of precipitation distribution between evapotranspiration and runoff. The observed change is due to land surface parameters which in turn can induced modification in atmosphere, which response back on land surface and energy fluxes (Zhao et al. 2001). Several relevant research have shown that changes in the sequence of vegetation can have a strong impact on the regional climate by distributing sensible and

latent heat fluxes. Others research also show the importance of vegetation in soil moisture and the role of soil moisture as an important source in forecasting rainfall. Vegetation may regulate the quantity of soil moisture at the surface, and enhanced vegetation depletes more soil moisture over time and this the process continue (Wang et al. 2009). After rain event, water last long for evaporation on a vegetated surface than on bare soil. Vegetation land unit affect the variability of soil moisture, and this is claimed to be evidence for a potential feedback between vegetation enhancement and cloud formation (De Ridder 1998; Mahmood et al. 2011).

West Africa (WA) is the most affected by the risk of climate change disruption (drought and flood), and experienced a decreased of precipitation following with a severe drought during the last 70s -80s severe drought. Agriculture in WA is primarily rainfed, and there is the need to understand the regional climate variation and future change impact and found the best adaptation strategic for mitigation (Yu et al. 2015). Most research work have showed that be said sea surface temperature which strongly influence rainfall variability over Sub-Sahara Africa (SSA), we have land surface properties and processes comprised vegetation conditions and dynamics (Nicholson 2013). Land-atmosphere interact between each other through climate by controlling vegetation modification abd dynamic and through vegetation through biogeophysical and biochemical processes by modifying surface albedo, roughness length Bowen ratio (Bonan 2008; Swann et al. 2012).

Change on land surface characteristic through clearing and deforestation affect moisture phase. Its change albedo, surface roughness and canopy resistance. As the result, land surface energy elements are then being reallocated and change in the partition of latent and sensible heat fluxes which will impact the boundary layer formation and the vertical transport in the atmosphere of heat and water vapour (Xinmei and Lyons 1995). Cloud

may form earlier over region with hight sensible heat flux (Rabin et al. 1990; lyons et al. 1993). Vegetation cleaning through deforestation and desertification sensitivity could induced to increase of albedo and decreased of precipitation in the region of WA (Charney 1975; Xue and Shukla 1993). The mechanism of cloud formation appeared earlier over the regions characterised by highest level of sensible heat flux (Rabin et al. 1990; Lyons et al. 1993). Land cover changes through land clearing induised change in the land surface energy balance by increasing sensible heat flux and decreasing latent heat flux. The decrease in latent heat flux attenuates the availability of moisture and leads to a decrease in the maximum available convective potential energy, which in turn leads to a decrease in total amount of seasonal rainfall. However, in comparison of the above statement, the increased of sensible heat flux increased land cover change surface temperature and by elevating planetary boundary layer height and enhanced levels of free convection and raised condensation, and transporting more water vapor into the atmosphere over the land modification surface (crop land, city areas) increasing the occurrence and the magnitude of extreme precipitation.

Abiodun et al. (2008) founding showed that both deforestation and desertification are liable to strengthen the monsoon flux over West Africa. However, Zheng and Eltahir (1998) highlighted that coastal areas deforestation over West Africa may result to the loss of monsoon flows but that desertification between the Sahara and West Africa has a minor impact on regional rainfall. Hoffmann and Jackson (2000) argued that the switch from savannah to grassland in the Sahel induces a warmer climate with an unimportant decrease in precipitation. According to Taylor et al. (2002), expansion of forest conversion to cropland projected during the last four decade has led to a decline in rainfall linked with a delay in the onset of the wet season peak in July.

Cropland ecosystems impact on land-atmosphere interactions and atmospheric boundary layer (ABL) processes has been assessed among a number of modelling studies. McPherson and Stensrud (2005) assessed the influence of changing of vegetation to winter wheat on the ABL trend. The result show that the enhanced value of latent heat flux and atmospheric moisture close to surface drive a less deep ABL. Tsvetsinskaya et al. (2001) researchers reported that change from standard crop to specific crop generate a difference in the simulation of turbulent het fluxes, which leads to changes in temperature, humidity, winds and precipitation. Levis et al. (2012) evaluated the impact of crop activities in land surface energy fluxes simulation and found that change in heat fluxes produce changes in precipitation. A number of modelling studies of the effects of land-use change on the hydrological and energy cycles have been developed, most of which deal with the conversion of natural landscapes to cropland. Bounoua et al (2002) studied landscape transformation caused by human conversion of large areas of forest and grassland, and found canopy cooling of as much as 0.7°C in summer because of enhanced latent heat flux from plants, and as much as 1.1°C in winter because of enhanced albedo. Diffenbaugh (2009) found statistically significant warm season cooling, due to changes in both surface moisture and surface albedo, in areas of crop/mixed cropping replacing shortgrass and interrupted woodland, and in areas of irrigation cropping. Mishra et al. (2010) found that complete conversion of forest to cropland reduced mean annual net radiation and sensible heat fluxes, partly due to the large effect of increased snow albedo in winter and spring. Although latent heat flux increased in summer, forest to cropland conversion also reduced annual ET.

The lifting condensation level (LCL) is defined as the height at which an air parcel get saturated when lifted adiabatically (Romps 2017, Wei et al. 2021). LCL has been used to estimated and predict the boundary layer of cloud cover level, precipitation

parametrization and convection in climate and weather models, and atmosphere dynamic interpretation (Romps 2017; Atreya et al. 2006). The cloud base or the base of the cloud is the height of the lowest visible part of the cloud. The LCL height has therefore been broadly used in the investigation of land-atmospheric coupling because its provides a good estimation of the average cloud base height and is an indicator of the probability of precipitation (Betts, 2009). Pass research funding showed that LCL height is mostly positively correlated with land surface sensible heat flux (SH) and temperature at 2 m and negatively correlated with precipitation rate, cloud albedo, soil moisture, surface relative humidity, evaporative fraction (EF), and latent heat flux (LH) (Betts 2009; Wei et al. 2021).

Numerous analytical, but approximate, expressions have been proposed for the height of the rising condensation level (LCL), including the widely used expressions of Espy, Bolton and Lawrence. Some previous LCL expression have been express and may have uncertainties of hundreds or thousands of meters. Romps have derive the accurate, expressive analytical expression of LCL of a parcel of air which is a function of of its temperature, relative humidity and surface pressure. While these studies provided many useful insight of the effect of land surface fluxes on the LCL height and precipitation event on large regional-scale processes, there have been few studies that assessed the capabilities of land surface models in simulating energy partitioning over VLU and CLU and compare their respective effect on ABLs and precipitation event over West Africa.

In this study, we evaluated the influence of crop, pristine vegetation and urban land cover interaction on the atmospheric condition (atmospheric boundary layer, precipitation events) over West Africa. We firstly evaluate the relationship between land surface fluxes and LCL height from CLU and assesses their influence on ABL and precipitation event,. In second part, we assess the relationship between of land surfaces fluxes and LCL height

over pristine vegetation land unit (VLU) and evaluated the their influence on ABL and precipitation event. At the end, we compare both the influence from both land unit and evaluate the most affecting ABL and precipitation event over West Africa using eCLM land surface model.

2.3 Impact of climate change on rice production

2.3.1 Climate change in Cote d'Ivoire

Climate change is an important issue for Côte d'Ivoire, and its vulnerability is among the highest in the world (World Bank 2018). A number of changes in the national climate have already been observed, such as lower and more erratic rainfall, shorter rainy seasons and a temperature increase of 0.5°C since the 1980s. An average temperature increase of 2°C across the country is projected by 2050, along with rainfall variability and a 30cm sea level rise along the country's coastline (World Bank, 2018). Côte d'Ivoire is one of the countries in the West Africa region. A region particularly vulnerable to climate variability and change, where a significant part of the population and crop production is concentrated (43% of the population and 53% of the area under cereals, roots and tubers; FAOSTAT). Rainfall in Côte d'Ivoire is dependent on the West African Monsoon (WAM), which originates in the Gulf of Guinea region. The WAM shows significant variability on interannual and interdecadal time scales: the long-term, large-scale drought of the 1970s and 1980s (Dai et al., 2004) and was considered the most extreme regional climate indicator in terms of precipitation in the middle of the last century (Trenberth et al., 2007). Such variability in WAM has a huge impact on the local population by highlighting their vulnerability to possible future negative changes in WAM in the context of global climate change (Roudier et al., 2011).

2.3.2 Crop models and model simulation

Predicting the potential impacts of climate change on crop yields requires a model that shows how crops will respond to future climate conditions due to natural factors and anthropogenic activities in climate change, such as the frequency of extreme temperatures, possible changes in mean precipitation, seasonal and temporal distribution, and warmer temperatures (Sultan and Gaetani, 2016). According to World Bank statistics published in 2008, crop yields are highly sensitive to climate variability, as 96% of all agricultural land is predominantly rain-fed. Therefore, with the widespread expansion of crop model applications, model performance and assessment need to be appropriately adjusted to increase confidence and reduce uncertainty in model simulations (Angulo et al., 2013). Crop simulation models take into account the complex relationships between weather, soil and management to assess and predict crop performance (Holzworth et al., 2014).

The setup of the application of crop growth models is mainly determined by the efficiency of the different parameters. Besides the fact that some parameters are difficult and hard to measure directly, the use of optimisation algorithms for parameter calibration is mostly required (Archontoulis et al., 2014ab; Kamali et al., 2018; Liu et al., 2019). Model calibration has mostly been applied to crop production by researchers in different ways (Ebrahimi-Mollabashi et al., 2019; Choruma et al., 2019; Bahri et al., 2019; Ahmed et al., 2016; Amarasingha et al., 2015a; Archontoulis et al., 2014a, 2014b; Bado et al., (2010); Gaydon et al., 2017a, 2017b, Fernando et al., 2015; Hammer et al., 2005; Bouman et al., 2001).

The Agricultural Production Systems Simulator (APSIM) model has been extensively parameterised, calibrated and validated in different environments and management conditions (Amarasingha et al., 2015). The APSIM model is a useful tool for assessing

the performance of cropping systems under different conditions and for improving water productivity (Katerji et al., 2013; Amarasingha et al., 2015). It is based on mathematical representations of real systems and, like other crop models, provides an efficient way to learn difficult biophysical systems (Holzworth et al., 2011). However, little or no work has been done using the coupled model (APSIM-ORYZA) to calibrate, validate and simulate rice production and yield under West African conditions, and also to establish a model simulation approach for different alternative management practices to mitigate the effects of climate change on crop yield.

2.3.3 Representative Concentration Pathways (RCPs)

The climate research community uses socio-economic and emissions scenarios to provide plausible descriptions of how the future might unfold with respect to a range of variables, including socio-economic change, technological change, energy and land use, and emissions of greenhouse gases and air pollutants. They provide input to climate models and underpin the assessment of potential climate impacts, mitigation options and associated costs (Van Vuuren et al., 2011). The scenarios provide a range of decision options for governments and other institutions around the world. Policy choices based on risk and values will help determine the way forward. The Fifth Assessment Report (AR5) of the Intergovernmental Panel on Climate Change (IPCC) introduced a new methodology for developing scenarios. These scenarios, called Representative Concentration Pathways (RCPs), cover the range of plausible radiative forcing scenarios (Jubb 2013). RCPs are concentration trajectories used in the IPCC's 5th Assessment Report. They have prescribed trajectories for greenhouse gas and aerosol concentrations, as well as land use change, that are consistent with a set of general climate outcomes used by the climate modelling community. The trajectories are characterised by radiative forcing at the end of the 21st century. Radiative forcing is the additional heat trapped in

the lower atmosphere by additional greenhouse gases, measured in watts per square metre (W/m^2). The complexity of possible future human emissions has been reduced to four representative pathways (Jubb 2013). RCPs include the effects of atmospheric concentrations of carbon dioxide and other greenhouse gases and aerosols. The time period covered by RCPs is 1850-2100.

The RCPs represent a broader range of scenarios in the research literature. They include a very low mitigation scenario (RCP 2.6), two intermediate stabilisation scenarios (RCP4.5 and RCP6) and a very high reference emissions scenario (RCP 8.5). RCP 2.6 is the most ambitious. It envisages an early peak in emissions, followed by a decline due to the active removal of carbon dioxide from the atmosphere. This pathway is also referred to as RCP3PD (representing a peak radiative forcing of ~$3W/m^2$ by mid-century, followed by a decline). RCP 2.6 requires early participation by all major emitters, including those in developing countries. It has no equivalent in the IPCC AR4 (Moss et al., 2008; Jubb 2013). Table has been proposed for projections of global warming for the mid and late 21st century (2046-2065 and 2081-2100, respectively). For these projections, it is proposed that temperature projections can be compared to a reference period of 1850-1900 or 1980-99 by adding 0.61 or 0.11°C respectively. Under all RCPs, global mean temperature is projected to increase by between 0.3 and 4.8°C by the end of the 21st century, while global mean sea level is projected to rise by between 0.26 and 0.82 m (Table 2:1).

2.3.4 Global and Regional Climate Models

Impacts of climate change will be far-reaching, and will largely be driven by natural and human-induced interactions that affect atmospheric and oceanic natural processes (IPCC, 2014). Many factors, including the land surface, polar ice sheets and the sun, determine global climate conditions. It is therefore imperative to develop computer programmes

that can collect, store and use adequate data to simulate these complex processes. The use of climate models is well established for assessing the impacts of climate change and variability. In many applications, due to the different responses/sensitivities of different GCM types combinations of multiple general circulation models (GCMs) are used to complement climate predictions (Chokkavarapu and Mandla, 2019).

Downscaling is an alternative way to assess climate variability at local scales, as climate models struggle to simulate climate variability at finer resolutions for local applications (Roux et al., 2018). There are two main methods of downscaling, namely dynamic downscaling and statistical downscaling. In dynamic downscaling, the results of the GCMs are used through the lateral boundary conditions of the regional climate models (RCMs) for a larger area down to a specific area of interest. However, dynamic downscaling is computationally intensive and costly (Schmidli et al., 2007). Statistical downscaling involves projecting the local climate into a process that links global and local scale parameters (Gudmundsson et al., 2012). Gutmann et al. (2012) compared statistical and dynamical downscaling and identified some uncertainties in using statistical downscaling to project climate events. The use of statistical downscaling approaches appears to be mandatory for precipitation prediction. The spatial coverage of precipitation is improved when additional statistical downscaling methods are considered. Thus, by comparing the main downscaling approaches, it is possible to understand and select the appropriate method for a field analysis (Gutmann et al. 2012). The Coordinated Regional Downscaling Experiment (CORDEX) has downscaled several GCMs across fourteen domains. Many papers have used this CORDEX dataset to study drought events (Diasso and Abiodun, 2015; Meque and Abiodun, 2015, Oguntunde et al, 2017), rainfall patterns in West Africa (Klutse et al, 2015), and the impacts of different

levels of global warming in specific regions (Abiodun et al., 2018; Klutse et al., 2018; Kumi and Abiodun, 2018).

In this study, the APSIM crop model was used to map the impacts of climate change in Côte d'Ivoire. The output of the GCM was used to produce a surface feature to predict climate in different time windows of future scenarios, spaced 30 years apart, including 2020, 2050 and 2080. The output produced daily weather data characteristic of the changed climate. These were used to predict crop yields using the APSIM crop simulator model. The rice simulation was performed with the combination of climate, soil and water management types in the study window and compared yield distributions now and for different future climate periods.

2.3.5 Bias Correction procedure

Climate models typically produce incorrect representations of observed time series, necessitating the use of bias correction methods (Teutschbein and Seibert 2012). Bias correction methods use a processing algorithm to correct RCM outputs. The basic idea and rationale for correcting the baseline and control RCM series is to identify possible biases between observed and simulated climate variables. The Climate Model Data for Hydrological Modelling (Cmhyd) tool was used in this study to perform the bias correction of the climate data (Yeboah et al., 2022). The observed climate variables (precipitation and minimum and maximum temperature) are stored in text files in the same directory. The observation files contain the start date of the time series, the number of daily records and the location files contain lat/long, altitude and the name of the file in the folder. Metadata from a netCDF file is used by a model to identify climate model grid cells above a station location. The model then converts the temperature and precipitation data into degrees Celsius and millimetres of rainfall respectively. CMHyd pre-processes the data prior to bias correction. The observed and modelled historical data are then

Table 2:1. Global warming (°C) and sea level (m) increase projections with four global radiative forcing pathways from greenhouse gas emissions from human activities, with radiative forcing of 2.6, 4.5, 6.0 and 8.5 W/m² by 2100. The corresponding respective greenhouse gas concentrations in the year 2100 are equivalent to 490, 650, 850 and more than 1370 parts per million (ppm) carbon dioxide.

RCPs		Global warming increase (oC)		Global sea level increase (m)	
Radiative forcing	Atmospheric CO2 equivalent (parts per million)	2046–2065	2081–2100	2046–2065	2081–2100
		Mean (likely range)		Mean (likely range)	
2.6	490	1.0 (0.4 to 1.6)	1.0 (0.3 to 1.7)	0.24 (0.17 to 0.32)	0.40 (0.26 to 0.55)
4.5	650	1.4 (0.9 to 2.0)	1.8 (1.1 to 2.6)	0.26 (0.19 to 0.33)	0.47 (0.32 to 0.63)
6	850	1.3 (0.8 to 1.8)	2.2 (1.4 to 3.1)	0.25 (0.18 to 0.32)	0.48 (0.33 to 0.63)
8.5	>1370	2.0 (1.4 to 2.6)	3.7 (2.6 to 4.8)	0.30 (0.22 to 0.38)	0.63 (0.45 to 0.82)

Source IGBP. http://www.igbp.net/download/18.1b8ae20512db692f2a680007120/NL75_one-planet.pdf

compared to assess performance. Delays for observed and historical data are then superimposed (Yeboah et al., 2022).

2.3.6 Bias correction Methods

Eight correction methods available in the CMhyd tool were analysed against the raw RCM data. These included linear scaling (multiplicative and additive), delta change correction (multiplicative and additive), local intensity scaling of precipitation, power transformation of precipitation, variance scaling of temperature and distribution mapping of precipitation and temperature. In this study, after the use of the 8 bias methods, only the delta change correction method was the best performing method. These methods are listed in Table 2:2. Bias correction for precipitation and temperatures (Table 2:2) and further details are given in the following sections.

2.3.6.1 Linear Scaling (LS) of Precipitation and Temperature

The LS methods consist of a permanent correction factor that is evaluated by the difference between the original RCM simulation and the observed. The aim is to have a perfect adjustment of the climate factors in the addition of the monthly means. For rainfall, the ratio of the long-term mean of the observed monthly rainfall ratios to that of the RCM simulated monthly rainfall ratios was defined and used for multiplying the simulated daily rainfall of the correction month (Eqs. 2.1 & 2.2; Lenderink et al. 2007).

$$P_{con,cor(d)} = P_{con(d)} \times \frac{\overline{P_{obs(m)}}}{\overline{P_{con(m)}}} \quad \text{(Eq2.1)},$$

$$P_{sec,cor(d)} = P_{sec(d)} \times \frac{\overline{P_{obs(m)}}}{\overline{P_{con(m)}}} \quad \text{(Eq2.2)}$$

$P_{con,cor(d)}$ is defined as the corrected daily precipitation, $P_{sec,cor(d)}$ is the unchanging future periods; $P_{con(d)}$ is the uncorrected daily precipitation in the equivalent month,

$P_{sec(d)}$ is identic during the future periods; $\overline{P_{obs(m)}}$is defined as the observed monthly mean precipitation in the equivalent month during the checking dated; $\overline{P_{con(m)}}$ is defined as the as the simulated monthly mean precipitation in the equivalent monthly during the future period.

However, for temperature time series, the difference between the long-term mean of the observed monthly temperature, and the one of the RCM simulations was defined as an addition term and then was added to the simulated daily temperature of the corresponding month (Eq 2.3 &2.4; Lenderink et al. 2007).

$$T_{con,cor(d)}=T_{con(d)}+(\overline{T_{obs(m)}} - \overline{\overline{T_{con(m)}}}) \quad \text{(Eq2.3)},$$

$$T_{sec,cor(d)}=T_{sec(d)}+(\overline{T_{obs(m)}} - \overline{\overline{T_{con(m)}}}) \quad \text{(Eq2 4)}.$$

Where, $T_{con,cor(d)}$ is the corrected daily temperature in the corresponding month during the control period; $T_{sec,cor(d)}$dowel unchanged during the future period; $T_{con(d)}$is defined as the raw daily temperature in the equivalent month throughout the checking period; $T_{sec(d)}$dowel the same throughout the future period; $\overline{T_{obs(m)}}$ is the observed monthly mean temperature in the corresponding month during the control period; $\overline{T_{con(m)}}$ is the simulated monthly mean temperature through the equivalent month during the future period.

2.3.6.2 Local Intensity Scaling (LOCI) of Precipitation

To further adjust the wet day frequencies, the LOCI method was developed using a wet day threshold. Since light rain days are often recorded in the original RCM outputs, this approach aims to eliminate the light rain effect. The scaling factor Sm is calculated to confirm that the mean of the corrected precipitation is equal to the observed precipitation. This is in accordance with the method and equation (5 to 9; Luo et al. 2018).

2.3.6.3 Power Transformation (PT) of precipitation

The LS method, also known as power PT (Zhang et al. 2018), corrects the mean and dispersion of the rainfall series using the exponential Pb. The LS method is based on the assumption that the mean and dispersion of the rainfall series are the same. The standard deviation of the RCM simulations is further adjusted with this method. First, the monthly mean precipitation was the same between the RCM simulated and observed precipitation time series (Teutschbein and Seibert 2012; Zhang et al. 2018), and the scaling factor bm was calculated to make the RCM variance coefficient equal to that of the observations on a monthly basis (Eq. 10; Zhang et al. 2018).

2.3.6.4 Variance scaling (VARI) of temperature

However, due to the use of the power function (Teutschbein and Seibert 2012; Zhang et al. 2018), PT, which is known as a method to correct both mean and variance, is limited to precipitation time series. However, variational adjustment (VARI) techniques have been applied to correct biases in temperature time series (Fang et al. 2015; Teutschbein and Seibert 2012).

2.3.6.5 Delta-change correction of precipitation and temperature

Rather than using the RCM simulations of the future state directly, the delta change method uses the RCM simulated future change as a perturbation to the observed data. For a good assessment, the baseline climatology (observed data) cannot be used. The observed time series is overlaid with monthly control and scenario simulations of the future scenarios. Multiplicative correction is used for precipitation (Equations 27 & 28; Teutschbein and Seibert 2012), and additive correction for temperature (Equations 29 & 30; Teutschbein and Seibert 2012).

2.3.6.6 Distribution Mapping (DM) of Precipitation and Temperature

The distribution function of RCM values in feet is corrected with the observed distribution function using the DM method. DM assumes that RCMs and observed climate variables follow a certain frequency distributions (Luo et al. 2018). Typically, two transfer functions suitable for climate data are the gamma and Gaussian distributions for precipitation and temperature, respectively. For precipitation, the cumulative probability of simulated precipitation was determined by first specifying a random precipitation intensity. Next, corrected rainfall values were chosen according to cumulated probabilities (Zhang et al. 2018). For temperature, the cumulative probability of simulated temperature was determined and the corrected temperature value was selected based on the probability (Zhang et al. 2018).

2.3.7 Rice for food security

Rice is a staple food essential to the food security of more than half the world's population. World rice production is expected to increase by 58 to 567 million tonnes (Mt) by 2030 (Mohidem et al., 2022). Rice contains a significant number of calories and a wide range of essential vitamins, minerals, and other nutritional values (Mohidem et al., 2022). Thus, it providing more than 21% of human caloric needs and up to 76% of the caloric diet of people in South East Asia (Zhao et al., 2020). Between 1994 and 2019, world rice production has increased, as shown in Figure 2.4 (FAOSTAT 2021). The United States Department of Agriculture (USDA) (USDA 2022) reports that primary rice production in 2020/2021 is 148.30 million tonnes (Mt) in China, in Africa, Nigeria with 5.04 Mt of production. Figure 2.5 shows rice and paddy production (average 1994-2019). Asia produces 90.6% of the world's rice, making it the world's largest producer (Bandumula 2018; FAOSTAT 2021). According to the OECD-FAO (2021), rice consumption is expected to increase significantly in Africa, while remaining stable or

decreasing in all other regions. Future demand for rice will be driven mainly by Africa, due to a combination of population growth, dietary changes and improved yields from existing land (intensification) (Van Oort et al., 2015). Cote d'Ivoire is one of the West Africa countries more depend of rice consumption. Rice paddy production is estimated to 1.09 Mt in 2020/2021. With climate change effect, the projected rice production is expect to decrease. This study assess the impact of climate change on farmers production and advise some alternative management practices to face this climate change challenges.

Table 2:2. Bias correction for precipitation and temperatures

Bias correction for precipitation	Bias correction for Temperature
linear scaling (LS)	linear scaling (LS)
Delta change correction (DCC)	Variance scaling (VARI)
Precipitation local intensity scaling	Delta change correction (DCC)
Power transformation (PT)	Distribution mapping (DM)
Distribution mapping (DM)	

Source : Yeboah et al. (2021)

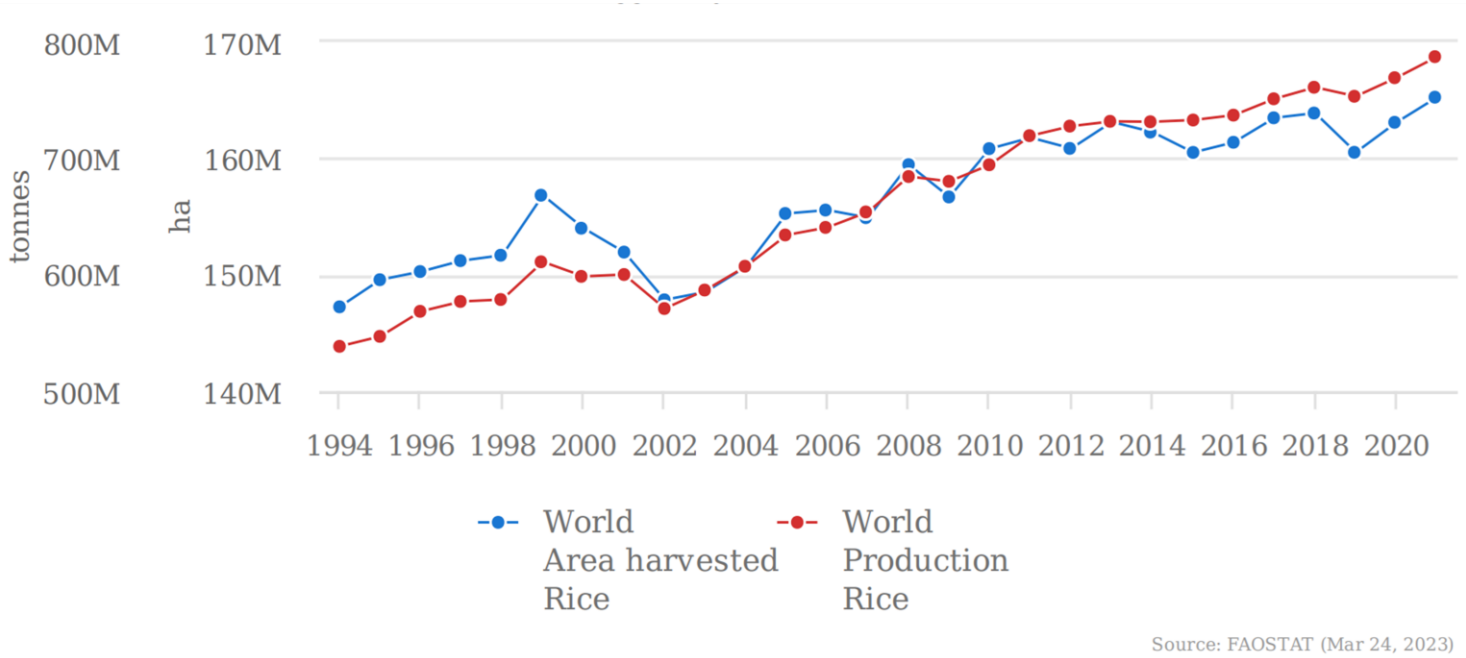

Figure 2.4. Production/yield quantities of rice paddy in the world (1994–2019) (FAOSTAT 2021)

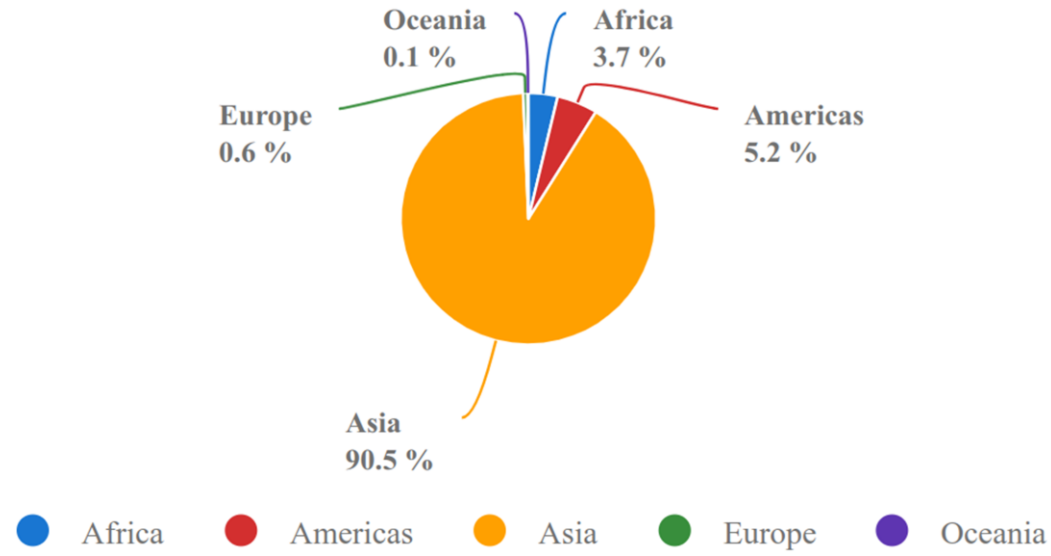

Figure 2.5. Production share of rice paddy by region (Average 1994–2019) (FAOSTAT 2021)

Chapter Three

3.0 Materials and Methods

3.1 Study area

The study area, West Africa (WA), lies roughly between longitudes 20∘ W and 20∘ E and latitudes 0◦ and 20◦ N (Figure 3.1). The region of the WA domain is divided into three climate zones: the Guinean (4◦N-8◦N), Sudanese (8◦N-11◦N) and Sahelian (11◦N-16◦N) (Abiodoun et al. 2012; Akinsanola et al. 2015). These three climate zones are spread over 11 countries (Benin, Burkina Faso, Côte d'Ivoire, Gambia, Ghana, Guinea, Mali, Niger, Senegal and Togo). Following a trend of decreasing rainfall from south to north, there is a progressive transition from forest, woodland, savanna woodland and savanna grassland to semi-desert grassland. The vegetation cover decreases with decreasing rainfall and the vegetation becomes smaller. The 10 selected eddy covariance sites (Table 3:1) cover two distinct ecological zones, 'Sahelian' and 'Sudanian', which differ mainly in the amount of rainfall and the length of the dry season. The Sudanian zone covers about 1.7 million km^2 and is cooler with 22-29 ºC and wetter with 600-1200 mm/year, and the Sahelian zone covers about 1.3 million km2 with average annual temperatures between 25 and 31 ºC and annual rainfall between 150 and 600 mm/year. The dry season lasts about four to seven months, with maximum monthly rainfall around August (Rahimi et al. 2021). The Guinean zone is characterised by a double rainy season under the intertropical discontinuity (ITD) effect (Quenum et al. 2019).

Data for model calibration and validation were collected at the AfricaRice Research Centre, 35 km from the city of Bouake North-West, where on-farm experiments were conducted in two irrigated rice systems in 22 fields under continuous flooding from March to June 2019. The 22 fields comprised two sites. 14 fields in Mbe (7◦53′58″ N, 5◦3′33″ W) for model calibration and 8 fields in Lokapli (7◦51′47″ N, 5◦3′35″ W) for

model validation. The two lowland rice sites are 5 km apart and are located in the Guinean savannah zone. The Mbe site and the Lokapli site are different in terms of fictional perspective and level of development. The Mbe site was poorly developed, while the Lokapli lowland site was moderately developed, with improved irrigation and drainage control on the plots. At both sites, surface water from the upstream dam was conveyed by gravity to the main and secondary canals through which water was directed to the fields selected for the study. In addition, small bunds were constructed to retain water and limit surface runoff (Dossou-Yovo and Saito, 2021). The climate of the study area is tropical with two dry seasons, the first from July to August and the second from November to March, and two rainy seasons from April to June and September to October (Dossou-Yovo and Saito, 2021). Bouake (Mbe and Lokapli sites) received an average minimum (min) and maximum (max) air temperature (T) and solar radiation (SolR) during the 2019 (Figure 3.2) growing season and within the 2015-2020 mid-range period.

3.2 Study datasets

3.2.1 Land surface model dataset

Observational data sets provide the atmospheric forcing required by the eCLM model. The Global Soil Wetness Project (GSWP) version 3 is the forcing provided by the model. For our study, the GSWP3 dataset has a spatial resolution of 0.5º x 0.5º and a temporal resolution of 3 hourly lateral boundary conditions.

Table 3:**2** shows the forcing data injected into the atmosphere. In the GSWP3 dataset, fluxes are provided at 3 hourly intervals. The data atmosphere model linearly interpolates these fields at the model time step. The land model is forced with the current atmospheric state at the given time step. In our study cases, 2000 to 2014 are the time periods provided to the model. Two parameters, the soil and vegetation data, characterise the land surface

flux data sets. The effect of different physical parameterisations on the coupling between the LCL and the land surface fluxes over the study area can be quantified from the simulation results (

Table 3:**2**).

The model results were validated against different sets of observed eddy covariance data from three sites, two in Ghana and one in Burkina Faso, and against ERA5-Land. ERA5-Land is a reanalysis dataset that provides a consistent view of land variable evolution over decades with improved resolution compared to ERA5. The resolution of the dataset is 0.1° x 0.1°, the native resolution is 9 km and the temporal resolution is monthly. The study area is West Africa. It covers the period 2000-2014.

3.2.2 Observational Data

Half-hourly observed sensible (*H*) and latent heat fluxes (LE) for 2013 were determined using eddy covariance (EC) technique, and meteorological data of air temperature (∘C), surface pressure (hPa), rainfall intensity (mm h^{-1}), incoming solar radiation (W m^{-2}), outgoing longwave radiation (W m^{-2}), specific humidity (g kg^{-1}) were also obtained from the EC site and were available between January and December 2013 (Quansah et al., 2017). We also estimate relative humidity as required by the method of Rompt (2017) for LCL expression. The observe data and ERA5 land data set were used to evaluate the simulation output.

For crop simulation scenarios, climate data include daily maximum and minimum temperature and daily precipitation from 1980 to 2020, collected by the AfricaRice station at Mbe, Bouake, Cote d'Ivoire.

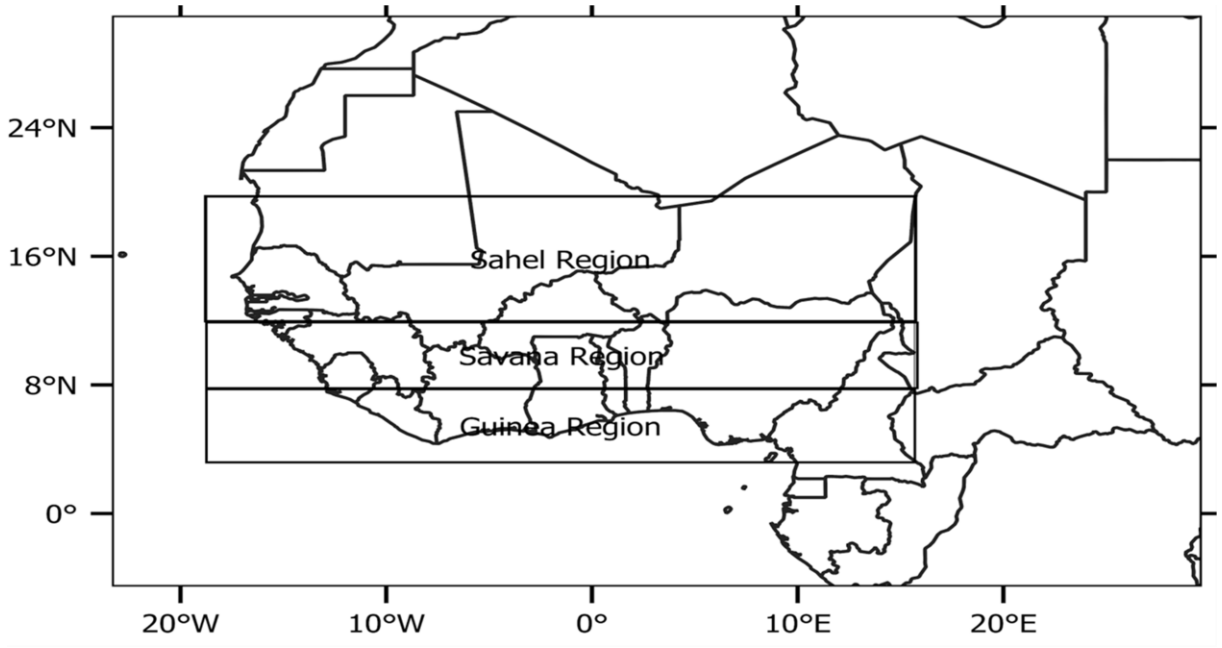

Figure 3.1. Study area highlighting the three climatic zones

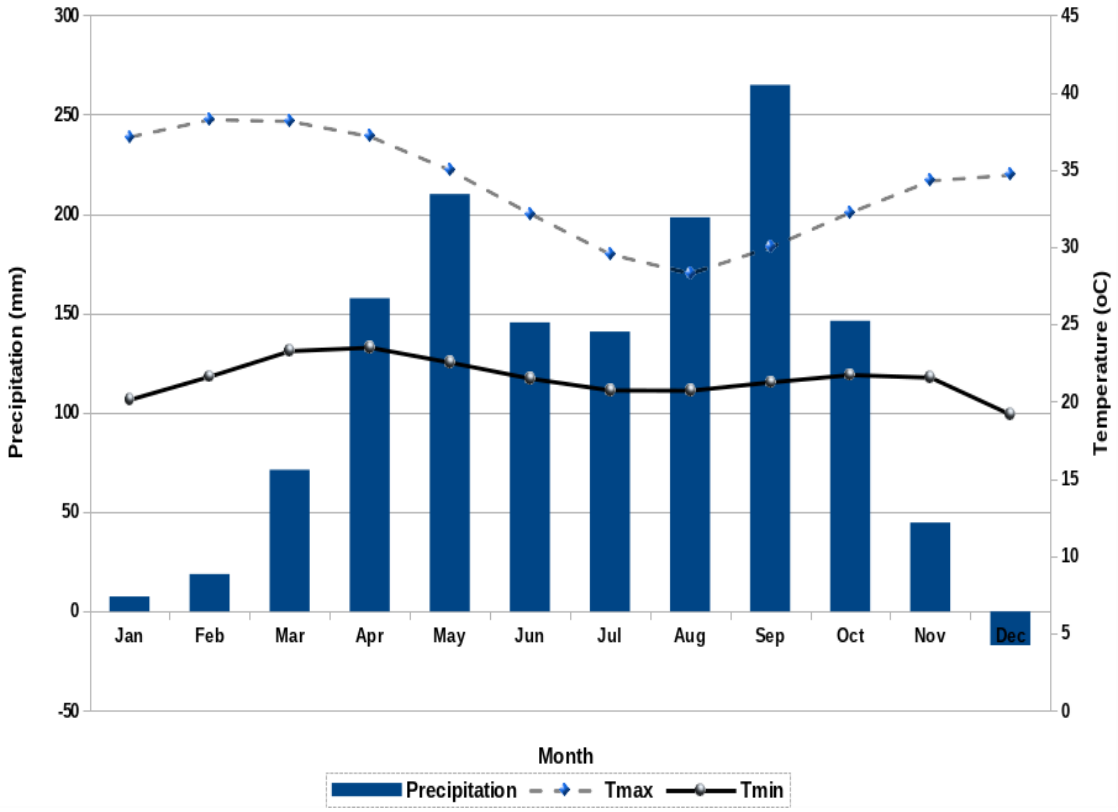

Figure 3.2. Long term average weather data during rice growing season (2019) and cumulated monthly rainfall and temperature in Mbe, Bouake, Côte d'Ivoire

Table 3:1. Characteristic of the selected site modify and adopted from Rahimi et al (2021)

EC Site name	Country	Lat; Lon	Zone	Ecosystem	Type of land cover
Agoufou	Mali	15.34◦N, 01.48◦ W	Sahelian, grass dominated	Open grassland with sparse shrubs	Grass, grazed
Kelma	Mali	15.22◦ N, 01.57◦ W	Sahelian, grass dominated	Seasonally flooded open woodland	Trees and grass
Wankama	Niger	13.65◦ N, 02.63◦ E	Sahelian, grass dominated	Fallow land with bushes	Grass
Bellefoungou	Benin	9.79◦ N, 01.72◦ E	Sudanian tree–shrub, dominated	Protected woodland	Trees and grass
Bontioli	Burkina Faso	10.88◦N, 03.07◦ W	Sudanian tree–shrub, dominated	Grassland/Shrubland	Grass

Kayoro	Ghana	10.92◦ N, 01.32◦ W	Sudanian, cultivated	Cultivated land	Agriculture (sorghum, peanut, millet)
Nalohou	Benin	9.74◦ N, 01.61◦ E	Sudanian, cultivated	Cultivated savanna	Agriculture (maize, Cassava, sorghum, peanut)
Nazinga	Burkina Faso	11.15◦ N, 01.58◦ W	Sudanian, tree–shrub dominated	Pristine woody savanna	Trees and grass
Niakhar	Senegal	14.50◦ N, 16.45◦ W	Sudanian, cultivated	Cultivated land	Agriculture (peanut, millet)
Sumbrungu	Ghana	10.85◦ N, 00.92◦ W	Sudanian, grass dominated	Savanna grassland	Grass, grazed

Table **3:2**. Land and meteorological forcing used for the historical simulation of GSWP3

Variable and units	Description
RH (%)	atmospheric relative humidity
THBOT (ºC)	atmospheric air potential temperature
QBOT (kg/kg)	atmospheric specific humidity
Psurf (Pa)	atmospheric pressure at surface
FSH_G (W/m^2)	sensible heat from ground
EFLX_LH_TOT (W/m^2)	total latent heat flux
Rain (mm/s)	atmospheric rain, after rain
FSDS (W/m^2)	atmospheric incident solar radiation
TG (ºC)	ground temperature
TSA (ºC)	2m air temperature
TSOI (ºC)	soil temperature
Tair (ºC)	atmospheric air temperature

Source : Compo et al. (2011)

3.3 Methods

3.3.1 Couple land surface and LCL processing

3.3.1.1 Lifting Condensation Level (LCL) height expression

The model used in this study is the re-engineered Community Land Model (eCLM). eCLM is a land component model of the Community Land Model Version 5 (CLM5). eCLM has the same modelling capabilities as CLM5. The latest updated version of the CLM has incorporated some changes such as soil and plant hydrology, snow density, river modelling, carbon and nitrogen cycling and coupling, and crop modelling with a more comprehensive and explicit representation of land use and land cover change. In addition to its power, eCLM uses a much "leaner" script to build and run a model. What makes eCLM better and more useful is the ability of users to design their own workflows (i.e. write their own scripts) for building and running a model, as opposed to CLM5 which uses more sophisticated tools to do the same job. eCLM models include mechanistic formulations of physical, biophysical and biogeochemical processes that simulate land surface radiation, heat, water and carbon fluxes in response to climate forcing. However, the biophysical processes of vegetation interact strongly with the land component. The ECLM of CLM5 describes the interactive physical, chemical and biological processes between the terrestrial ecosystem and the climate. A nested subgrid architecture is used to represent the spatial variability of the land surface, including five land units (glacier, lake, urban, vegetation and crop), soil/snow columns and 16 plant functional types (PFTs). Fifteen soil layers and up to five snow layers are defined. Biogeophysical and biogeochemical mechanisms in the terrestrial ecosystem are considered.

eCLM features a hierarchical data structure in each grid cell, and spatial land surface

heterogeneity in eCLM is compose of different land unites, and land unit can have different columns and each columns a different or multiple plant functional types (PFTs). In our study, we consider, three land unit (Vegetation, crop and default PFT). Default is defined as a composed of different classis (built-up/urban, vegetation, cropland, tree cover, mangroves, bare soil, shrubland, grassland, wetland).

Vegetated surfaces are composed of up to 15 possible plant functional types (PFTs), including bare ground. On the surface dataset, vegetation is referenced to the percentage natural vegetation index (PCT_NAT_VEG). Each PFT type differs in leaf and stem optical properties, which control reflection, transmission and uptake of solar radiation; root allocation parameters, which control soil water uptake; aerodynamic properties, which control resistance to heat, moisture and kinetic energy transfer; and photosynthetic properties, which control stomatal resistance, photosynthesis and transpiration.

The crop functional type is represented by the crop percentage (PCT_CROP). To allow crops to coexist with natural vegetation in a grid cell, the vegetated land unit is divided into a natural vegetation land unit and a managed crop land unit.The eLCM model includes eight actively managed crop types (PFTs) (temperate soybean, tropical soybean, temperate maize, tropical maize, spring wheat, cotton, rice and sugarcane), which were selected based on the AgroIBIS algorithms (Dirmeyer 2015; Levis et al., 2016). However, the default PFTs that included vegetation, crop, and urban PFTs in the CLM included a managed irrigated and non-irrigated crop C3, which is considered to be grass. The default list of crop types includes twenty-three non-functional crop types that are not associated with the required active management parameters. They are simulated using the parameters of the closest crop types similar to the PFTs required to maintain close phenological parameters based on temperature cut-offs.

To compare the lifting condensation level (LCL) high over the different land cover

changes (default, vegetation and crop land units) and to assess the impact on ABL and precipitation event over West Africa, an algorithm was written to run the surface data set used for the model simulation. The script written to compute each case is made to maintain urban land unit (PCT_Urban) constant for the three cases while vegetation percentage (PCT_NAT_VEG) or forest are made to be zero percent at each iteration to obtain vegetation case or cropland units (PCT_CROP) are made to be zero percent at each iteration to obtain crop case during eCLM simulation over West Africa. The default case (PCT_DEFAULT) is defined by leaving each land unit as default. This means that the grid cell is equal to the sum of the urban and the specific land unit.

$$G = PCT\_URBAN + PCT\_NAT\_VEG + PCT\_CROP = 100\% \quad \text{(Eq 3.1)}$$

$$G = PCT\_URBAN + 0 + PCT\_CROP = 100\% \quad \text{(Eq 3.2)}$$

$$G = PCT\_URBAN + PCT\_NAT\_VEG + 0 = 100\% \quad \text{(Eq 3.3)}$$

where G is the land unit grid cell for the specific case, Crop takes the value zero when running the vegetation land cover surface dataset cases, and vegetation is assigned the value zero when running the crop land cover dataset cases.

3.3.1.2 eCLM Model Simulation

A 30-year historical forcing dataset (1979-2010) was simulated by both CLM5 and eCLM to assess the robustness of the model to adequately simulate the land-atmosphere interaction. The simulation was performed based on the existing land use, land cover component or plant functional type (PFT) in the CLM5 model by running the simulation with eCML. Firstly, we evaluated the output of CML5 and eCLM (Table 3:4). Secondly, we analyse the relationship between the lifting condensation level (LCL) height and the land surface fluxes (RH, SH, LH and SR). The analysis will help to accurately constrain

the atmosphere interaction simulations. The results from both the eCLM and CLM5 models show a good correlation with a correlation coefficient of 1 and PBIAS of -0.1 and 0.6 respectively at Kayero in Ghana and Nazinga in Burkina Faso, two sites randomly selected for model evaluation.

3.3.1.3 LCL Height calculation

The lifting condensation level (LCL), i.e. the height of the cumulus cloud base, is closely related to the dew point depression. However, the exact expression of the LCL height has been a challenge for researchers over the last century. From the first equation given by Espy (1836, p. 244) to Lawrence (2005) with a diagnosis of the LCL height consistency, the air surface temperature at 2 m and the surface dew point temperature have been used. For this study, we used the exact expression of the LCL of Romps (2017) with the analytical saturation vapour pressure.

$$z_{LCL}=z+\frac{C_{\rho m}}{g}(T+T_{LCL}) \quad \text{(Eq3.4);}$$

$$T_{LCL}=c[W-(RH_l^{1\alpha}ce^{c})]^{-1}T, \quad \text{(Eq3.5)}$$

$$P_{LCL}=P(\frac{T_{LCL}}{T})^{c_{\rho m}/R_m} \quad \text{(Eq3.6);}$$

$$\alpha=\frac{c_{\rho m}}{R_m}+\frac{c_{\upsilon l}-c_{\rho \upsilon}}{R_\upsilon} \quad \text{(Eq3.7);}$$

$$b=-\frac{E_{0\upsilon}-(c_{\upsilon\upsilon}-c_{\upsilon l})T_{trip}}{R_\upsilon T} \quad \text{(Eq3.8);}$$

$$c=b/\alpha \quad \text{(Eq3.9)}$$

Where z_{LCL} is the lifting condensation level (LCL) height, z is the parcel's height in Eq1, T is the absolut temperature, $RH_l$is the parcel's relative humidity with respect to the

liquide, which range from 0 to 1, $c_{\rho m}/g$is the inverse of the dry adiabatic lapse rate with $g = 9{,}81\ ms^{-2}$ the gravitational acceleration and $c_{\rho m}$ is the specific heat capacity at constant pressure, R_m is the air parcel's specific gas constant. The subscript m denotes that these are the appropriate values for moist air. R_v is the specific gas constant for water vapor, c_{vv} is the specific heat capacity of water vapor at constant volume, $c_{\rho\upsilon}=c_{\upsilon\upsilon}+R_\upsilon$is the specific heat capacity of water vapor at constant pressure, c_{vl} is the specific heat capacity of liquid water, p_{trip} is the triple point vapor pressure, T_{trip} is the triple-point temperature, and E_{0v} is the difference in specific internal energy between water vapor and liquid at the triple point.

The LCL height level was calculated based on the three hourly data to identify the exact parcel height of LCL and the exact correlation between each land cover unit on LCL height. The couple between land surface fluxes and lifting condensation level height was presented to identify the correlation of each land surface flux from each land unit on LCL height. The Sahara region in northern West Africa, which is considered to be the hottest desert on Earth, was excluded from our simulation post-processing. This was done due to its arid conditions and mineral dust, which can significantly influence cloud formation and consequently atmospheric circulation, rainfall and storm formation, and land surface conditions (Pausata 2021). To avoid these effects and to assess the effect of the urban land cover condition, vegetation (pristine vegetation/forest) and crop land cover on the coupling between land surface and LCL, the Sahara region was removed.

3.3.2 Climate change datasets and emissions scenarios

3.3.2.1 Future climate data and climate scenarios

While many climate change projections exist, we used future climate data (precipitation and minimum and maximum temperatures) from the Coordinated Regional Climate Downscaling Experiment (CORDEX) climate simulation experiments (Giorgi et al. 2009) to better understand and estimate future climate. Four forcing global climate models (GCMs), including the Max Planck Institute for Meteorology Earth System Model version 1.2 (MPI-ESM1.2) (Mauritsen et al. 2019), the Centre National de Recherches Météorologiques (CNRM-CM5) (Voldoire et al. 2013), the Hadley Centre Global Environmental Model Earth System (HadGEM2 -ES) (Jones et al. 2011), and the GFDL NOAA Earth System Models (ESMs) (Dunne et al., 2020). In addition, we consider two Representative Concentration Pathways (RCPs) emission scenarios, such as RCPs (4.5 and 8.5). The RCM and RCP considered in this study were used in the Fifth Assessment Report of the Intergovernmental Panel on Climate Changes (AR5, IPCC 2014). The future scenarios were divided into three different time frames with 30year intervals, except for the first time window, which includes 2010 to 2040 (2020s), 2041 to 2070 (2050s) and 2071 to 2100 (2080s). RCP4.5 is a medium emissions scenario with CO2 equivalent concentrations between 580 and 720 ppm in 2100, while RCP8.5 is considered a high emissions scenario with CO2 equivalent concentrations above 1000 ppm in 2100 (Zhang et al., 2018).

3.3.2.2 Bias Correction procedure

To perform the bias correction of the climate data, the Climate Model data for hydrological modelling (CMhyd) tool was used in this study (Rathjens et al., 2016; Yeboah et al. 2022). CMHyd pre-processes the data before bias correction. The observed and modelled historical data are then compared to assess performance. Delays for observed and historical data are then superimposed. For this study, eight correction

methods available in the CMhyd tool, including linear scaling (multiplicative and additive), delta change correction (multiplicative and additive), local intensity scaling of precipitation, power transformation of precipitation, variance scaling of temperature, and distribution mapping of precipitation and temperature, were analysed and the output of the bias correction was used for the crop simulation.

3.3.2.3 Change analysis and extreme indices

The observed time series, defined as the baseline periods (1980-2005), were compared with the ensemble mean of the 4 model variables (precipitation, minimum and maximum temperature). Absolute changes in precipitation (equations 3.9 to 3.14) and relative changes in temperature were obtained for the periods 2020, 2050 and 2080 (Yeboah et al. 2022).

$\Delta 2020 \quad \frac{(\theta_{2020s}-\theta_{base}) \times 100}{\theta_{base}}$ (Eq3.9) $\quad \Delta 2050 \quad \frac{(\theta_{2050s} -\theta_{base}) \times 100}{\theta_{base}}$ Eq3.10

$\Delta 2080 \quad \frac{(\theta_{2080s} -\theta_{base}) \times 100}{\theta_{base}}$ (Eq3.11), $\quad \Delta 2020 \quad (\theta_{2020s} -\theta_{base})$ (Eq3.12),

$\Delta 2050 \quad (\theta_{2050s} -\theta_{base})$ (Eq3.13), $\quad \Delta 2080 \quad (\theta_{2080s} -\theta_{base})$ (Eq3.14).

Where Δ is the relative or absolute change, θ represents either precipitation or minimum and maximum temperature and is based on the reference baseline periods (1980-2005). The observed positive and negative changes are due to the increase and decrease of the future periods (Yeboah et al. 2022).

3.3.2.4 Climate indices

This section presents some climate index methods used in the present work. For the extreme indices, four indices of observed and future climate extremes are taken into

account, including the Standardised Rainfall Index, which measures potential future droughts, the total annual rainfall contribution of extremely wet days (R99pTOT), the number of hot days (TX90p) and the number of warm nights (TN90p). ClimPACT2 software (Alexander and Herold, 2016) was used to calculate the indices of extremes. Table 5 provides a description of these indices.

3.3.2.5 Evaluation of Bias-Correction Methods

Different bias correction methods are used for precipitation and temperature, as mentioned above. Frequency and time series statistics are used to evaluate the efficiency of each bias correction method. We used four time series-based statistics: coefficient of determination (R^2), Nash-Sutcliffe coefficient (NSE), root mean square error (RMSE) and percentage bias (PBIAS) to assess the accuracy of the bias-corrected model. We also used mean, median, standard deviation (STD), coefficient of variation (CV) and 10th and 90th percentiles (X10, X90) as frequency-based statistics for both precipitation and temperature (Table 3:3). For simplicity, only the results for March, corresponding to the dry season, and August, corresponding to the wet season, are presented. The RMSE was used as a goodness of fit technique to indicate the standard deviation of the model in simulating the observed data. The model performs better when the RMSE is smaller. The NSE ranges from - ∞ to 1, with NSE values $\geq$ 0.5 being satisfactory and NSE values $\geq$ 0.7 being a very good fit (Nash and Sutcliffe, 1970). The PBIAS was used to assess whether the model underestimated or overestimated the observed data. The model becomes more accurate as the PBIAS approaches 0.

Table **3:3**. Temperature and Rainfall indices, definition used in this study: TX and TN are temperature daily maximum and daily minimum respectively, and RR the daily precipitation

Climate Indices	Names	Definitions	Units
R99pTOT	Contribution from extremely wet days	100 ∗ r99p / PCP	%
TX90p	Amount of hot days	Percentage of days when TMAX > 90th percentile	%
TN90p	Amount of warm nights	Percentage of days when TMIN > 90th percentile	%
SPI	Standardized Precipitation Index	Measure of "drought " using the Standardised Precipitation Index on time scales 12 months.	unitles s

Source : http://www.wmo.int/pages/prog/wcp/ccl/opace/opace4/expertteam.php. Date of access (January 2022)

3.3.3 Crop simulation processing

3.3.3.1 APSIM-ORYZA for simulating adequately climate change impact on rice production

For this study, APSIM version 7.10 was used to parameterise the APSIM-Oryza module for the rice growing season on the 22 farmers' fields in 2019 for the rice variety most used by the farmers (WITA9).The rice module in APSIM-Oryza was used to simulate rice growth and yield under potential production, continuous flood water management and limited fertiliser simulation over the study area in Cote d'Ivoire (Gaydon et al., 2017b). The APSIM-Oryza simulation must interact with other APSIM components/modules such as soil water, surface organic matter, irrigation, fertiliser and crop management to simulate crop growth and yield. Rice growth, development (stage) and yield parameters are used to parameterise APSIM-Oryza for yield assessment.

The Soil Water Model (SoilWat) module in APSIM is one of the two soil water components available in APSIM and was used for model calibration. A daily water balance was run in APSIM. Drainage and runoff, dry and wet season data, soil albedo and soil water content (SWCON) were included in the modelling process. The soil parameters obtained are shown in Table 3:5. In APSIM-Oryza, the soil nitrogen (SoilN) model was used to simulate soil mineralisation, control, denitrification and urea hydrolysis. The simulated soil organic matter (SOM) module is divided into different sub-modules consisting of organic carbon (OC), the rapidly decomposing organic matter (BIOM), an intermediate (HUM) and the stable organic decomposition pool (INERT). The rapidly decomposing pool (FBIOM) is a separate sub-module that includes previous crop roots and crop residues if they have been incorporated into the soil by tillage.

Table 3:4 Validation of the robustness and accurate of eCLM Vs CLM5

Site Name	R2	PBIAS	NSE	RMSE
Kayoro	1	-0.1	0.994	80.10
Naziga	1	0.6	0.996	69.59

Table **3:5**. Soil properties for experiments conducted in the two sites and used in simulation studies

Soil Properties	Depth in cm (Lokakpli)			Depth in cm (Mbe)		
	0-10	10-20	20-30	0-10	10-20	20-30
EC (dS m-1)	0.2	0.3	0.3	0.23	0.2	0.2
pH	5.99	6.22	6.97	5.64	5.75	5.96
N (%)	0.039	0.037	0.027	0.039	0.037	0.027
Nitrate-N (mg kg-1)	38	38	38	38	38	38
P (mg kg-1)	15	15	15	15	15	15
K (mg kg-1)	14	14	14	14	14	14
Organic C (%)	3.62	2.26	1.51	2.82	3.02	2
Silt (%)	11	12	7	9	24	18
Sand (%)	46	64	77	56	49	53
Clay (%)	41	24	16	35	27	29
BD (g cm-3)	1.5	2	2	1.230	1.340	1.310
LL (cm3 cm-3)	0.145	0.232	0.29	0.275	0.243	0.282
Soil texture	very humusy, silty texture	very humusy, silty-sandy texture	humus-rich, silty-clay texture	Humus, with clay-silt texture	low ahumus, clay-silt texture	non-humus, clay texture
DUL (cm3 cm-3)	0.313	0.299	0.334	0.4	0.4	0.4
SW (cm3 cm-3)	0.312	0.312	0.324	0.46	0.39	0.38
Ks (cm h-1)	0.004	0.002	0.003	2.51	1.16	1.87

Ks=Saturated hydraulic conductivity; EC= Electrical conductivity, LL: Soil lower limit (Wilting point) and DUL: Soil drain upper limit (Field Capacity), P = phosphorus, K = Potassium, N = nitrogen, OC = organic carbon, BD = Bulk Density, SW = soil water .

3.3.3.2 Crop phenology

Phenological parameters were derived from the time of plant establishment to flowering and physiological maturity. The phenological parameters used were: development rate of juvenile stage (DVRJ, $^{o}Cd^{-1}$), development rate of photoperiod sensitive stage (DVRI, $^{o}Cd^{-1}$), development rate of panicle stage (DVRP, $^{o}Cd^{-1}$) and development rate of reproductive stage (DVRR, $^{o}Cd^{-1}$) as summarised in Table 8. Rice yield in APSIM-Oryza is represented by output parameters such as total above-ground dry matter (WAGT, kg/ha), storage organ dry weight (WSO) and raw rice dry weight (WRR, kg/ha). In this research study, 10 parameters were considered out of the 20 basically considered in the ORYZA initiative file (Tan et al. 2017). The description and variation of the changes of these parameters are presented in Table 3:6. Most of the parameters not listed in the table out of the 20 were obtained from the default values in the model file, especially leaf area and partitioning factors.

3.3.3.3 Soil data

Soil characteristics were collected from the experimental plots at both sites (Mbe and Lokapli). Soil data samples were collected prior to experimental planting. Per field, 12 single auger samples from 0-30 cm depth were mixed, air dried and sieved (2 mm) to determine sand and clay content, pH and soil organic carbon. A pH meter (pH 2700; Eutech Instruments Pte Ltd) was used to measure pH. Soil organic carbon was determined by chronic acid digestion. Additional sol data and soil water content required by the APSIM-Oryza model were calculated using the formula of (Saxton and Rawls, 2006) and the methods of (Burk and Dalgliesh, 2012).

APSIM-Oryza was configured using the Soil Water Management module tool. The parameterisation of the soil water module uses sub-modules such as Crop Lower Limit

(CLL) and Drained Upper Limit (DUL), which were calculated based on sand, clay and bulk density (BD) values collected in the field. CLL was calculated using clay sand and soil depth (Eq3.15), while DUL was calculated using sand, clay and bulk density (Eq3.16) (Burk and Dalgliesh, 2012). Soil saturation (SAT) data are difficult to obtain and generally have to be calculated from total soil porosity (PO), determined by soil bulk density measurement, and rock density, assumed to be 2.65. The SAT is calculated by subtracting the assumed percentage of entrapped air in the rock density for the specific texture class (3% for heavy clay soils, 7% for sandy soils and 0.5 for loam soils) [Eq3.17; Dalgliesh and Foale, 1998]. Saturated hydraulic conductivity (Ks) was calculated using the equation of Saxton and Rawls, (2006) adapted from Rawls et al. (1998) and Campbell (1974). The Ks equation is a power function of the moisture held at low tension in the larger pores that conduct water most effectively (Eq3.18). The value of λ (Eq3.19) is the inverse of the slope of the exponential tension moisture curve B (Eq3.20).

CLL = 0.0826 + 0.00255(Clay) – 0.000713(Sand) + 0.000382(Depth); (Eq3.15)

DUL = 0.453 + 0.00245(Clay) – 0.00144(Sand) – 0.123(BD); (Eq3.16)

PO-SAT = e and PO = (1-BD/2.65) *100; then, SAT = [(1-BD/2.65) *100] – e (Eq3.17)

Where PO (volumetric water is in %), e is the specific textural class, clay and sand are weighted in % and soil depth in cm.

$$Ks = 1930(\theta_s| - \theta_{33})^{(3-\lambda)} \quad \text{(Eq3.18)}$$

$$\lambda = \frac{1}{B} \quad \text{(Eq3.19)}$$

$$B = [\ln(1500) - \ln(33)]/[\ln(\theta_{33}) - \ln(\theta_{1500})] \quad \text{(Eq3.20)}$$

Where Ks is the saturated hydraulic conductivity; is the Saturated moisture (0 kPa) in %v; 1500 kPa moisture in %v; λ is the Slope of logarithmic tension-moisture curve; B is the

Coefficients of moisture-tension; is the 33 kPa moisture, normal density in %v.

3.3.3.4 Crop management

The WITA9 rice variety was grown by the farmers selected for this on-farm trial. The selected rice varieties and information collected from farmers were grown at two sites (Mbe and Lokakpli) with similar soil characteristics, irrigation management system and fertiliser application, but with different dates of sowing, fertiliser application and harvest. Data were collected during weekly field visits followed by a field survey to collect information on agricultural management practices, including irrigation amount and timing, fertiliser amount and timing, planting densities, land preparation (tillage, straw and management), crop establishment, frequency and dates of weeding, and seedling age. A standard agricultural management practice was established by the farmers in the two different sites where data were collected. The irrigation method was maintained as continuous flooding with a total maximum of 453 mm irrigation and 515 mm rainfall per growing season received by the crop in Mbe and Lokapkli, respectively. All farmers applied 144 kg/ha nitrogen in 2019.

3.3.3.5 Data collection

Rice field trials were conducted in Mbe and Lokapli in 2019. These field trials were conducted to assess farmers' farming practices, yield potential and variety stability. The WITA9 rice variety was grown by the farmers selected for this on-farm trial. The selected rice varieties and information collected from farmers were grown at two independent sites (Mbe and Lokapli) with similar soil characteristics, irrigation management system and fertiliser application, but with different sowing, fertiliser application and harvesting dates.

Data were collected during weekly field visits followed by a field survey to collect information on agricultural management practices, including irrigation amount and timing, fertiliser amount and timing, planting densities, land preparation (tillage, straw and management), crop establishment, frequency and dates of weeding, seedling age. A standard agricultural management practice was established by the farmers in the two different sites where data were collected. The irrigation method was maintained as continuous flooding with a total maximum of 453 mm irrigation and 515 mm rainfall per growing season received by the crop in Mbe and Lokapkli, respectively. All farmers applied 144 kg/ha nitrogen in 2019.

3.3.3.6 Model evaluation

The model was evaluated in two steps. The first was to adjust the empirical parameters by repeatedly comparing simulated and observed data with field datasets (calibration). The second step is to test the calibrated model against independent datasets collected from the field experiment designed to assess model performance through a range of seasons, practices and environments (validation).

3.3.3.6.1 Model Setup and Calibration Protocol

Model calibration was developed to produce a model capable of simulating cropping system performance. Several steps were used to calibrate APSIM-Oryza. In the first step, climate data were provided in the MET module, followed by soil information parameterised based on site information, soil properties and condition, and rice management. In the second step, field measurement data were incorporated into the platform to allow APSIM to be used for graphical and statistical purposes. Calibration of APSIM involved several steps: (i) we provided climate, soil and management data to the model; (ii) we incorporated the measurement data (Table 3:6) into the model; next, (iii)

Table **3:6**. The parameter description and variance in the APSIM-ORYZA model

Parameters	Description	Unit	Variance		Base value
			Min	Max	
DVRJ	Development rate in juvenile phase	$(°C\ Day)^{-1}$	0.0007	0.0013	0.0001
DVRI	Development rate in photoperiod-sensitive phase	$(°C\ Day)^{-1}$	0.000525	0.000975	0.00075
DVRP	Development rate in panicle development	$(°C\ day)^{-1}$	0.000595	0.001105	0.00085
DVRR	Development rate in reproductive phase	$(°C\ day)^{-1}$	0.0014	0.0026	0.002
RGRLMX	Maximum relative growth rate of leaf area	$(°C\ day)^{-1}$	0.00595	0.01105	0.0085
RGRLMN	Minimum relative growth rate of leaf area	$(°C\ day)^{-1}$	0.0028	0.0052	0.004
WGRMX	Maximum individual grain weight	kg/grain	0.0000175	0.0000175	0.00002 5
Outputs					
WRR	Crop yield	kg/ha			
WAGT	Total aboveground dry matter	kg/ha			
WSO	Dry weight of storage organs	kg/ha			

Table **3:7**. : WITA9 rice variety phenological parameters and their values used for model calibration

Parameters	WITA9 variances	
	Minimum	Maximum
Development rate in juvenile phase	0.000523	0.000673
Development rate in photoperiod-sensitive phase	0.000590	0.000758
Development rate in panicle development	0.000630	0.000730
Development rate in reproductive phase	0.001100	0.001250
Maximum relative growth rate of leaf area	0.00600	0.00860
Minimum relative growth rate of leaf area	0.0020	0.0040
Maximum relative growth rate of leaf area (RGRLMX)	0.00400	0.00650
Minimum relative growth rate of leaf area (RGRLMN)	0.0020	0.0040

we incorporated the rice initiative (Oryza) into the model and inserted our own rice variety (WITA9) into the model to best simulate the observed value and (iv) Several aspects of the model were tracked and evaluated : crop phenology, soil water, soil N, irrigation, rice transplanting, pond depth, fertiliser, biomass production and grain yield. APSIM-Oryza requires daily values of rainfall, maximum and minimum temperature and solar radiation. In addition, it needs measured soil physical parameters for different soil strata, including bulk density, saturated water level, field capacity and wilting point. The SWCON factor is the amount of water that exceeds the capacity of the field and drains into the next layer in a day. Soil parameters required for APSIM-Oryza include soil pH, organic carbon, initial mineral N. The saturated hydraulic conductivity (Ks) was estimated using Saxton and Rawls, (2006) formula. The parameters that were not directly measured had to be calculated using Saxton and Rawls, (2006) and calibrated in a repetitive manner.

Soil organic matter (SOM) mineralization capacity varies between location and is function of soil biota ecology and is characterized in APSIM-Oryza with Fbiom and Finert as describe in our last section (Gaydon et al., 2017). The values of Fbiom and Finert were progressively modified within physically plausible limits (Probert et al., 1998). This was done until the simulated N supply in the N-free treatments allowed a simulation that approximated observed crop yields (Gaydon et al., 2017). Concerning crop phenology, Oryza initiative model was parameterized base on the rice variety (Table 3:7) used and incorporated in the APSIM model and were calibrated by varying the Oryza initiative model until the modelled phenology dates matched the observed dates. The same rice variety was used by farmers over both sites. The main dates selected for APSIM-Oryza phenological parameterization are those related to sowing, transplanting, maximum tillering, panicle initiation, flowering and physiological maturity. Soil water

dynamics and rice water uptake were used to calibrate rice rooting parameters and water lower limits (LL) which is function of soil layer. Therefore, the model calibration was completed when a good value for the evaluated variables was found between the field measurement and the predicted values. In the context of this study, the data required for model parameterisation were collected from 14 farmers (Mbe site), of which 3, 7 and 4 farms were located very close, in the middle and close to the irrigation system, respectively.

3.3.3.6.2 Models' validation

Model validation is the most important phase of model verification (Andarzian et al., 2011). Model validation comprises comparison between the observed data (field measurement) and the output generated by the model (Ahmed et al., 2016). The term 'model robustness' refers to the model's reliability under a range of experimental conditions (Bellocchi et al., 2010; Confalonieri et al., 2010b). In our case study, after model parameterised and calibration was performed and result is in agreement with grain yield in calibration experimental site, the parameterised and calibrated model was used to simulated the second experimental site (Lokakpli) with experimental dataset collected, as means of checking the veracity of the model. These simulated/observed validation data sets were used to evaluate the performance of the model from different perspectives (Gaydon et al., 2017). This validation was performed to evaluate i) the ability of APSIM-Oryza to robustly simulate rice phenology for sowing date trials, ii) simulate rice sequences by examining residual error as a function of crop progression, iii) soil water and soil carbon dynamics in conjunction with crop production, iv) system water balance components and irrigation water use, and v) CO_2 response.

3.3.3.6.3 Statistical Validation

Several statistical indices including the coefficient of determination R^2, the agreement index (D-index) from (Willmott, 1981; Willmott et al., 1982), the absolute root mean square error (RMSE), the normalised root mean square error (%RMSE) from (Loague and Green, 1991) and the model efficiency (ME) were used to check the agreement between observed and simulated values. In addition, we determined the slope (α) and intercept (β) of the linear regression between the simulated and measured values, which were used to compare the measured and simulated grain yield for rice cultivation among the different selected farmers. Model performance was also evaluated using Student's t-test of means assuming unequal variance P(t).

$$D\text{ - index} = 1 - \frac{\sum_{i=1}^{n}\left[\left(p_i - \bar{O}\right) - \left(p_i - \bar{O}\right)^2\right]}{\sum_{i=1}^{n}\left[\left(\left|p_i - \bar{O}\right|\right) - \left(\left|p_i - \bar{O}\right|\right)^2\right]}$$

$$RMSE = \left[\sum_{i=1}^{n}\frac{(Pi - Oi)^2}{n}\right]^{0.5}$$

$$\%RMSE = \left[\sum_{i=1}^{n}\frac{(Pi - Oi)^2}{n}\right]^{0.5} x \frac{100}{O}$$

$$ME = 1 - \frac{\sum_{i=1}^{n}(Pi - Oi)^2}{\sum_{i=1}^{n}(Oi - O)^2}$$

where Oi and Pi are the observed and simulated values for all variables considered, and O is the mean value of the observed variable. The normalised RMSE, also called N-RMSE, gives a percentage (%) measure of the relative difference between the simulated and observed data. The simulation is considered excellent if the normalised RMSE is less than 10%, good if the N-RMSE is greater than 10% and less than 20%, fair if the N-RMSE is greater than 20% and less than 30% and poor if the N-RMSE is greater than 30% (Jamieson et al., 1991).

3.3.4 Alternative management practices to mitigate climate change impacts on rice yield

The achievement of this section was done with the simulation of different alternative scenarios. Seven alternatives have been kept for assessing their impact on rice yield in order to mitigate climate change effect.

3.3.4.1 Scenario 1: Crop establishment

APSIM-ORYZA was used to parameterize the model with two crop establishment methods such as direct seeding and translated method. This is to assess the base on the historical climatic data the potential yield of WITA9 over the study area by comparing the output in order to identify the best adapted method to mitigate climate change impact with the result of rice yield improvement. Factor mode in APSIM was activated by keeping the others parameters per default and set the model with two alternative, “direct seeding” or “transplantation method”(Table 3:8).

3.3.4.2 Scenario 2: Soil Organic Matter (SOM) application

Organic matter has long been used to improve soil productivity and provide plant nutrients. Different types of organic matter are used in agriculture, but unfortunately most of these materials remain under-utilised, especially in developing countries in sub-Saharan Africa.

The manure scenario is well developed in the APSIM model using factor parameters. Manure organic matter is defined in terms of its parameters such as mass, type and its inorganic and organic nitrogen and carbon content (Akponikpè et al. 2010). For this scenario, a constant potential rate is specified as input in the APSIM factor windows and was applied 15 days after transplanting. The reference fertiliser application for setting the

model scenarios is "no application". The potential fertiliser application rates set in the model are 30, 60 and 100 kg N/ha by keeping the moisture, temperature and C:N ratio of the fertiliser at basal rates.

3.3.4.3 Scenario 3: Mulch amount application

In farmers' production systems, weeds are a major constraint on crop yields in sub-Saharan Africa (SSA), especially for smallholder farmers who are financially unable to purchase herbicides. It has been argued that the use of herbicides is detrimental to the environment and soil quality. However, the literature argues that the practice of mulching with crop residues suppresses weeds and is a best alternative management practice to mitigate the effects of climate change and increase rice yield. For this scenario, different ranges of mulch application of 0, 5 and 10 Mg dry matter were parameterised in the APSIM-ORYZA model (Table 3:8). Rice yield and biomass production were compared with the baseline application.

3.3.4.4 Scenario 4: Mineral fertilizer application

Efficient fertiliser management has been used to increase crop production to adequately mitigate the effects of climate change. Nitrogen fertiliser is the most important input in rice production and optimal management of its rate and timing improves the sustainability of the production system. For this scenario, different nitrogen (urea) application rates were parameterised in the APSIM-Oryza model, specifically in the factor module. Five nitrogen rates (45, 90, 120, 150 and 180 kg N/ha) were applied using the same rice variety WITA9 (Table 3:8). The basal nitrogen application was 114 kg N/ha, applied once by the farmers. Basal phosphorus and potassium applications were maintained at 44 and 42 kg ha-1, respectively

Table 3:8 Soil organic matter scenarios: Manure application 15 days before early rice transplanting (30, 60 and 100 kg N ha-1) and nitrogen application scenarios (45, 90, 120, 150, 180 kg N ha-1).

Parameter	Baseline	Range test
Crop establishment	Transplanting	Direct seeding
Soil organic matter application (kg/ha)	0	30, 60 and 100
Mulch application (Mg/ha)	0	5 and 10
Mineral fertilizer application (kg N/ha)	144	45, 90, 120, 150 and 180
Seeding age (day old)	21	10, 14 and 35
Sowing date	01 April	1st February, 15th February, 1st March, 15th March, 1st May, 15th May, 1st June condition

3.3.4.5 Scenario 5: seedling age

The production of strong seedlings and their transplanting at the right age are the most important factors for achieving high performance in rice production. The effect of seedling age was parameterised in this scenario using the APSIM-ORYZA model. Different transplanting dates of 10, 14 and 35 days old seedlings (Table 3:8), grown with different seeding rates during the historical rice growing seasons, were set up in the model

3.3.4.6 Scenario 6: sowing date

The effect of changing the planting date on lowland rice yield was simulated using the APSIM-ORYZA model based on historical climate. The APSIM-ORYZA model was parameterised to simulate rice yield in the study area under nine different planting dates (1) planting on 1 February; (2) planting on 15 February; (3) planting on 1 March; (4) planting on 15 March fifteen days earlier; (5) planting on 1 April, the baseline condition; (6) planting on 15 April condition; (7) planting on 1 May condition; (8) planting on 15 May condition; and (9) planting on 1 June condition (Table 3:8).

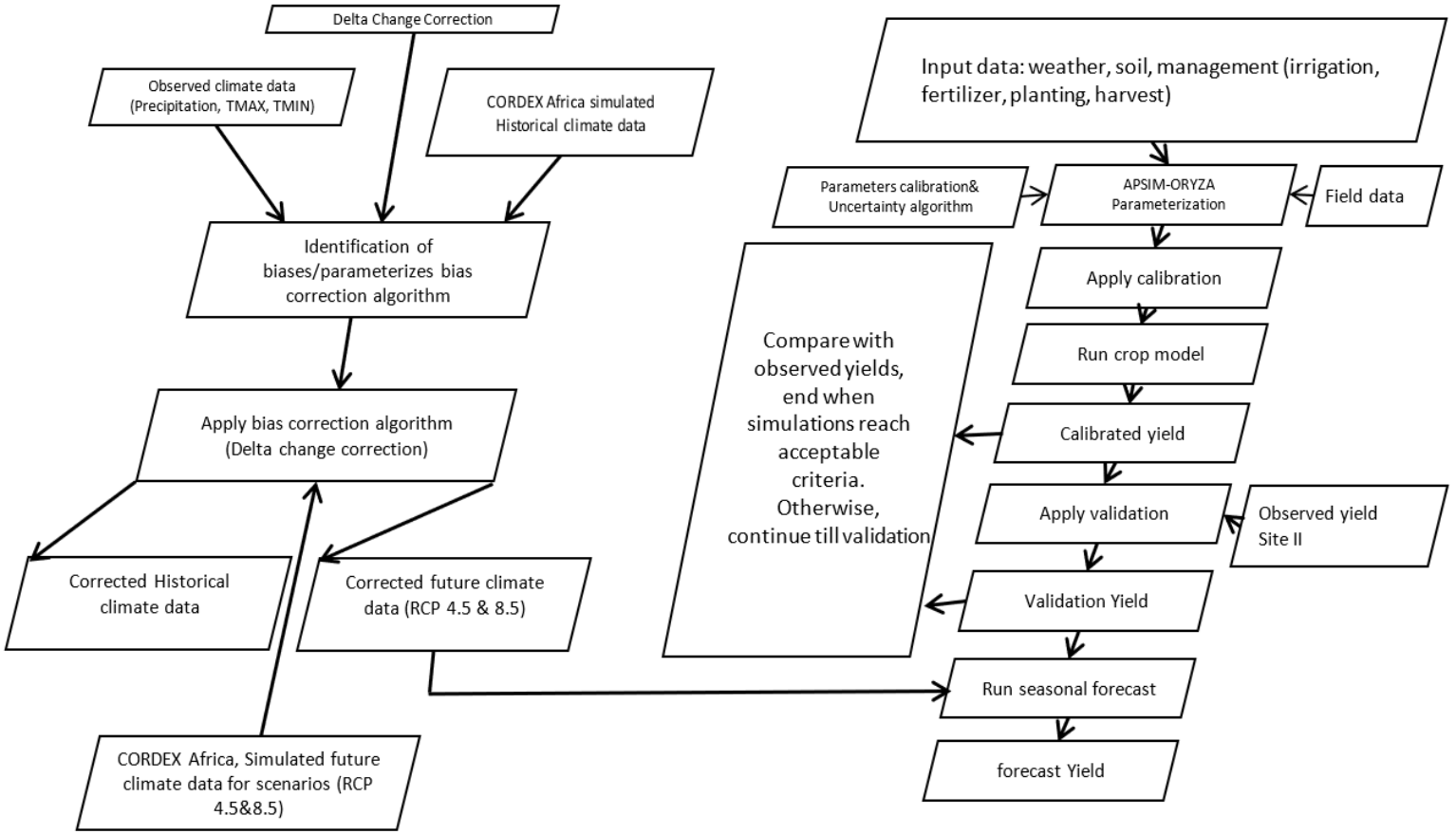

Figure 3.3 Flowchart showing the crop simulation procedure, bias correction methods and rice simulation and forecast

Chapter Four

4.0 Result and Discussion

In this chapter, the research finding relative to land-atmospheric interaction and its impact atmospheric boundary layer and precipitation event over West Africa, and on rice production are develop.

4.1 Coupling of land surface model fluxes and lifting condensation level (LCL) height simulations with the present climate

4.1.1 Model Configuration

The lifting condensation level (LCL) height was estimated using the land surface fluxes output from the simulation. The numerical simulations were performed with eCLM, a variant of CLM5, using three Plant functional type (PFT) parameterisations. The experiments were carried out over West Africa using the GWSP version 3 forcing with a resolution of 50 km and a temporal resolution of 3 hours over a period of one year from 2000 to 2014. The simulations were performed with integration time steps of 3 hours, with model results submitted at the same frequency. The three-hourly LCL was estimated using the equations of Romp et al. (2017).

4.1.2 Comparison of simulated energy fluxes

The performance of the different function sets in reproducing 3 hourly land surface fluxes (latent and sensible heat) is shown, as well as the correlation and comparison between the different plant function types with the observed and ERA5 land datasets. For example, at the Kayoro site in Ghana (Figure 4.1, Figure 4.2, Figure 4.3A&D, Figure 4.4(A)), where observations are collected, the results of the simulation agree well with the observed and ERA5 land in terms of phase, with good correlations for latent heat with unchanged correlation coefficient ($r = 0.74$, $r = 0.60$) for the three land units respectively and root mean square error (RMSE = 19 and 25) for the three PFTs respectively. We observe a

similarity between observed and simulated for sensible heat with a slight correlation in trend and amplitude with a change in correlation coefficient (r = 0.30, r = 0.44) for the observed and ERA5 land with the three PFTs respectively and unchanged root mean square error (RMSE = 14, RMSE = 28 w/m2) (Figure 4.4(A)). For example, at Nazinga in Burkina Faso (Figure 4.1, Figure 4.2), we observe a low and weak correlation between simulation, observed and ERA5 with unchanged correlation coefficient (r = 0.44, r = 0.46) and root mean square error (RMSE = 34) for latent and sensible heat respectively (r = 0.036, r = 0.039) (Figure 4.4 (B)). However, at Sumbrungu, Ghana (Figure 4.1, Figure 4.2) we observe good agreement with a strong correlation between simulation, observation and ERA5 land (r = 0.84, r = 0.55) for latent heat and a weak correlation (r = 0.4, r = 0.3) for sensible heat. We observe an underestimation of latent heat for all sites (Kayoro, Nazinga and Sumbrungu in 2013) for the three PFTs, and improvements in trend and amplitude of fluxes were obtained with observation and ERA5 for latent heat and an underestimation with sensible heat flux.

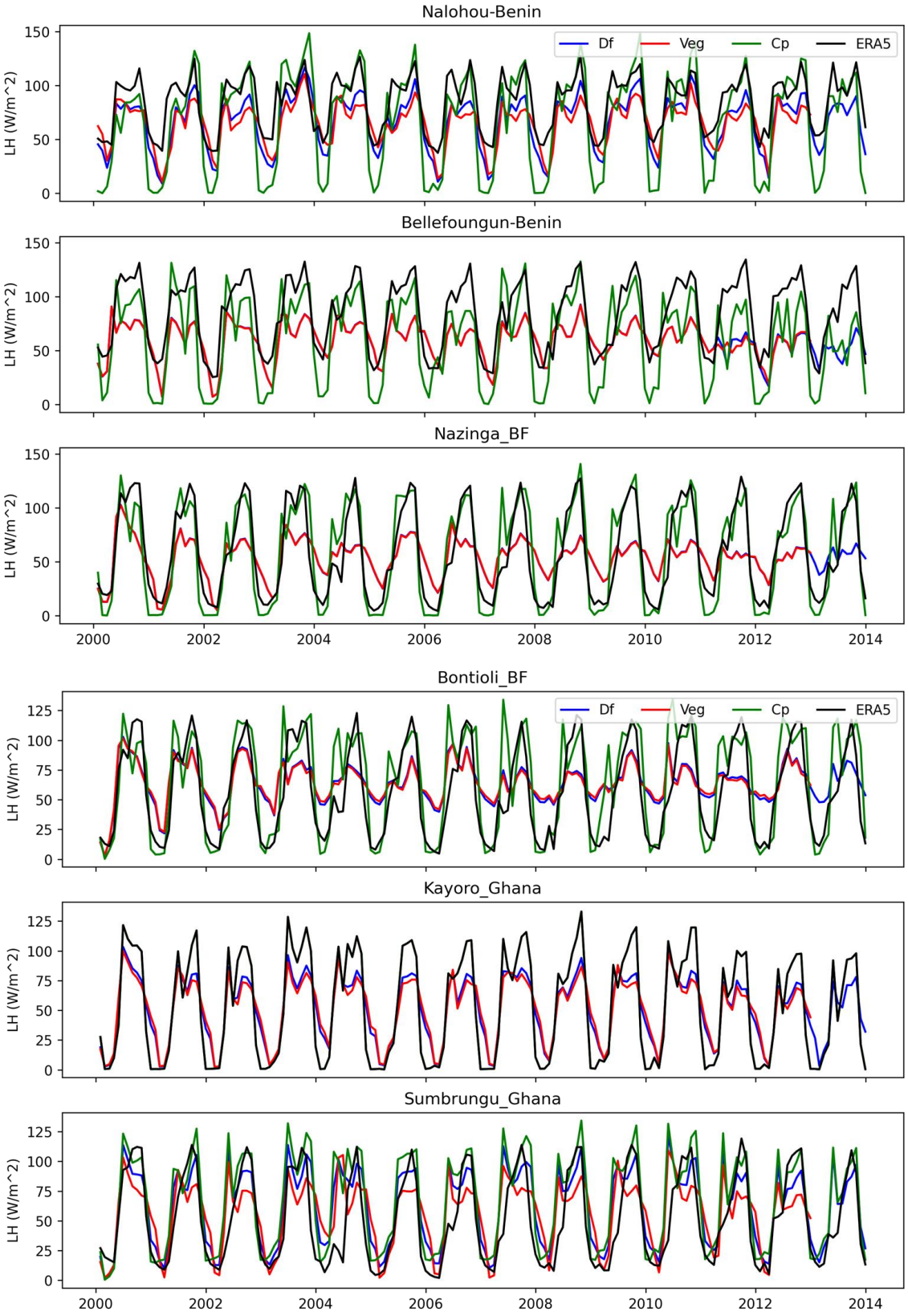

Figure 4.1. Comparison of monthly latent heat (LH) between simulation output and ERA5-land reanalysis data over the 11 eddy covariance selected sites in West Africa

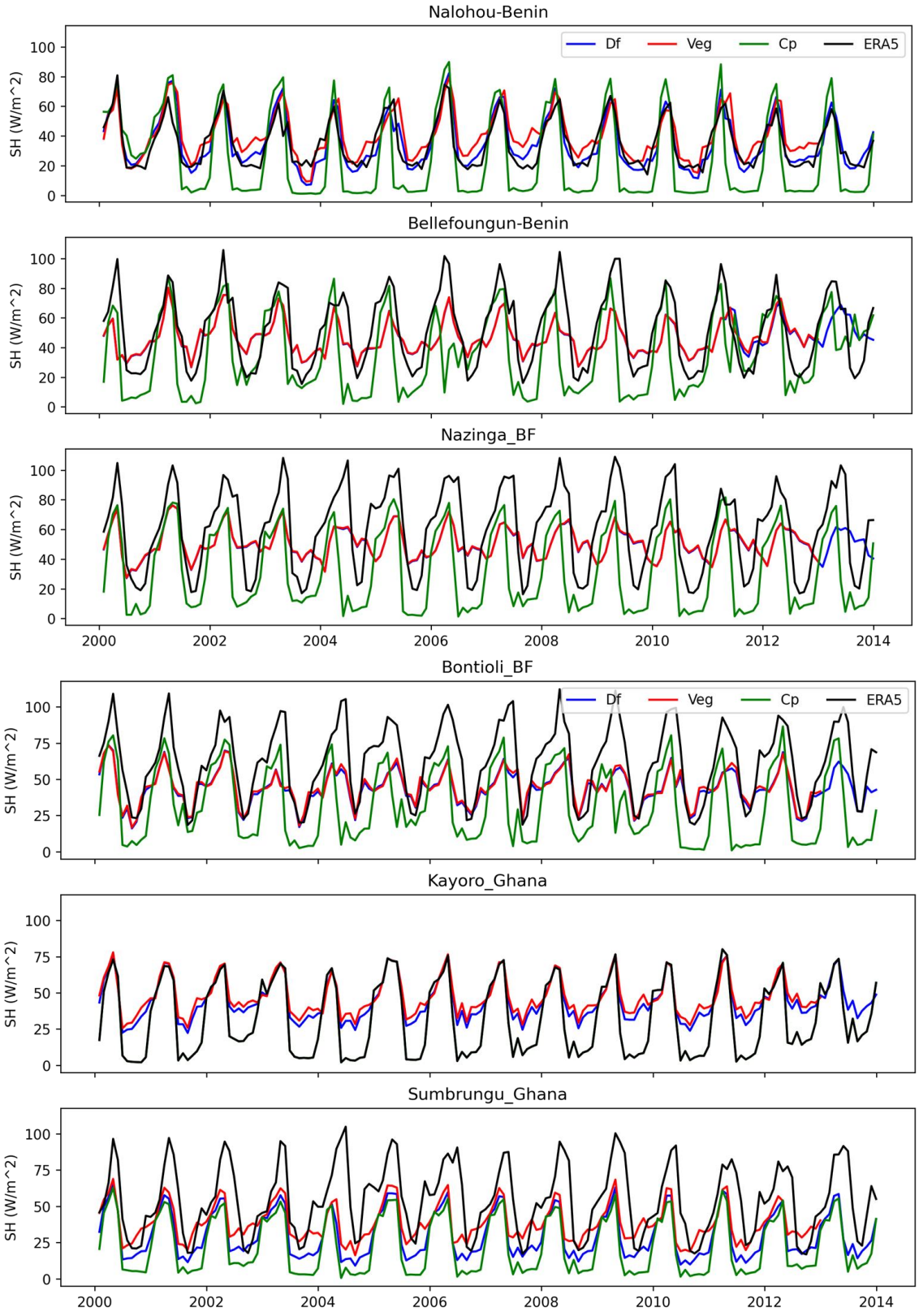

Figure 4.2. Comparison of monthly sensible heat (SH) between simulation output and ERA5-land reanalysis data over the 11 eddy covariance selected sites in West Africa

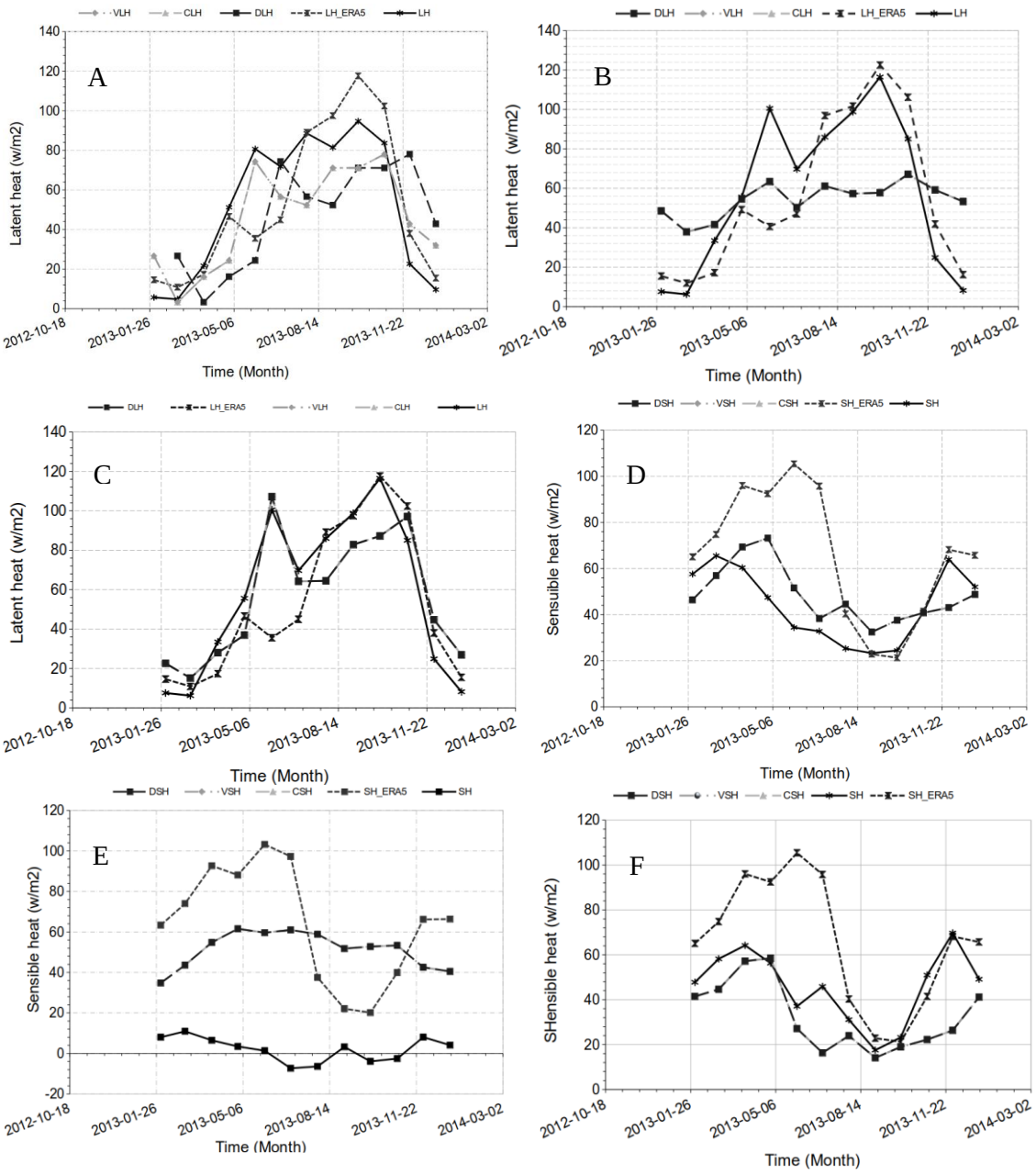

Figure 4.3. Variation of latent (LH) and sensible (SH) heat fluxes times series of observed, ERA5 and simulated monthly averaged diurnal cycle over (A, Kayoro; B, Nazinga; C, Sumbrumgu) for LH, and SH (D, Kayoro; E, Nazinga; F, Sumbrumgu) in 2013. DLH, VLH, CLH for latent heat flux simulated from default, vegetation and crop land vegetation types respectively; DSH, VSH, CSH are sensible heat flux simulated from default, vegetation and crop vegetation types respectively.

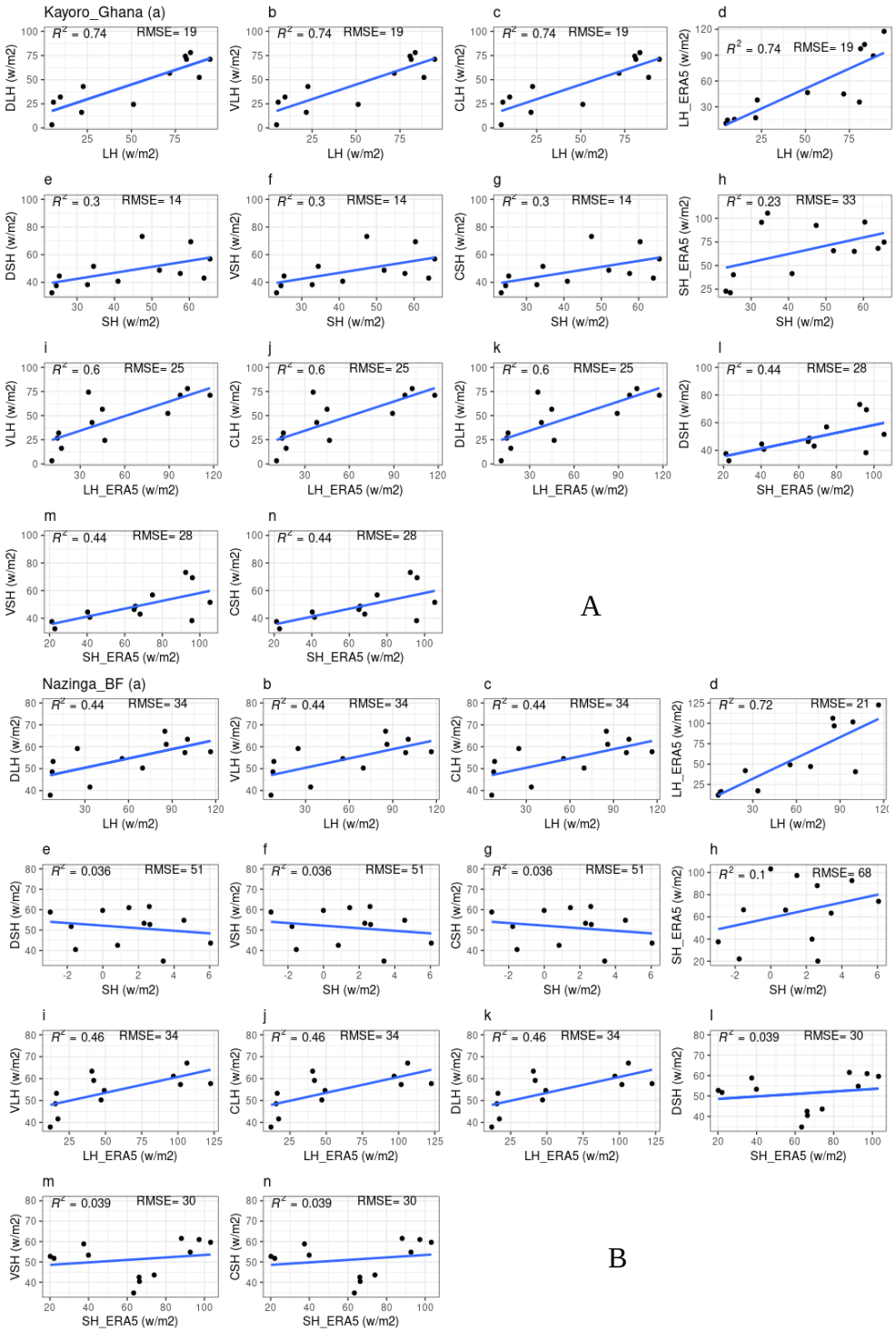

Figure 4.4. Correlation between simulation land surface fluxes, ERA5-land and observe (eddy covariance) data over the selected sites in (A) Kayoro station in Ghana and (B) Nazinga in Burkina Faso. LH, latent heat flux form EC data, DLH, VLH, CLH, latent heat flux from default, vegetated and crop land cover simulated output, LH_ERA5, latent heat from ERA5 land data. SH, sensible heat from eddy covariance station; DSH, VSH, CSH, are sensible heat from default, vegetation and crop simulated vegetation types; SH_ERA5, sensible heat from ERA5 land dataset.

4.1.3 Comparison of Lifting Condensation Level (LCL) with different PFT types and current climate

The simulated land surface fluxes (latent and sensible heat) were significantly improved with the three plant functional types in West Africa. The LCL pattern was computed for each 3 hourly average monthly period and the minimum and maximum LCL value over the study area is recorded in Table 4:1 as well as the comparison between simulation, observation and ERA5. Figure 4.5 and Figure 4.6 show the variability of LCL height over the three sites where eddy covariance data was collected (Figure 4.5) and the variability over the eleven selected site in West Africa (Figure 4.6). We observe that the LCL is higher above the crop PFT (4.5 km) and the minimum level simulated is 0.3 km above the crop PFT. Over vegetation PFT, the maximum level of LCL height is recorded by 4.3 km and the minimum level (0.3 km). The comparison of the LCL between simulated, ERA5 land and observed datasets shows a good agreement in trend and amplitude between simulated observed and ERA5. The relationship between each expressed LCL PFTs with observed and ERA5-land are very strong and high ($r^2 > 80$) over the selected site for model evaluation (Figure 4.7). Evaluating the high of LCL in the West Africa according to each land cover, we also observe a good agreement with a slight overestimation of the LCL from the crop PFT in West Africa. In Nalolou, Niakhar, Kayoro and Wankama EC sites characterised by crops (maize, groundnut, sorghum, cassava, millet), the LCL value is higher (Figure 4.6) and in the EC sites (Agoufou, Dahra, Kelma, Bellefoungou, Bontiola, Nazinga and Sumbrungu) (Quansah et al., 2015, Rhaimi et al. 2021, Ago et al. 2016) characterised by vegetation PFT (forest, trees, grassland, shrubland), we observe an underestimation of LCL estimated by vegetation PFT ((Figure 4.6). When West Africa is covered only by vegetation land cover, the height of the LCL level is slightly than when it is covered by cropland.

Table 4:1 Statistical analysis result from simulation output and ERA5 land: DLCL= lifting condensation level calculated from default land cover; VLCL= lifting condensation level express from vegetation type; CLCL= lifting condensation level express from crop vegetation type; LCL_ERA5=lifted condensation level calculated from ERA5 land dataset

Statistic parameter	DLCL (km)	VLCL (km)	CLCL (km)	ERA5 Land (km)
	Mean	Mean	Mean	Mean
Max	4.4	4.3	4.5	4.5
Min	2.1	2.1	2.2	2.5
Lowes	0.3	0.3	0.3	0.1

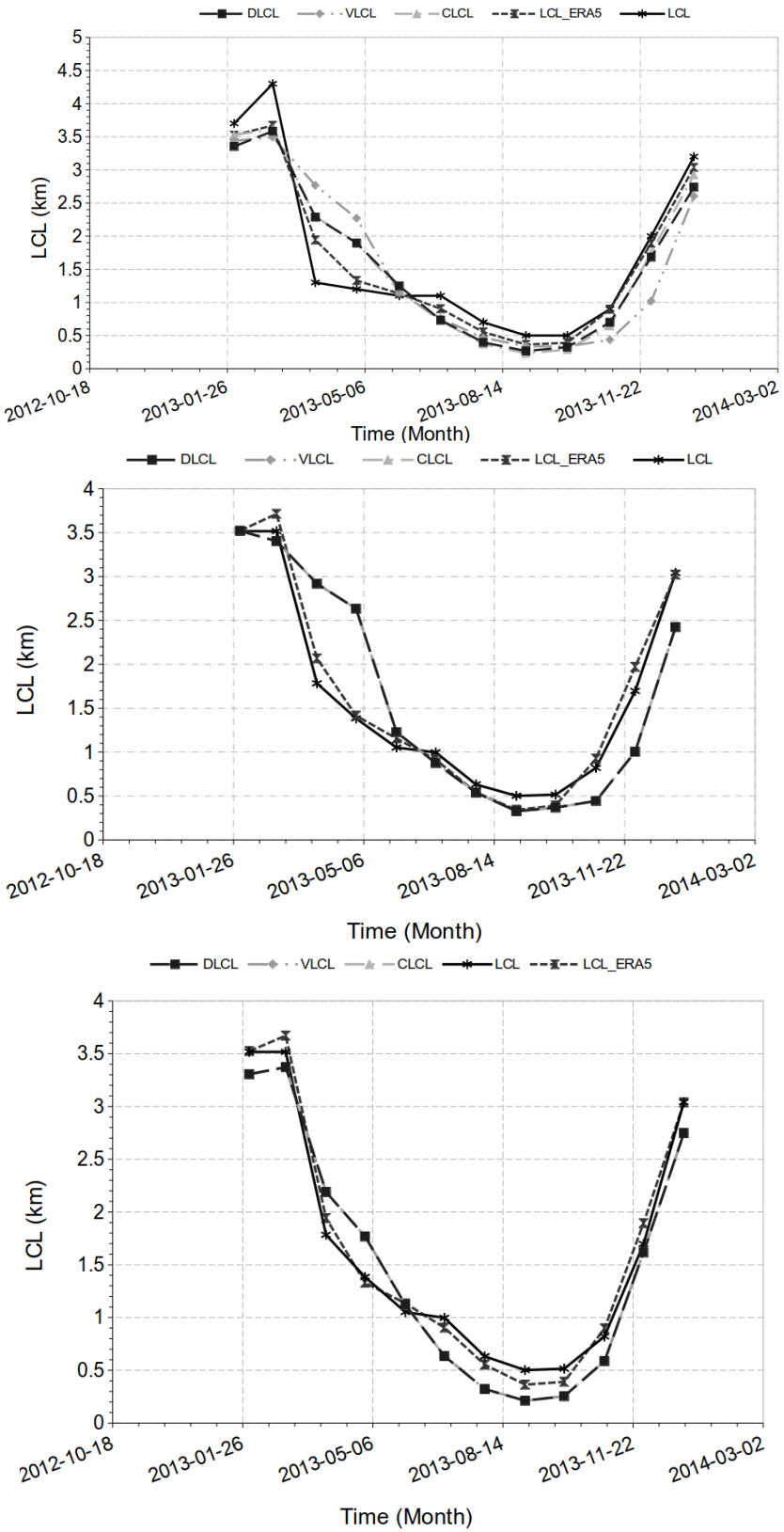

Figure 4.5. Observed and simulated monthly averaged diurnal cycle of (A) latent heat, (B) sensible heat, and (C) Lifting condensation level (LCL) height at the Sumbrungu, in

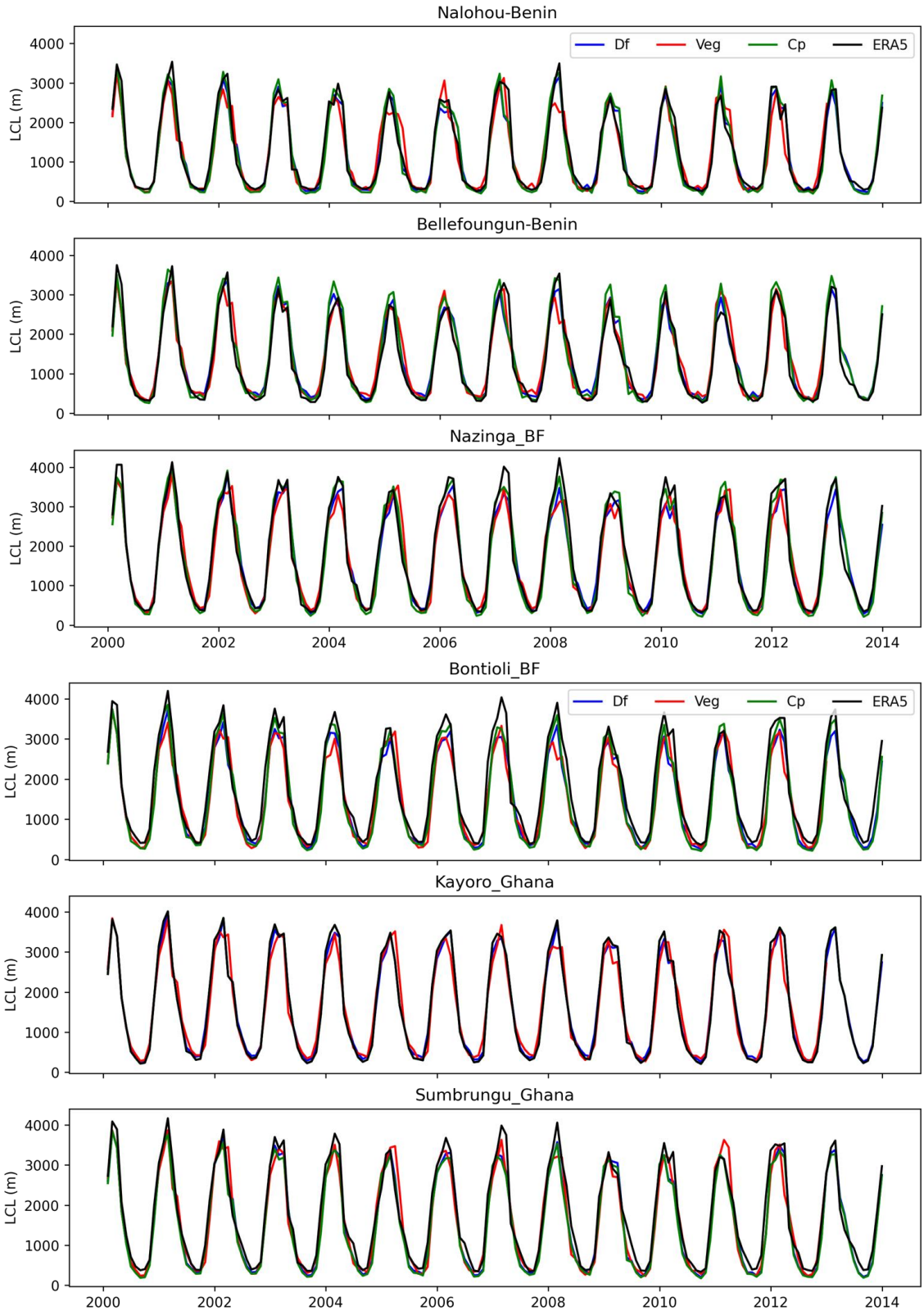

Figure 4.6. Comparison of monthly lifting condensation level (LCL) height between simulation output and ERA5-land reanalysis data over the 11 eddy covariance selected sites in West Africa

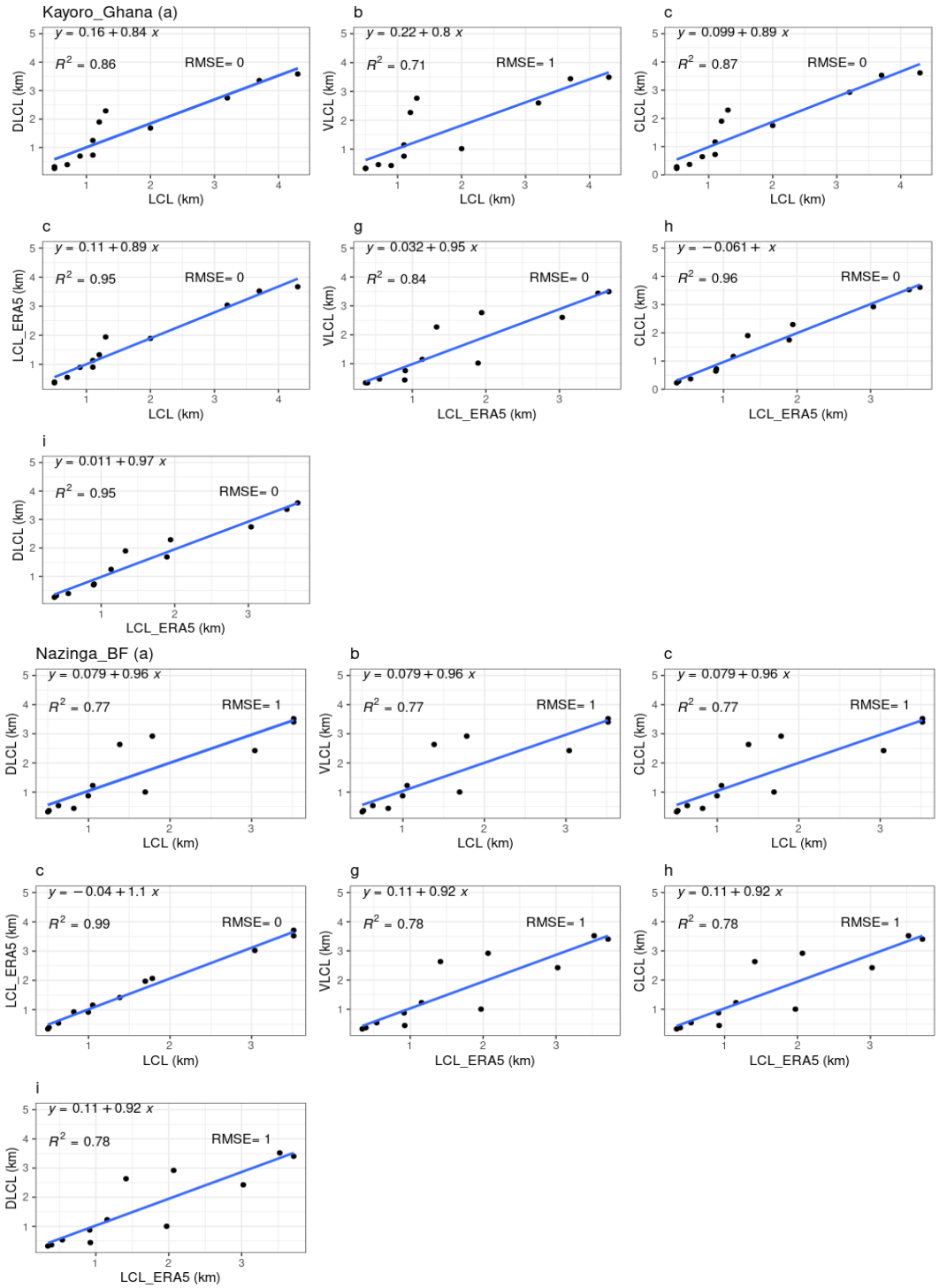

Figure 4.7. Linear correlation (coefficient of determination and root mean square error) of the mean 3 hourly in monthly sensible and latent flux from the default (DLH, DSH), vegetation (VLH, VSH) and crop PFT (CLH, CSH) with observe eddy covariance data (SH, LH) and ERA5 land (LH_ERA5, SH_ERA5) over Kayoro in Ghana and Nazinga in Burkina Faso

Figure 4.8 shows the minimum and maximum LCL pattern over West Africa for the period 2000 to 2013. The minimum and maximum heights of the LCL level have been calculated for different PFT land cover. For the minimum height of the LCL level, we observe that the lowest level is observed along the coastline in the Guinean region (longitude 15^{o}W to 15^{o}E and latitude 5 - 10^{o}N) at 0.3km for the default (DLCL) and vegetation (VLCL) PFT functional types and 0.25km for the crop (CLCL) PFT. This is shown in dark blue. The red light colour indicates the maximum level and can be up to 2.1km for DLCL and VLCL and 2.2km for CLCL. The same applies to the maximum height of the LCL level. For example, in the Sahelian zone (4.4 km, 4.3 km and 4.5 km) the highest level height is observed for DLCL, VLCL and CLCL respectively (latitude 12^{o}N to 22^{o}N) and is observed in red light colour. For example, in the Soudanian zone (latitude 9^{o}N to 12^{o}N), the height of the LCL level is in the middle (2.1 km for DLCL and VLCL and 2.2 km for CLCL; Figure 4.8)

The climate of West Africa (WA) is determined by the West African monsoon circulation and seasonality. The climatology of the region, with the exception of the coastal areas, is dominated by two seasons: a rainy season with rainfall almost equal to the total annual rainfall, and a dry season with little or no rainfall. The monsoon mechanism provides most of the rainfall in summer. Rainfall generally begins in June, peaks in August and decreases from September onwards. The Figure 4.9 shows the climatology of the LCL level height for different land cover type. For example, for the urban/default land cover, the LCL decreases steadily from over 4.1 km in April to less than 0.5 km from June to October, corresponding to the rainy season and monsoon activity. From November to March, the LCL increases to less than 0.5 km, reaching 3 km in December and more than 4 km in March (Figure 4.9(A)). A similar pattern is observed for the pure vegetation cover over West Africa. The LCL steadily decreases from more than 4.1 km in April to less than

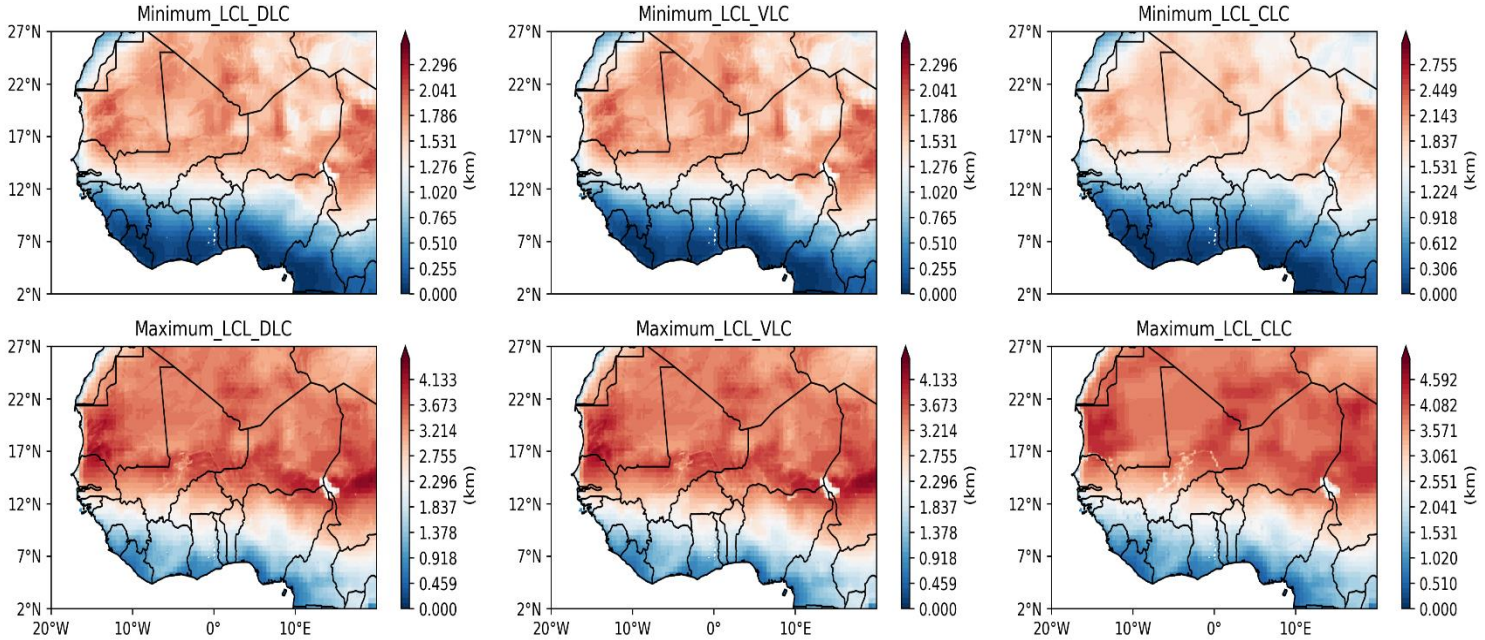

Figure 4.8. Mean maximum and minimum of lifting condensation level height for the three hourly land cover DLCL = default plant functional type (PFT), VLCL = vegetation PFT and CLCL = crop PFT

(A)

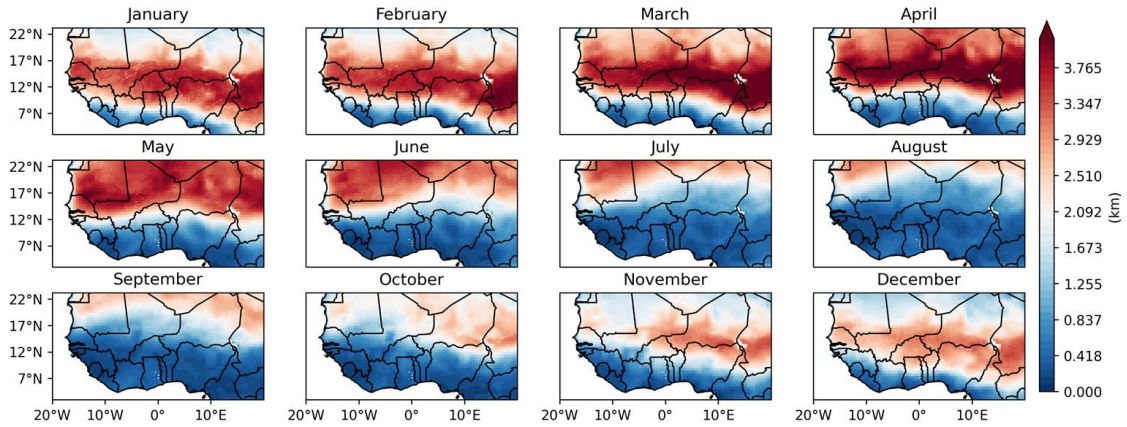

(B)

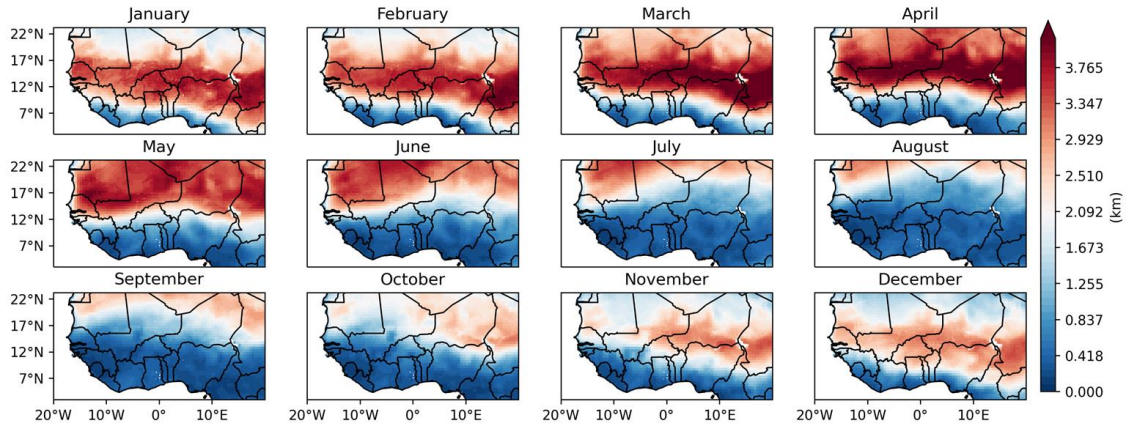

(C)

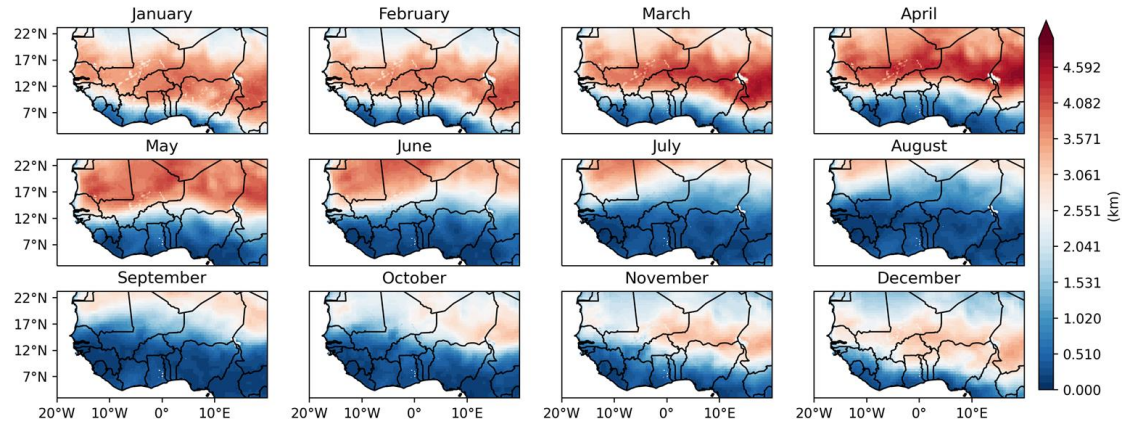

Figure 4.9. The climatology pattern of 14 years average of lifting condensation level (LCL) height from (A) default, (B) vegetation and (C) cropland land units over West Africa

0.5 km from June to October and starts to increase from less than 0.5 km (0.3 km) to 4 km in March (Figure 4.9(B), Figure 4.5(B,C)). For the Crop Land Unit, considering that West Africa is covered by cropland only, the LCL decreases steadily from a level above 4.5 km in April to less than 0.3 km in the June to October period. When WA is covered with cropland PFT, the model simulates a higher LCL level in April and a lower LCL level in the dry and wet seasons except March-April-May (Figure 4.9(C), Figure 4.5(A)) while when WA is covered with vegetation or a default PFT parameterisation, we observe a higher LCL level in the dry season (January-February) and during wet periods (March to June) over the Sahelian region (> 3. 5 km) and a slightly higher LCL level over the Sahelian and Sudanaen zone (<3 km) from September to December. However, for vegetation and standard land cover, the height of the LCL level over the Sahelian zone increases from January to June (> 3.5 km), while it is lower over the region from September to December (< 2.5 km). A meaningful relationship between LCL and precipitation and the interaction between cloud cover, precipitation and LCL is proposed and investigated.

4.1.4 Difference between the different land cover for the express LCL

Figure 4.10 shows the difference in LCL from the different land cover changes over West Africa. The change in difference is calculated to assess the significant level of LCL from each land cover of the PFTs. The difference between the percentage vegetation PFT and the percentage default PFT showed no change in significance. This is due to the insignificant change between the two datasets. However, we observe a slight increase in LCL over the WA region (Figure 4.10A). The difference between VLCL and CLCL has been performed and the result shows a significant change compared to VLCL-DLCL. Over WA (5^{o}N - 17^{o}N) we observe a high LCL, which implies more strong winds and less precipitation associated with a lower albedo and more downward solar radiation at

(A)

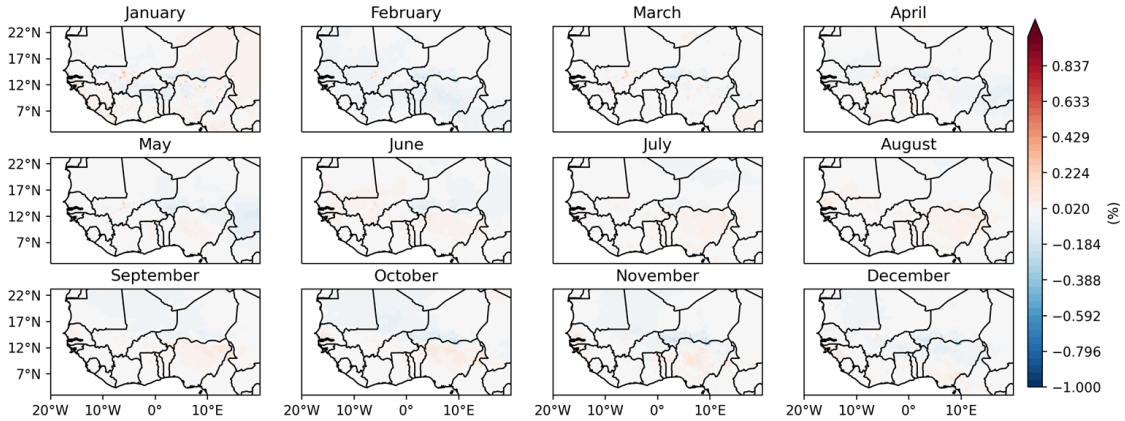

(B)

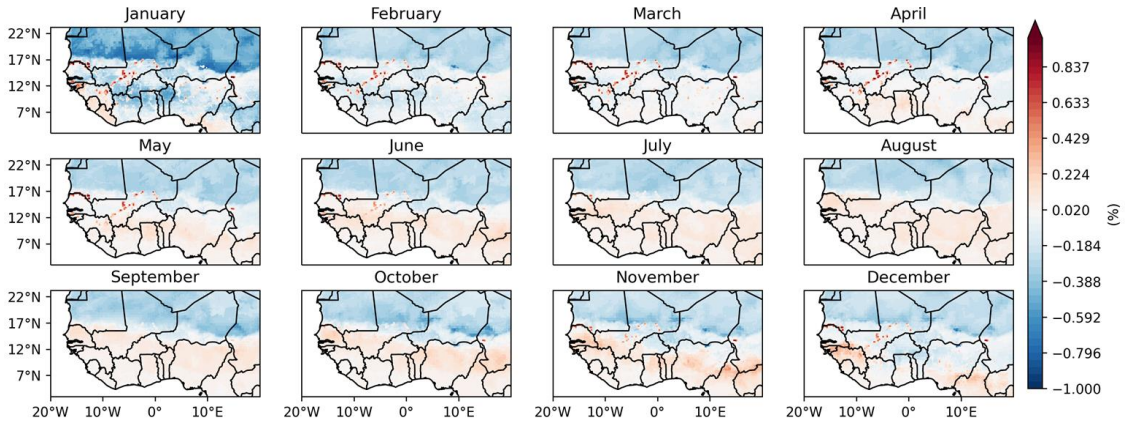

(C)

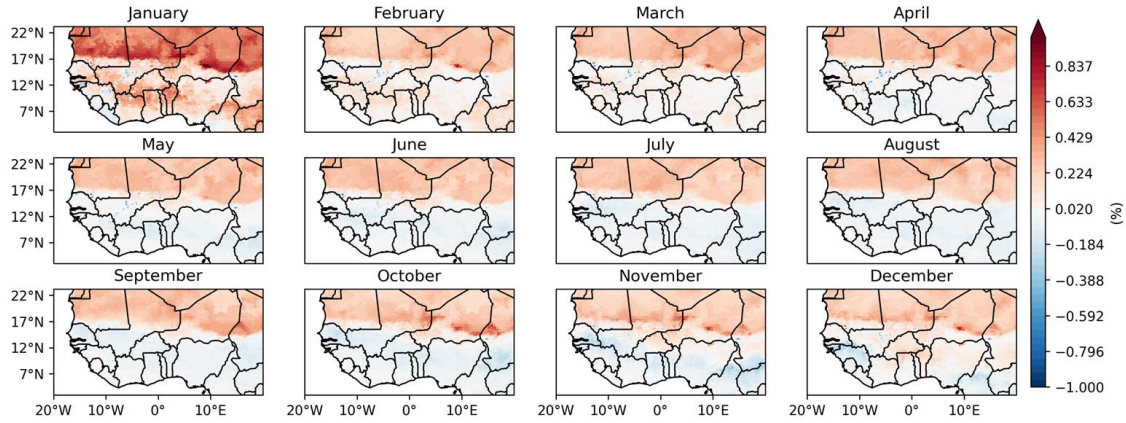

Figure 4.10. Level of significance change of LCL height between the three PFTs : (A) difference (VLCL-DLCL), (B) difference (VLCL-CLCL), (C) difference (CLCL-DLCL)

the surface. The high LCL is observed from March to December and of particular note is the low LCL observed over the WA region in January and February (Figure 4.10B). However, a lower LCL height is observed over the Sudanian and Sahelian region of WA (17ºN - 22ºN) and is observed from January to December. Figure 4.10C shows the significant change when cropland is extracted from the standard PFT, and this is in contrast to the analysis above. A low LCL is observed from the Guinea to Soudan region of WA (5ºN - 17ºN) and a high LCL is observed over the Sahelian region (17ºN – 22ºN) with in January and February a high LCL is observed over the whole region of WA (Guinea, Soudan and Sahel).

Vegetation PFT consists of trees, grass, broadleaf and crops. If the standard PFT is subtracted from vegetation, then the WA landscape is dominated by vegetation characterised by trees and some grass. However, if the standard is subtracted from Crop Cover/PFT, the WA landscape is dominated by a crop cover (vegetated grassland).

4.1.5 Couple LCL and land surface fluxes

In this section, we investigate the relationship between land surface fluxes (sensible and latent heat, solar radiation, relative humidity) and LCL height. The correlation coefficient of the 14-year (2000-2013) mean value in JJA for the different land cover: default (DLC), vegetation (VLC) and crop (CLC) was calculated to analyse the level of the relationship. We also calculated the evaporative fraction (EF), which is the ratio of LH to the sum of LH and SH. EF, defined as the ratio of latent heat flux to available energy at the land surface, is an important parameter that reflects the distribution of available energy at the surface and interprets the components of the energy budget, and is strongly related to soil moisture (Liu et al., 2020). The left two columns of the Figure 4.11 show the LCL-LH and LCL-SH correlations obtained from the simulation output and LCL estimation. The correlation pattern of the default and vegetation and crop PFTs appears to be broadly

similar. However, the default and vegetation PFTs have a more negative LCL-LH correlation over the WA region than the crop PFT, while the LCL-SH correlation is positive over the whole region with the crop PFT than with the default and vegetation (over the Soudan and Sahel regions).

The last columns on the right of the figure show the correlation between LCL and Evapotranspiration (EF). EF was estimated due to the unavailability of soil moisture data and its close relationship with soil moisture. The relationship between LCL and EF is almost positive over the entire Guinean and Sudan-Guinean region and negative over the entire Sahelian region of WA. In WA, four stations (Bellefoungou, Kayoro, Nazinga-Sumbrungu and Wankama, based on their specific ecosystem) were selected from the 11 EC stations as an example for detailed analysis. The four selected sites are located in the transition zone between the Sudanian and the Sahelian in WA. The Bellefoungu ecosystem in Benin is characterised by protected forest (trees and grass), the Kayoro ecosystem in Ghana by cropland (sorghum, groundnut and millet), the Nazinga ecosystem in Burkina Faso by pristine wood savannah (trees and grass) and the Wankama ecosystem in Niger by cropland (millet). Based on the magnitude of the EF, we observe from the scatterplots in Figure that the LCL-LH correlation remains negative over the selected region and for the three land cover types, but is stronger during the rainy season and lower during the dry season, while the LCL is stronger during the dry season and lower during the rainy season. The LCL-SH correlation remains mostly positive throughout the region.

Our results, along with the findings from previous studies (Betts, 2009; Kollias et al., 2009; Romps, 2017; Sulis et al., 2014; Wei et al., 2021) illustrate the extent to which the characterisation of the land surface change from one plant functional type to another particularly vegetation to crop or crop to vegetation could influence climate simulations in West Africa. According to Wei et al., (2021), The SH is found to be positively correlated with LCL in general, while its negative correlation with soil moisture and EF, the LCL-LH correlation is sensitive to the local climate and it is concluded that only

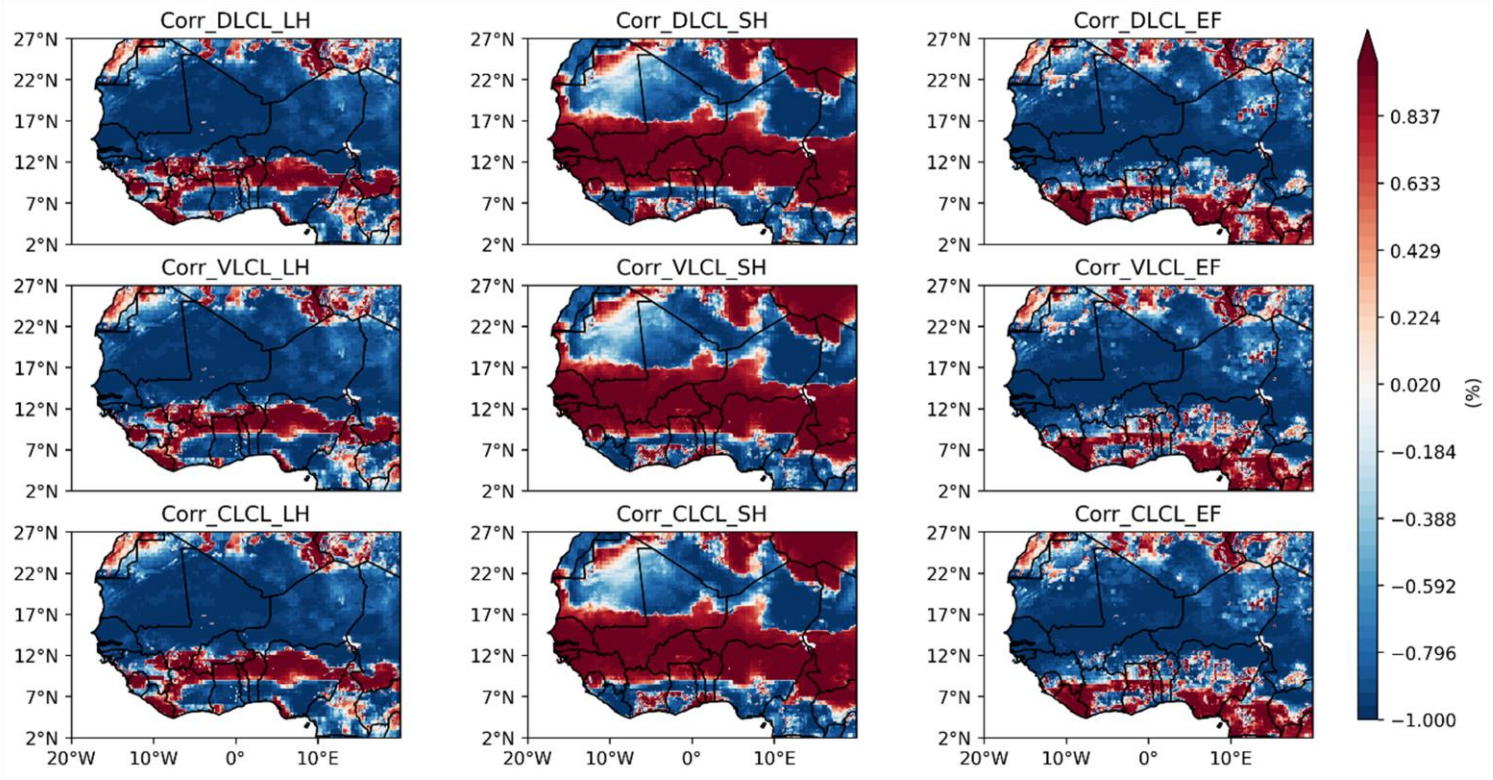

Figure 4.11. Fourteen years average correlation coefficient between LH and LCL height, SH and LCL height, EF and LCL height for the three land cover over West Africa during 2000-2013. DLCL, default PFT; VLCL, vegetation PFT; CLCL, crop PFT; LH, latent heat, SH, sensible heat; EF, evaporative fractional; PFT, plant functional type; LCL, lifting condensation level

correlations can account for a possible influence of LH on LCL. Betts (2004, 2009) found a general positive correlation between LCL with land surface sensible heat fluxes (SH) and 2 m temperature (T2M), and a negative correlation with precipitation, cloud albedo, soil moisture, surface relative humidity, evaporative fraction (EF) and latent heat fluxes (LH).

4.1.6 Relationship between LCL, precipitation and Cloud base

In this section, we were not able to set the crop and vegetation functional type characteristics during model parameterisation to observe the specific difference in rainfall pattern for each land cover or PFT type. Figure 4.12 shows the climatology of the rainfall pattern from the simulation output over West Africa during the period 2000-2013. An increase in rainfall during the June-July-August-September monsoon period is observed, with a large increase over the Guinean and Soudan regions of WA specifically associated with a southward shift of the monsoon core.

We also assess any relationship between the surface parameter and changes in precipitation and LCL to see how changes in surface fluxes are reflected in the atmosphere. The relationship between precipitation and LCL (PCP-LCL) is shown in Figure 4.13. The correlation is calculated using the fourteen year averages of the JJA correlation between land surface fluxes, LCL and precipitation. The first three columns in each row are LCL-PCP. There is a strong relationship between the two variables for the three land cover types DLC, VLC and CLC. The correlation pattern between LCL and precipitation (Figure 4.13) is similar for all three land cover types. However, a positive correlation is observed in the Soudan region (latitude 7ºN to 11ºN). This is consistent with the below analysis (Figure 4.18 and Figure 4.19). The monsoon season,

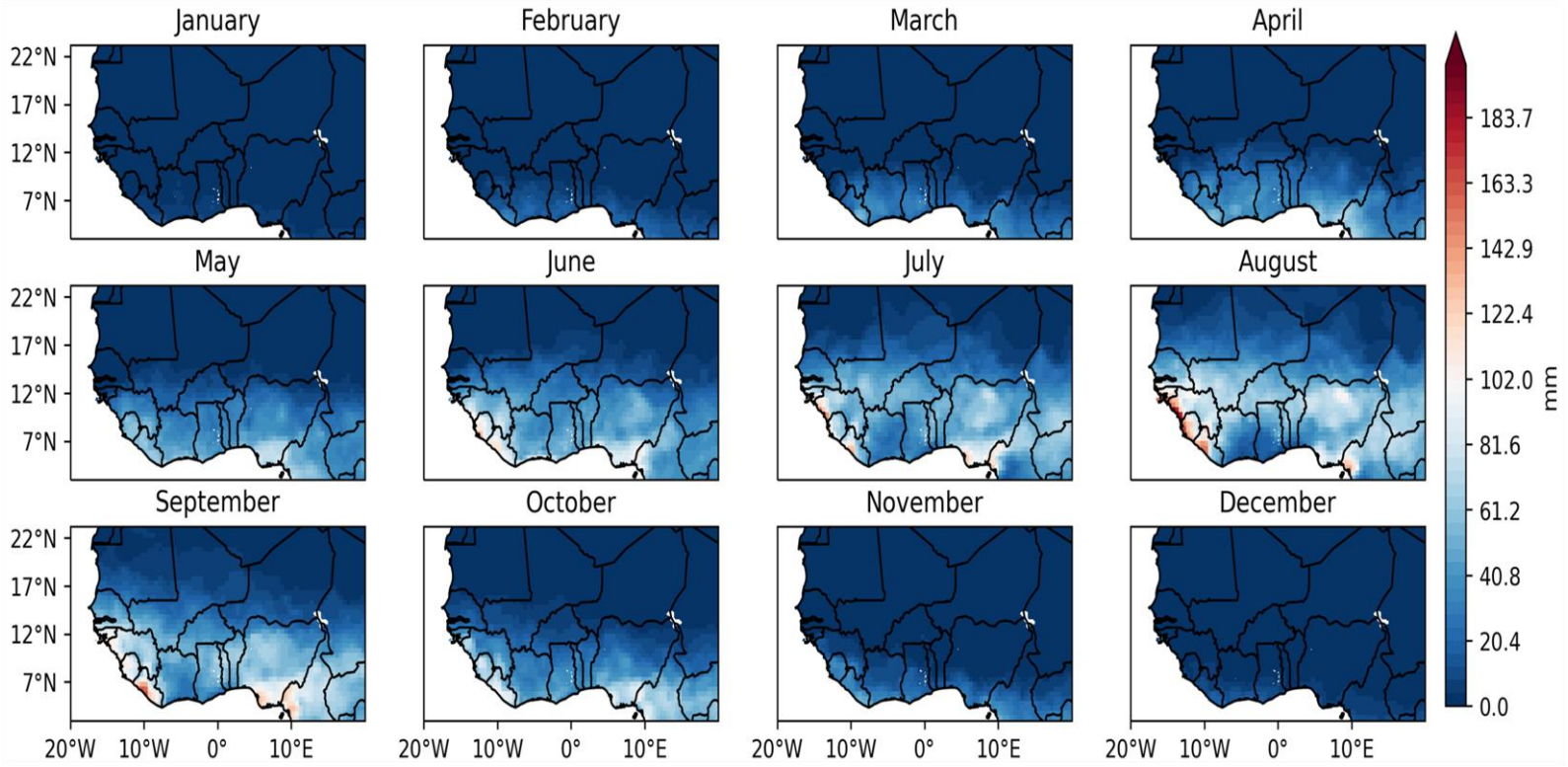

Figure 4.12. Climatology of Simulated rainfall mean monthly from 2000-2013 over West Africa

from May to September, is associated with convective clouds of varying depths that produce rainfall of varying magnitude. The maximum ground rainfall is observed in August and the highest daily rainfall rates are observed from July to September. During this period, the LCL is observed to decrease as the monsoon progresses and there is a strong correlation between the height of the LCL and rainfall (Figure 4.12) (Kollias et al., 2009).

LCL height is related to cloud base height, so a high (low) LCL height implies more high (low) clouds, which is usually associated with less (more) cloud moisture, less (more) precipitation, lower (higher) cloud albedo, and more (less) solar radiation that reacts with the ground (Wei et al. 2021). If West Africa is assumed to be covered only by crop PFT, the LCL height will be higher, implying more very high clouds associated with very low cloud moisture, resulting in very little precipitation over the region of West Africa. On the other hand, if we assume that West Africa is covered only by vegetation, then the LCL height will be lower than the crop PFT, implying fewer high clouds and therefore a slight increase in cloud moisture associated with a slight increase in precipitation. According to Boone et al. (2016), the change from vegetation land cover state to crop PFT mostly leads to an increase in the Bowen ratio and a decrease in net radiation, and a significant decrease in surface evaporation, especially over the Sahelian region. This in turn leads to a decrease in the convergence of moisture and precipitation. Yu et al. (2021) show that vegetation dynamics, through their interaction with climate, significantly increase precipitation in the region around the expected vegetation growth limit. Thus, the vegetation response affects the seasonal variation of precipitation changes, increasing precipitation before and after the monsoon season and decreasing precipitation during the peak of the monsoon season.

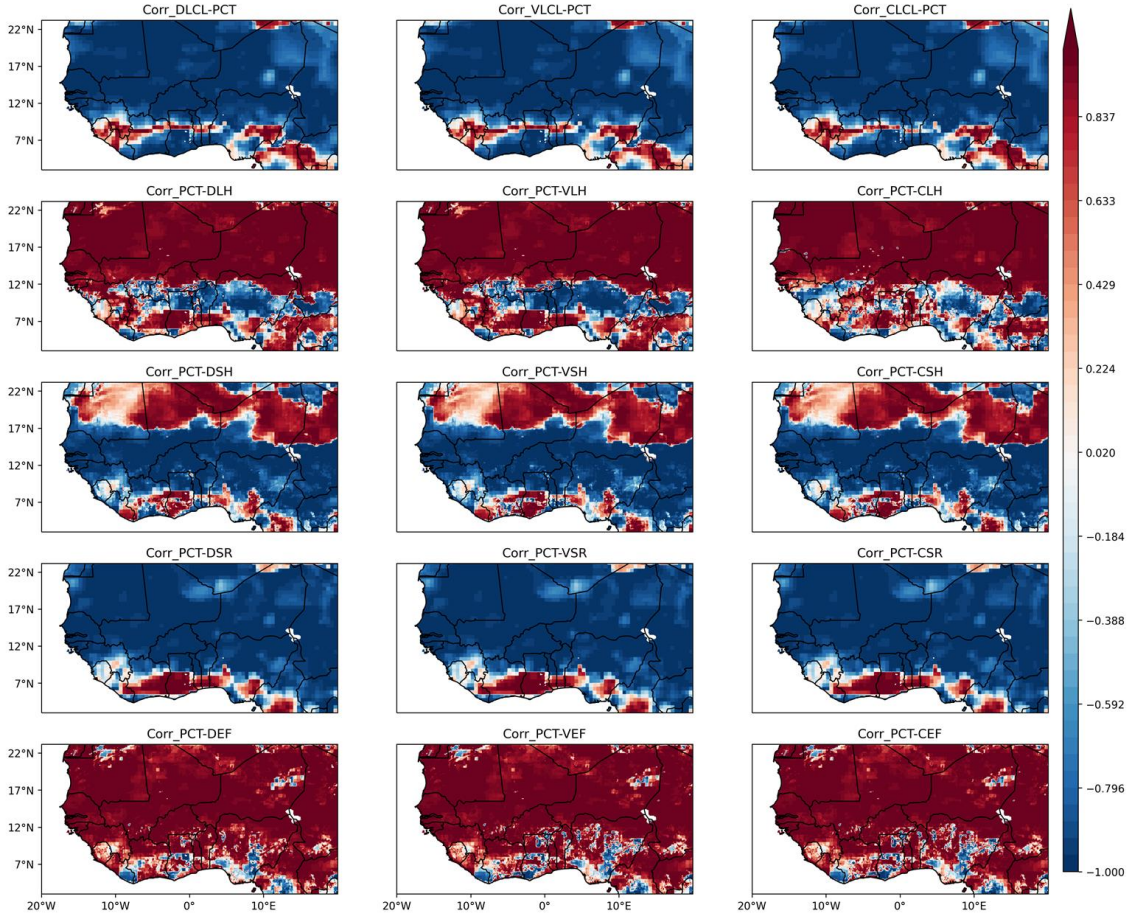

Figure 4.13. Fourteen years average correlation coefficient between rainfall, energy and water fluxes and LCL in West Africa during 2000-2013. DLCL, default PFT; VLCL, vegetation PFT; CLCL, crop PFT; LH, latent heat, SH, sensible heat; EF, evaporative fractional; PFT, plant functional type; LCL, lifting condensation level; PCT, rainfall.

The relationship between precipitation and latent heat flux (PCP-LH) is shown in Figure 4.13 (second row) in West Africa with water scarce conditions over the land surface. A strong relationship between LH and EF is observed over the three land cover types, indicating a strong correlation between LH and soil moisture. The reduction of LH can significantly influence moisture convergence. PCP-LH have more positive correlation over the Guinea cost and Sahel region, while we observe negative correlation in the Sudanian zone (8^{o}N-12^{o}N) for default and vegetation plant functional type and positive correlation for crop PFT. The pattern of PCP-SH correlation (Figure 4.13, third row) is similar and negative but slightly positive over the coastal region, the same is observed for solar radiation (PCP-SR) for the three land cover types (Figure 4.13, fourth row).

The PCP-EF plot shows a strong and positive correlation across the WA region. In this study, vegetation types are grouped into ten natural plant functional types (PFTs) such as evergreen and deciduous trees, C4 and C3 grasses, and crop PFTs are grouped into two super-grasslands, bare soil, plant C3 and C4. Crop PFTs differ from natural grasses only in their specified height carboxylation and Rubisco replenishment rates. A number of PFTs can be found in the same grid (mosaic vegetation). These PFTs share the same climate forcing, but land surface fluxes are calculated according to their own properties (de Noblet-Ducoudré et al. 2004). Vegetation and crop parameterisation in the eCLM model is static, not dynamic. The conversion of 'vegetation (forest) PFT to cropland (agriculture) changes the distribution of net radiation between latent and sensible heat fluxes (Pielke et al. 2002). The decrease in transpiration from cropland leads to a decrease in cloud formation over the WA and, in contrast, an increase in the height of the LCL.

4.1.7 Relationship between LCL height, the monsoon seasonal cycle and convective cloud

Figure 4.14 shows the climatology of average minimum daily of LCL for wet and dry season from the simulation output over West Africa during the period 2000-2013. We observe a low high of LCL height during the wet season JJA covering the Guinea and Sudanian zone and can reach 0.3 km of high, while over the Sahelian region, the high of LCL height range between 1 km to 2km. This LCL pattern is observe with the three vegetation types. In the dry season DJF, a high LCL height is observe over the Sudano-Sahelian and Sahelian region with a high reaching 2.5 km for vegetation and default land cover. Over the region with crop land cover, the coverage of LCL height is less that the one observe with vegetation and default but with a high reaching 3 km. Nevertheless, we observe a very low high of LCL height (0.3 km) through the coastal zone, while over the Sudanian zone the LCL height for the three land cover range between 1 km and 2 km.

Figure 4.15 show the climatology of average maximum of daily LCL height for wet and dry season over WA. During the wet season JJA, the le LCL height is low over the Guinea and Sudanian zone and can reach 1 km high from the land surface while over the Sahelian zone the LCL height reach a high range between 3 km to 4 km. We observe during the DJF dry season, an elevated LCL height from the coastal through the Sahelian region. Over the coastal zone the high of LCL height is lower over the ocean as show in Figure 4.15 last line where its reach a high of 1 km, while from Guinea to Guineo-Sudanian, it reach 3 km and from Sudano-Sahelian and Sahelian zone it reach 4.5 km of high.

The subtract method between different vegetation types have been apply in order to evaluate the dominant land cover and the associated LCL height. Figure 4.16 show the difference daily average of minimum LCL over JJA and DJF season between vegetation (Veg) and default (Def), and between crop (Crop) and default (Def). The result

observation show during JJA a low LCL over the whole of West Africa except over the Sudanian region (7°N-15°N) where we observe a high of LCL in the northern part of Nigeria, Togo and in the southern part of Niger. In the southern part of Niger we also observe a very concentrate low LCL high. However, in DJF, we observe a high LCL height with a very concentrate high in some particular place (northern of Nigeria and Southern of Mali and Senegal) over the Sudanian zone of West Africa. When subtracting default from crop vegetation type, we observe during the JJA and DJF a high of LCL height. The LCL is more higher over the Sahelian zone than the two others climatical zone Guinean and Sudanian. Nevertheless, very low LCL height is observe over Guinea, Senegal and Southern part of Mali.

Figure 4.17 show the difference daily average of maximum LCL over JJA and DJF season between vegetation (Veg) and default (Def), and between crop (Crop) and default (Def). When subtracting default from vegetation land cover type, we in JJA a high LCL height over West Africa, but more higher over the Guinea and Sudanian region with except in Niger where it observe that the high of LCL height is lower in the southern part of the country. In DJF, we observe a medium high of LCL height with a very high in some particular place over the Sudanian region of West Africa. The subtraction of default land cover from crop vegetation type show during the seasonal JJA period, a high LCL height over the Sahelian zone and low high of LCL height from the coastal region (Guinea) to Sudanian zone and Sudano-Sahelian. In DJF seasonal period, we observe a very high LCL height over the Sahelian zone and a medium high of LCL height over the Guinea and Sudanian zone. However, a particular observation is made in Liberia, Mali, Guinea, and Guinea-Bissau.

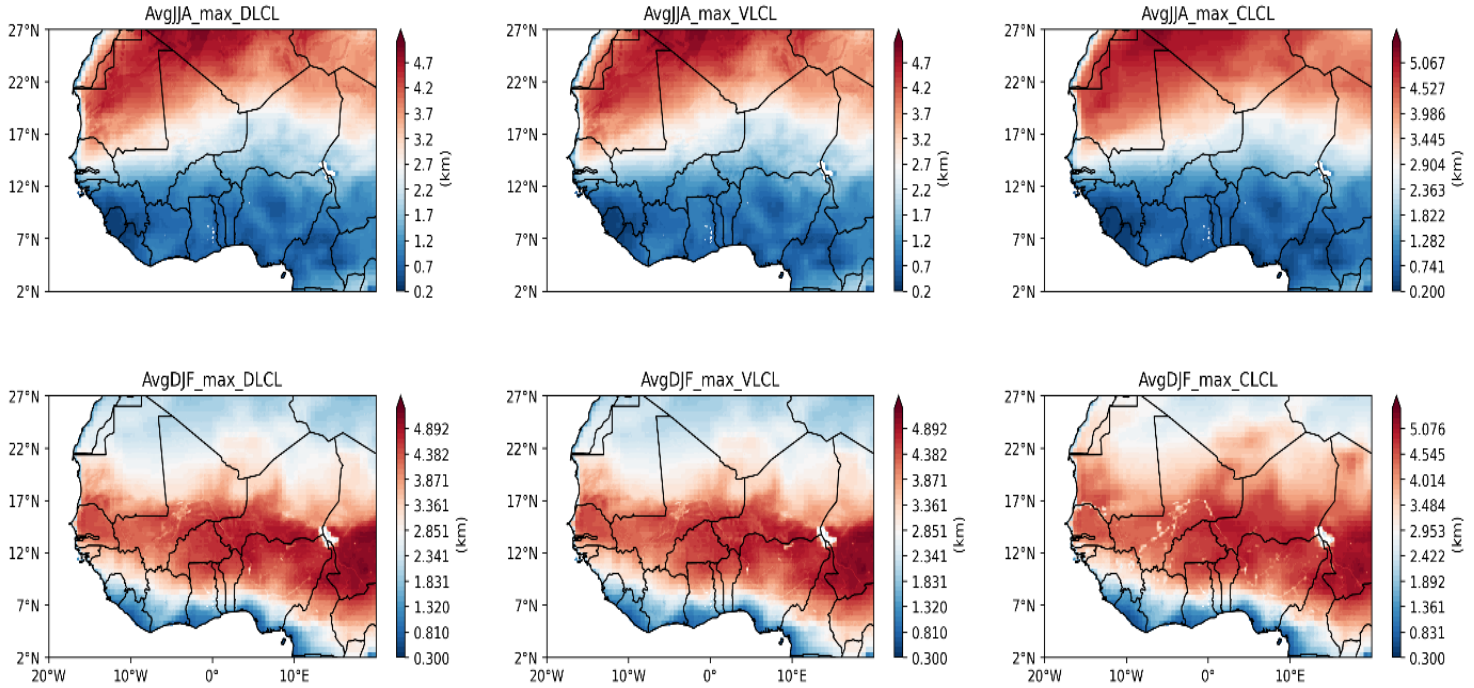

Figure 4.14 : Climatology of average minimum daily LCL for wet and dry season over West Africa. JJA, June-July-August, DJF, December-January-February, DLCL, Default land cover, VLCL, vegetation land cover and CLCL, crop land cover

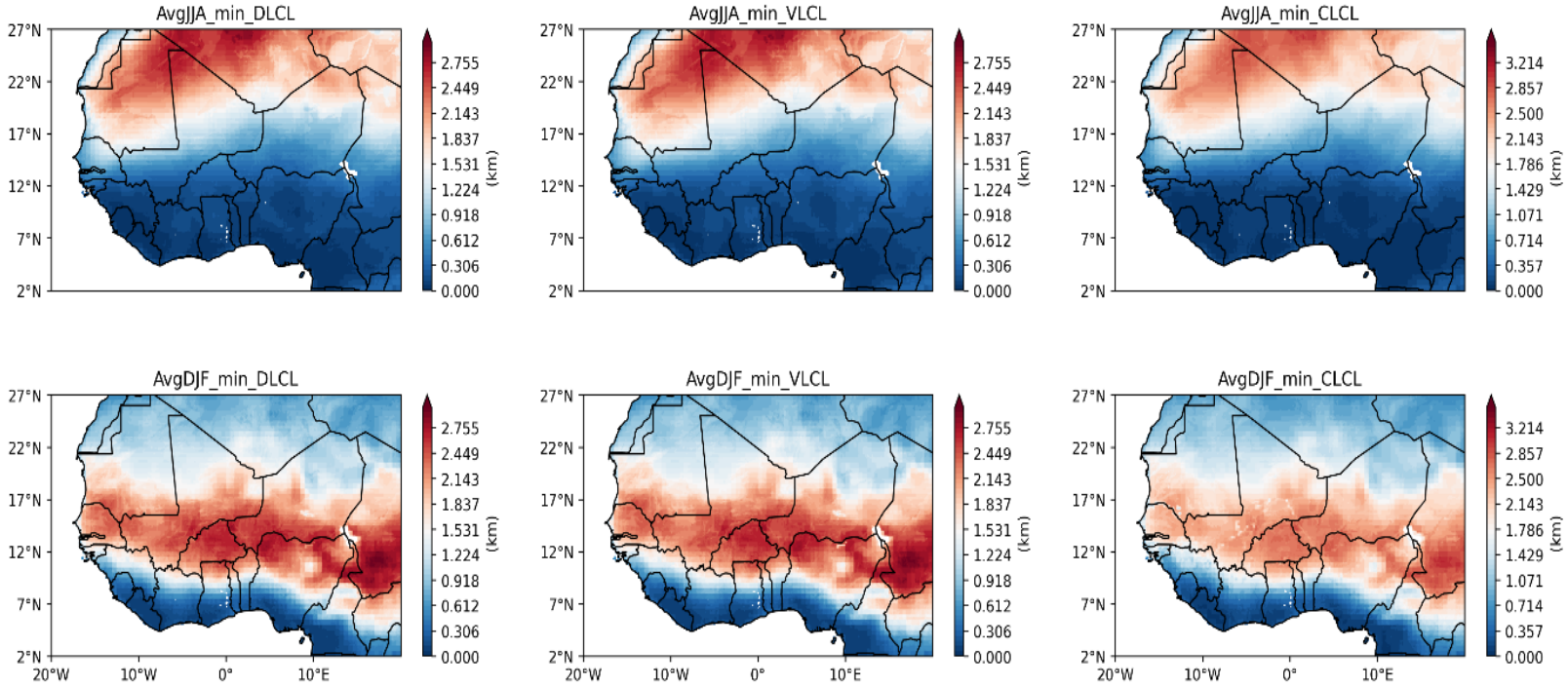

Figure 4.15 : Climatology of average maximum daily LCL for wet and dry season over West Africa. JJA, June-July-August, DJF, December-January-February, DLCL, Default land cover, VLCL, vegetation land cover and CLCL, crop land cover

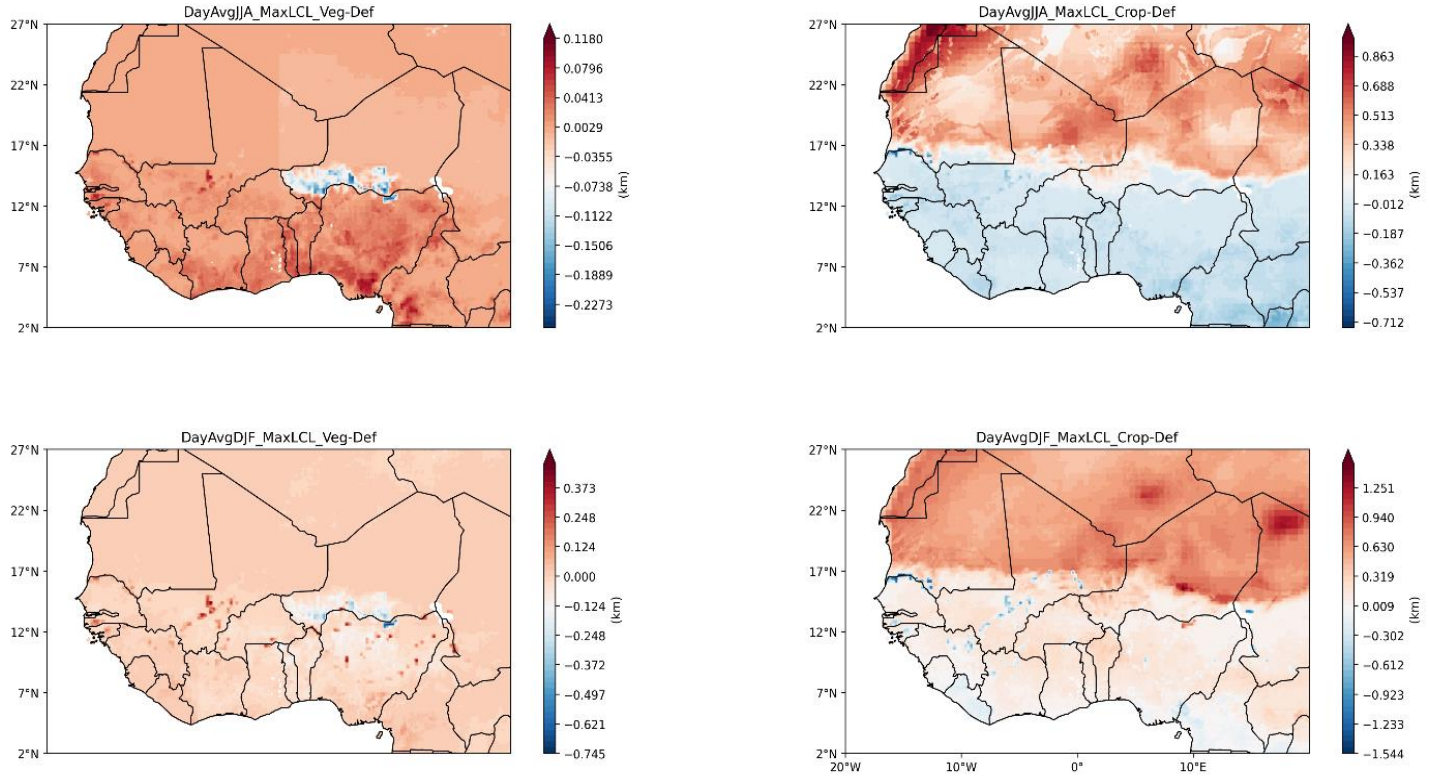

Figure 4.16 : Difference for maximum daily average over JJA and DJF seasonal LCL between vegetation and default (Veg-Def), and between crop and default (Crop-Def) over West Africa. JJA, June-July-August; DJF,

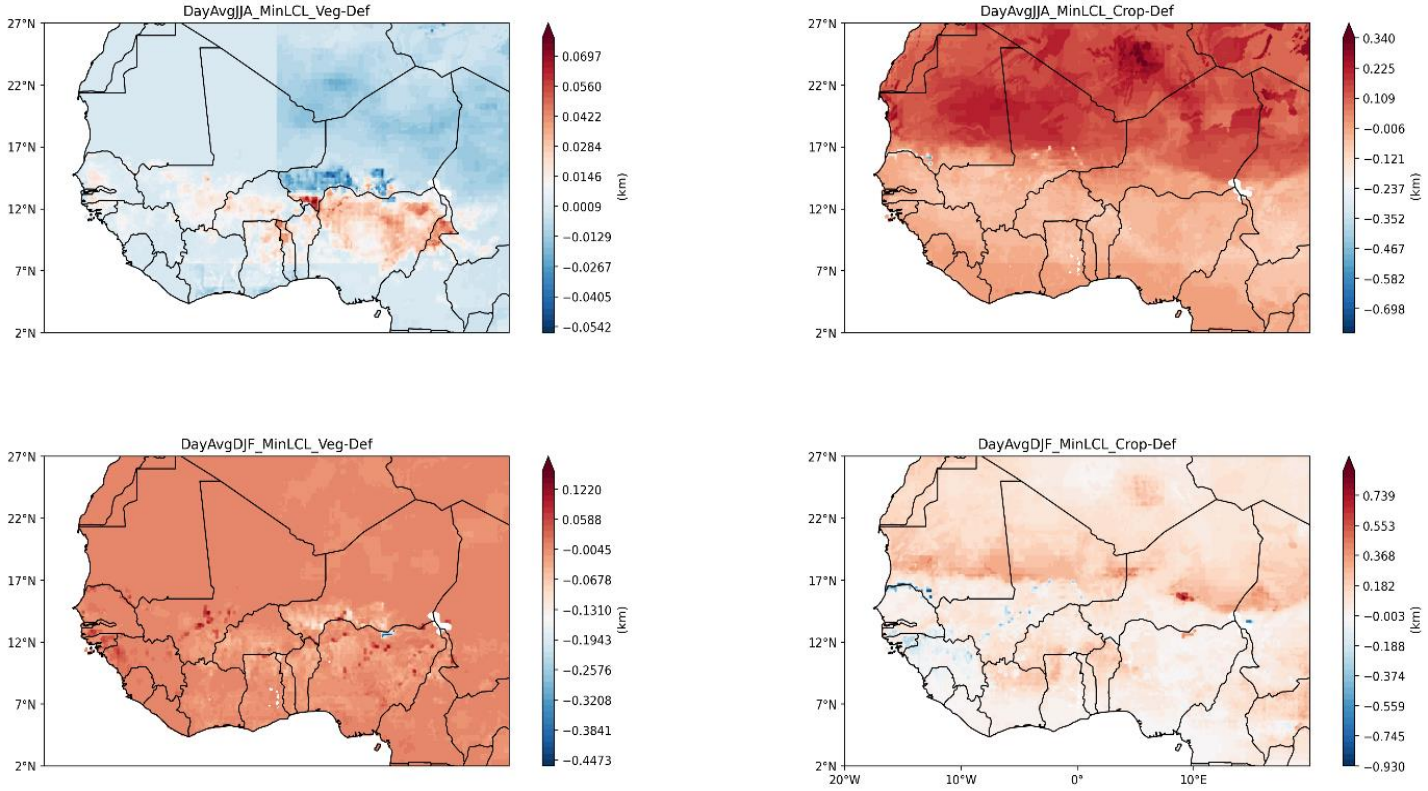

Figure 4.17 : Difference for minimum daily average over JJA and DJF seasonal LCL between vegetation and default (Veg-Def), and between crop and default (Crop-Def) over West Africa. JJA, June-July-August; DJF,

The next step in this study is to assess the relationship between the lifting condensation level height, the cloud base and the monsoon cycle over the West Africa. There are several unique features of the climate over West Africa. Annual rainfall is almost constant at all latitudes. However, from about 1500 mm near the coast at 5^{o}N to about 20^{o}N, annual rainfall decreases sharply from south to north, with a gradient of about 1 mm per km. The months of June, July, August and September (JJAS) are roughly the rainy season. As a result, the length of the dry season, although variable, is generally longer than that of the rainy season. Figure 4.12 show the rainfall pattern during the monsoon cycle. During that Period JJAS, the high of LCL is observe to decrease as the monsoon progresses. During the dry season December, January and February (DJF), the high of LCL height is higher. The LCL height is related to the cloud base height, so a high (low) LCL height implies more high (low) clouds, which is usually associated with less (more) cloud moisture, less (more) precipitation, lower (higher) cloud albedo, and more (less) solar radiation that reacts with the ground (Wei et al. 2021).

In this study, vegetation types are grouped into ten natural plant functional types (PFTs), such as evergreen and deciduous trees, C4 and C3 grasses, and crop PFTs are grouped into two super-grasslands, bare soil, plant C3 and C4. Crop PFTs differ from natural grasses only in their specified height carboxylation and Rubisco replenishment rates. A number of PFTs can be found in the same grid (mosaic vegetation). These PFTs share the same climate forcing, but land surface fluxes are calculated according to their own properties (de Noblet-Ducoudré et al., 2004). Vegetation and crop parameterisation in the eCLM model is static, not dynamic. The conversion of vegetation (forest) PFT to cropland (agriculture) changes the distribution of net radiation between latent and sensible heat fluxes (Pielke et al., 2002). The decrease in transpiration from cropland

leads to a decrease in cloud formation over the WA and, in contrast, an increase in the height of the LCL.

When West Africa default land cover is change and covered only by crop PFT, the LCL height will be higher, implying more very high clouds associated with very low cloud moisture, resulting in very little precipitation over the region of West Africa. On the other hand, when WA land cover landscape is change and covered only by vegetation, then the LCL height will be lower than the crop PFT, implying fewer high clouds and therefore a slight increase in cloud moisture associated with a slight increase in precipitation. According to Boone et al. (2016), the change from vegetation land cover state to crop PFT mostly leads to an increase in the Bowen ratio and a decrease in net radiation, and a significant decrease in surface evaporation especially over the Sahelian region. This in turn leads to a decrease in the convergence of moisture and precipitation. Yu et al. (2021) show that vegetation dynamics, through their interaction with climate, significantly increase precipitation in the region around the expected vegetation growth limit. Thus, the vegetation response affects the seasonal variation of precipitation changes, increasing precipitation before and after the monsoon season and decreasing precipitation during the peak of the monsoon season.

4.1.8 Role of Plant functional type (PFTs) on LCL height and present day climate

Figure 4.18 and Figure 4.19 show the correlation diagram plot of the major impacts linking the LCL height sensible, latent heat, net solar radiation, relative humidity and evaporative fractional over Kayoro in Ghana (Figure 4.18) characterise of crop land and Nazinga in Burkina Faso (Figure 4.19) characterise of trees, woodland and grassland. The circle symbol define the positive /negative and the strength of correlation. The red circle mean a negative correlation, and the blue a positive correlation. The red dark and blue dark design the strength of correlation (negative and positive).

The study assesses the contribution of three PFTs (default, vegetation and cropland) to lifting condensation level (LCL) height, cloud base formation and precipitation events over West Africa. LCL has long been used to express cloud base height (Stackpole 1967). Cloud formation is responsible for the current climate event. Pielke (2001) examines the various links between surface moisture, surface heat fluxes and convective cloud precipitation. They found a significant decrease in the sensible heat flux to the atmosphere during the cold winter and spring, which may be related to the decrease in winter precipitation observed across the agricultural region. The role of land cover type or plant functional type cannot be ignored. Based on the above analysis, the contribution of vegetation land cover to the formation of cloud base height is different from that of cropland and the default (urban PFT) over West Africa. Chase et al. (2000) simulate the General Circulation Model (GCM) and show that a change in land cover type, from cropland to vegetation PFT or from vegetation to cropland PFT, can lead to a change in surface fluxes elsewhere in the region. Changing the West African landscape from default (urban PFTs) or vegetation (forest PFTs) to cropland changes the partitioning of net radiation into the corresponding latent and sensible heat fluxes. There is a strong correlation between land surface fluxes, soil moisture and LCL height (LCL-LH, LCL-SH, LCL-EF) (Figure).

Higher LH usually leads to low LCL during JJA and low LH leads to higher LCL during DJF. Higher LH provides more moisture to the atmosphere and lowers LCL, whereas higher SH leads to higher LCL during the JJA wet season and lower LCL during the DJF dry season and lower near-surface humidity (Santanello et al., 2011; Wei et al., 2021). Thus, changes in water and energy fluxes may directly affect soil moisture and surface fluxes, which may also affect LCL height (Wei et al., 2021). Changes in the WA landscape from vegetation to cropland are associated with reduced transpiration, resulting in

reduced storm activity over the region (Pielke et al., 2002). The mean minimum LCL height is 2.2 km and the mean maximum LCL height is 4.5 km. The change in standard PFTs to cropland may lead to a reduction in rainfall over the Guinea and Soudan region of West Africa, which is already characterised by forest, savannah and grassland, and an increase in humidity and mean precipitation over the Sahel region. Research by Charney (1975) shows that the reduction of vegetation in the Sahel could lead to an increase in albedo and a decrease in precipitation, which could then trigger a positive feedback with drought in the region. As the region is transformed with irrigated cropland, this will reduce albedo and LCL and increase precipitation over the region.

The natural vegetation of West Africa varies from rough grass on the desert border (Sahelian region) to humid rainforest on the southern border of the region near the Atlantic coast (Guinean region). The intermediate zone (Sudan region) is occupied by several vegetation zones, ranging from tropical forest to woodland, savannah, scrub and short grass. Change of WA landscape from default (urban) or cropland to vegetation PFTs by assuming the vegetation to be static in the eCLM model simulation. Zheng and Eltahir (1998) study the role of vegetation in the dynamics of the West African monsoon and their results show the development of a robust monsoon circulation and that vegetation cover on the coast of West Africa has a significantly greater influence on the simulated monsoon than vegetation cover near the desert margin. Vegetation in the form of dense forests increases net surface radiation and sensible and latent heat fluxes. These fluxes are strongly correlated with the lifting condensation level (LCL) (Figure 4.18 and Figure 4.19).

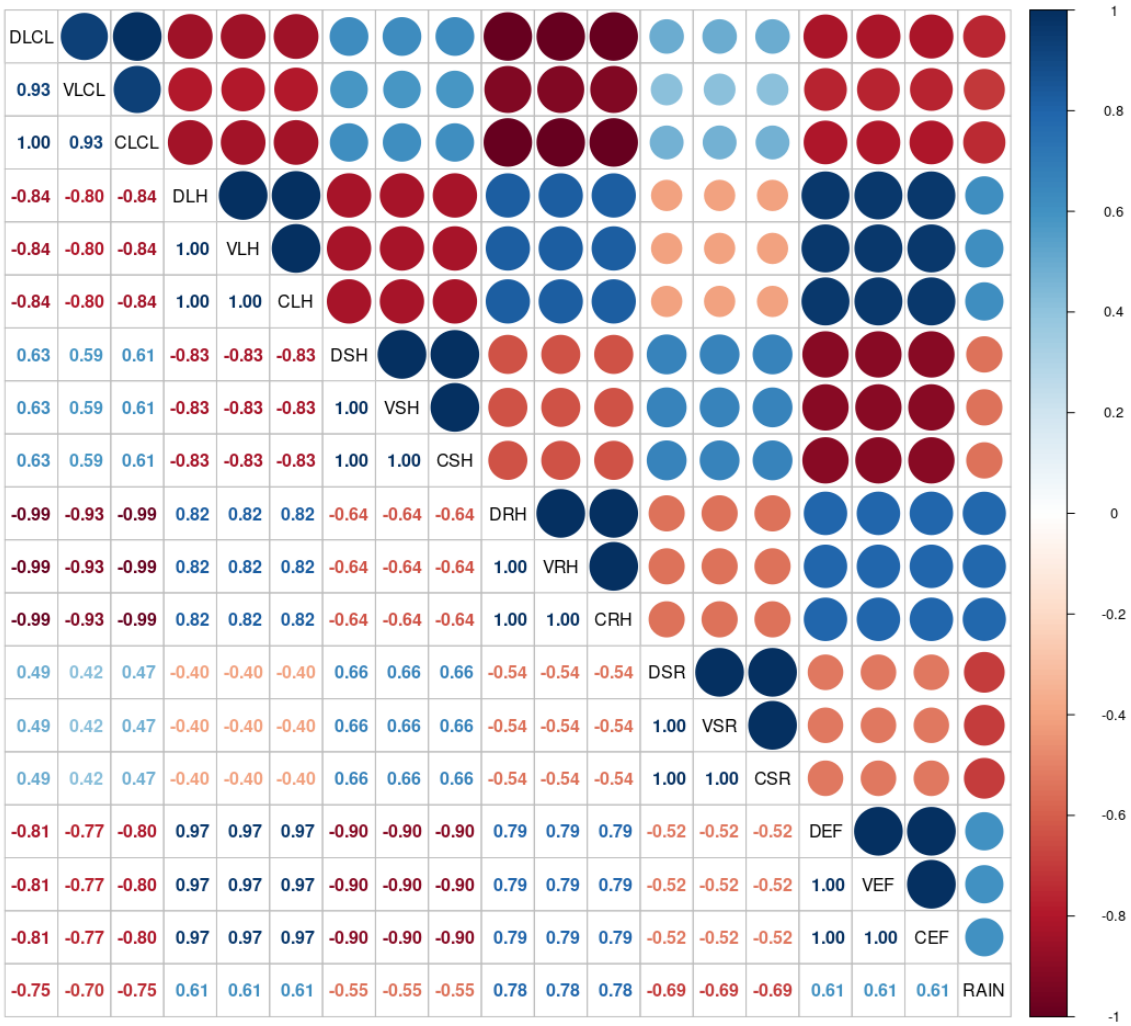

Figure 4.18. Correlation plot of the 14 years averages surface fluxes (latent LH and sensible SH heat), net radiation (SR), relative humidity (RH), evaporative fraction (EF), and LCL height in West Africa during the periods 2000-2013 in Kayoro, Ghana characterise with cropland (Dark blue colour reveal a strong positive correlation, medium light blue show a low positive correlation, light blue show a low positive correlation while the contrast in red colour

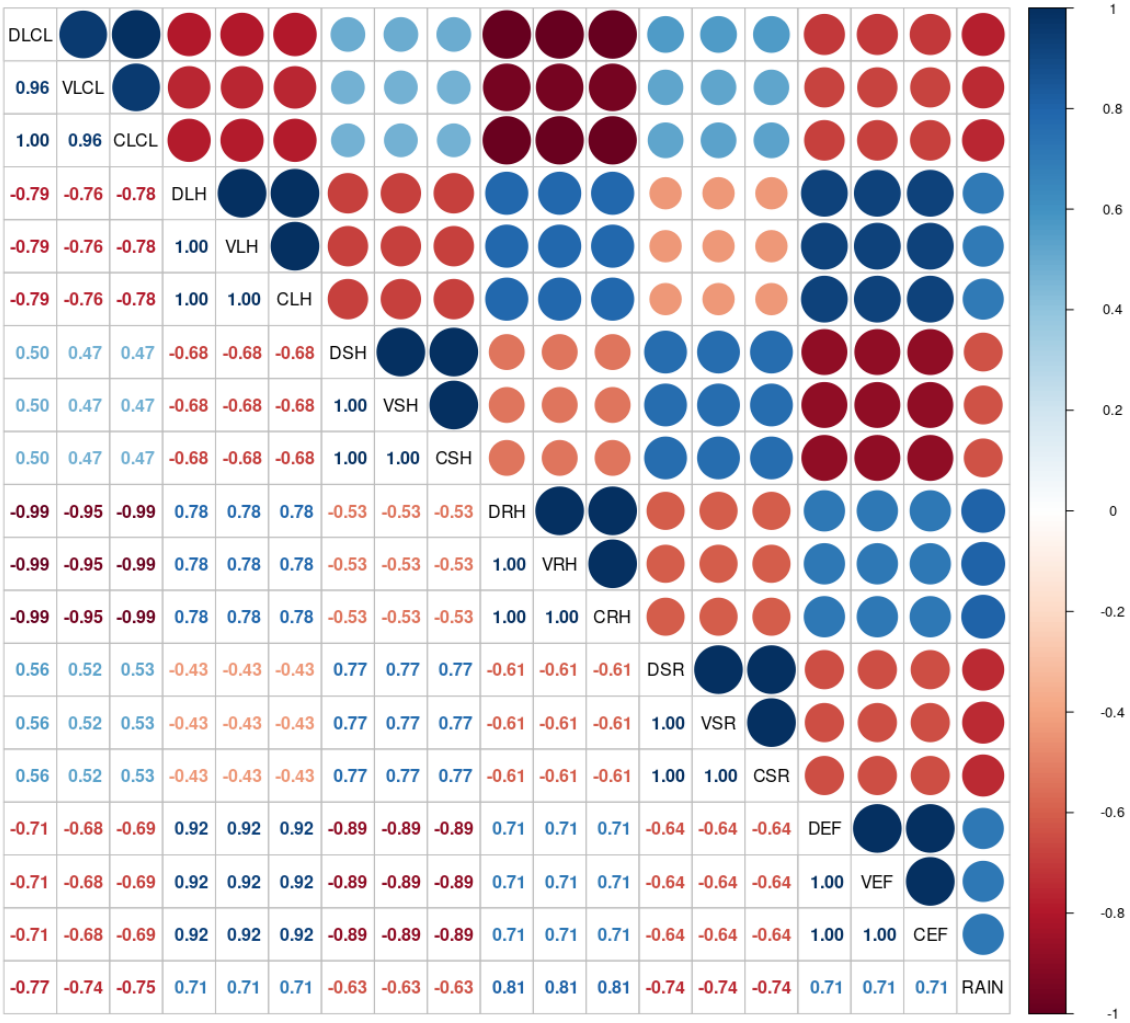

Figure 4.19. Correlation plot of the 14 years averages surface fluxes (latent LH and sensible SH heat), net radiation (SR), relative humidity (RH), evaporative fraction (EF), and LCL height in West Africa during the periods 2000-2013 in Bontioli, Burkina-Faso characterise with trees and grassland. Dark blue colour reveal a strong positive correlation, medium light blue show a low positive correlation, light blue show a low positive correlation while the contrast in red colour

A high SH generally results in a higher LCL due to the entrainment of warm, dry air and lower humidity near the surface, while a high LH provides more latent heat. atmospheric moisture and lowers the LCL (Wei et al., 2021). These fluxes supply energy and entropy to the boundary layer and generate a significant gradient of entropy between the land and the ocean, which is the driving factor in the monsoon circulation.

Due to many positive and negative feedbacks, changes in vegetation composition can have significant effects on climate, not only at regional but also at global scales. In particular, conversion of WA vegetation PFT landscape to cropland PFT landscape can increase surface albedo (Myhre and Myhre, 2003) and reduce evapotranspiration because grasses and annual crops do not have access to as much soil water for transpiration as native vegetation/trees. The increase in albedo leads to a reduction in surface shortwave radiation (SSR) and hence surface temperatures. In a negative feedback loop, lower surface temperatures further reduce evapotranspiration, resulting in less latent cooling and more sensible heat to rewarm the surface. In temperate and boreal regions, albedo-driven cooling is often considered to be the dominant factor (Govindasamy et al., 2001; Bounoua et al., 2002; Matthews et al., 2004; Brovkin et al., 2006; Bala et al., 2007). Reduced evapotranspiration is particularly important in the (sub)tropics. This is partly because it reduces convective cloud formation and hence convective precipitation. The LCL height is similar to the cloud base height, so a higher (lower) LCL height implies more high (low) clouds, which is usually associated with less (more) cloud moisture, less (more) precipitation, lower (higher) cloud albedo and more (less) downward solar radiation at the surface. Conversely, a lower LCL height implies more low clouds, which is usually associated with more cloud moisture, more precipitation, higher cloud albedo and less downward solar radiation at the surface.

4.2 Parameterisation of APSIM-ORYZA model

4.2.1 Model calibration output

APSIM-Oryza was calibrated for rice varieties during production in the 2019 season using data collected from selected farmers during the visit. Calibrating APSIM-Oryza allows accurate prediction of anthesis and maturity of rice varieties. Specific parameters, such as sowing date, plant density per hill and observation of initial soil water and soil nitrogen conditions, were used to initialise APSIM-Oryza. Phenology parameters to match simulated development stages and maturity dates with observed conditions were then derived by trial and error. In order to obtain accurate leaf area expansion and biomass production under different climatic conditions, it is very important to adjust the parameters of minimum relative leaf area growth rate and maximum relative leaf area growth rate. The observed and simulated crop characteristics after calibrating are shown below in Figure 4.20(Calibration a,b) which shows good agreement correlation between observed and simulated values.

4.2.2 Model validation output

Data collected from farmers in Lokakpli during the 2019 growing season, which were not used for model calibration, were used to validate the performance of the APSIM-Oryza model. Crop variables were used to validate crop phenology and grain yield. During the 2019 growing season, which was used for model validation, the phenology of rice varieties ranged from 103 to 130 days after sowing (DAS). Observed rice physiological maturity ranged from 104-143 DAS. As shown in Figure 3, the model simulated the anthesis date with good accuracy and model efficiency (ME > 97%). The RMSE (5 days), normalised RMSE (5%), ME (97.91%), R^2 (0.85) and PBIAS (2) values confirm the model robustness (Figure 4.20 validation a).

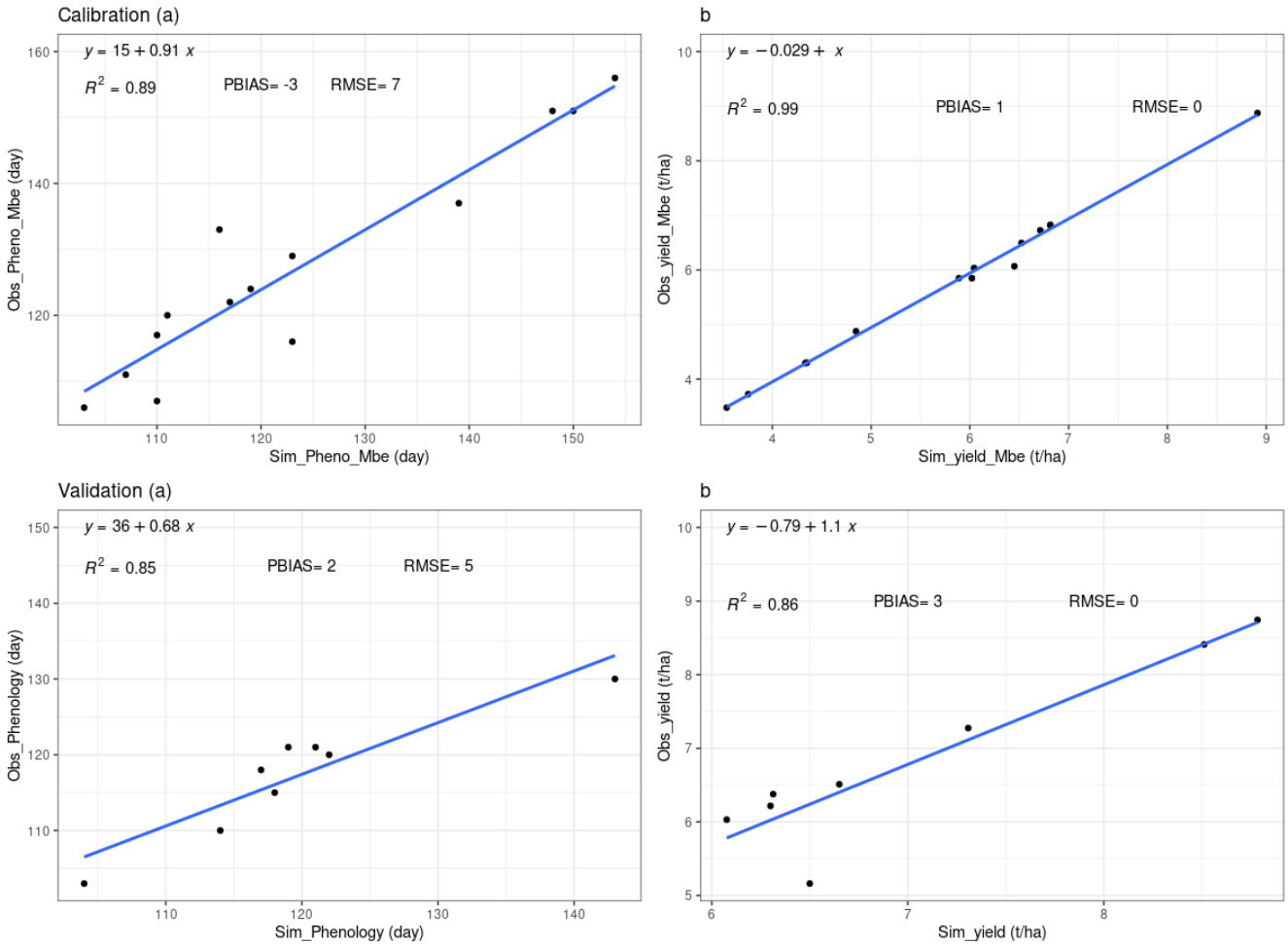

Figure 4.20 : Evaluation metric for APSIM-Oryza model calibration and validation

Table **4:2**. Model evaluation statistics after calibration and validation showing Model efficiency (ME), root-mean-square error percentage (RMSE), and percent bias (PBIAS) for yield and phenology, and the coefficient of determination R^2.

Model	Observed mean	Simulated mean	ME	RMSE	PBIAS	R^2
Calibration						
Rice grain Yield ($t\ ha^{-1}$)	5.7	5.8	1	0	1	0.99
Rice Phenology (day)	127	123	0.83	7	-3	0.89
Validation						
Rice phenology (day)	120	117	97.91	5	2	0.85
Rice yield ($t\ ha^{-1}$)	6.84	6.89	100	3	3	0.86

APSIM-Oryza is a very good simulator of rice yield. Simulated grain yield ranged from 5.2 to 8.9 t/ha, close to observed yield (5.2 to 8.7 t/ha) in crop year 2019. The observed and simulated rice yields were in good agreement. The robustness of the APSIM-Oryza model to simulate grain yield with high accuracy is confirmed by the model evaluation metrics RMSE (0 t/ha), normalised RMSE (8%), PBIAS (1) and ME (100%), R2 (0.99) (Figure 4.20 validation b).

Several work have been done calibrating and validating APSIM-Oryza in different climate condition. However, none were done calibrating and validating APSIM-Oryza under West Africa climate and soil condition using farmers' rice production dataset. Simulation outcomes from APSIM-Oryza in our findings showed that the model can be used as suitable tool in the selection of appropriate cultivars and to investigate the effect of climate change on rice growth and yield, and set up a model base approach to propose the best alternative management practices to farmers to mitigate climate change impact. Phenology of rice parameterised in Oryza rice module has a strong influence on development and grain yield of the cultivar. In our case studies, APSIM-Oryza predicted phenology stages close to the observed values (Gaydon et al., 2017). Model evaluation metric confirmed the robustness of APSIM-Oryza to simulate the phenology of rice (Figure 3C). Therefore, to calibrate the phenology of rice in APSIM-Oryza, a particular parameters s (DVRJ, DVRI, DVRP, DVRR) are very important to be considered (Liu et al., 2019). Calibration and validation of APSIM-Oryza (Liu et al., 2019; Ahmed et al., 2017; Gaydon et al., 2017; Gaydon, 2014) simulation indicated good to fair predictions of development and maturity time of rice cultivar as indicated by the different validation metrics scores. The results of the validation were used to project rice yield under climate condition in Cote d'Ivoire, which will be discuss in the next section

4.2.3 Performance of Bias-Correction Methods

4.2.3.1 Precipitation

For the evaluation of the capability of the CORDEX data in crop model simulations, precipitation and maximum and minimum temperatures from the GCM output are used in APSIM-Oryza. Only the delta change has the best performance when applying the different bias correction methods. It is assumed that if the original GCM output simulation is close to the observed one, the GCM results have small biases that can be overcome by calibrating the model. For the four models (CNRM-CM5, HadGEM2-ES, MPI and NOAA), the statistics resulting from the bias correction show an overall good result. Generally, there is a significant correlation between the simulated GCM and the site observations. Similarly, the GCM simulations are in line with the observations. The statistical outcome during the model simulation, in Mbe, the R^2 value gives 0.99, the NSE value gives 0.99, the RMSE value gives 0 and the PBIAS value gives 0.

In this study, 8 bias-corrected methods were applied and only the delta change map significantly improved the simulated precipitation time series, as confirmed by the fit. This is also the case for the statistics based on the frequency and the time series. Figure 4.22 shows the graphical comparison plot for the seasonal cycle between the observed, raw and bias-corrected forecast statistics for precipitation. The mean precipitation for both seasons is significantly underestimated by the raw historical data for the four models. The mean precipitation varies from 0.14 mm to 2.3 mm for the dry season and from 5.57 mm to 6.14 mm for the rainy season. The standard deviation is higher for the wet season, at 9.14, compared to 7.39 for the dry season. The historical data are strongly underestimates of the observations for the for model. The role of the variability coefficient is to measure the level of distribution around the mean, indicating the higher

value for historical series compared to observed data for dry and wet seasons. In a similar way to the mean, the 90th percentiles show the same distribution for both the dry and the wet seasons (Figure 4.21).

4.2.3.2 Minimum and maximum temperature

Figure 4.24 graphically compares the observations, historical raw and bias-corrected daily minimum temperatures for the dry/wet periods for the four GCMs. For the dry (March) and wet (August) seasons, the biased corrected value is almost similar to the observed data, while the opposite is observed for the historical raw value. The average (26.68 in March, 20.76 in August) of the historical raw values tends to overestimate the average of the observations for each season (23.14 in March, 22.61 in August). The same can be seen for the SD, where the historical raw SD for the dry period is 2.29, overestimating the SD of the observations, which is 1.18, while for the wet period in August, both the observations and the historical raw SD have the same SD. Nevertheless, during dry March, historical CVs are slightly higher at 23.94 than observed CVs at 21.83. Similar results are found for 90th percentile for both seasons, where calculated historical raw values overestimate observations. However, all historical raw values are found to agree with the observed data (Figure 4.23). The R2, NSE, RMSE and PBIAS values for the observed and historical raw data are identical for the four models from a time series based statistics point of view, unlike for precipitation. After applying the bias correction method to the delta change map, the performance of all four models was generally very good.

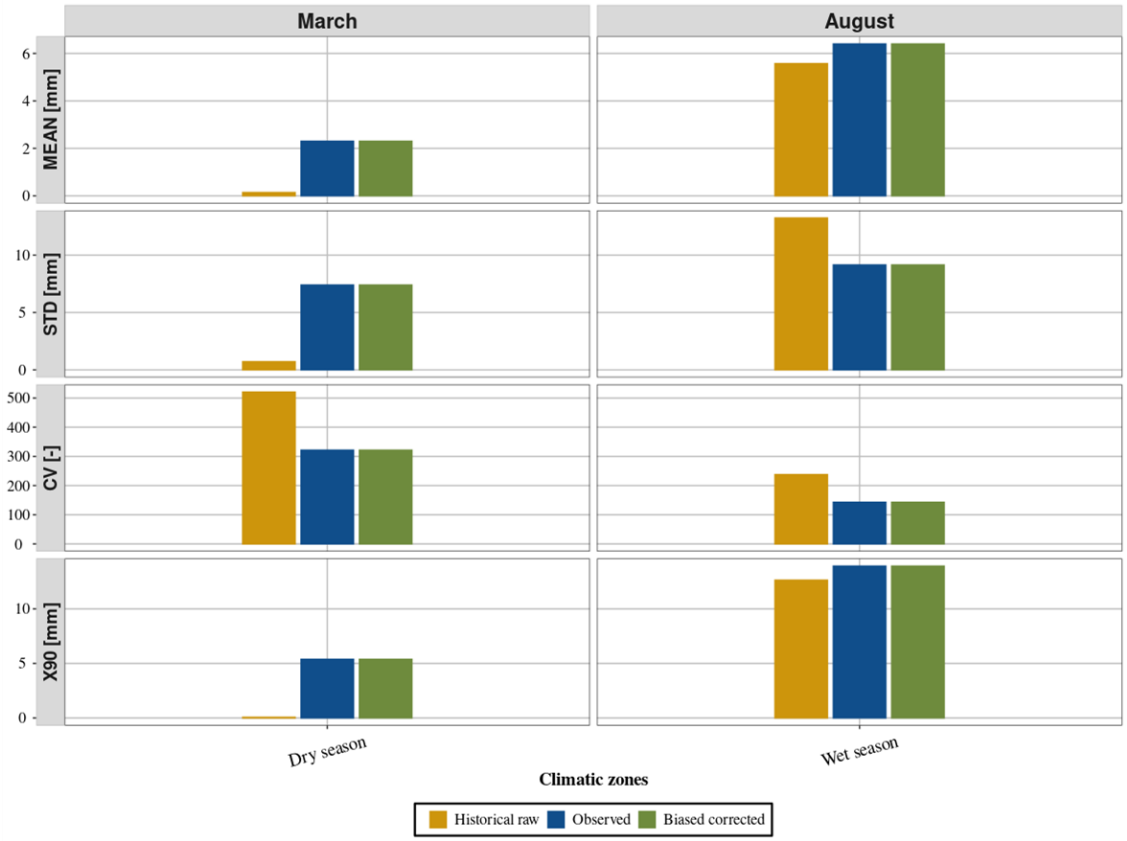

Figure 4.21. Relationship between the ensemble of the raw simulation, observed and bias-corrected daily precipitation series, measured by the mean, standard deviation (STD) and 90th percentile (X90) for the months of March (dry season) and August (wet season).

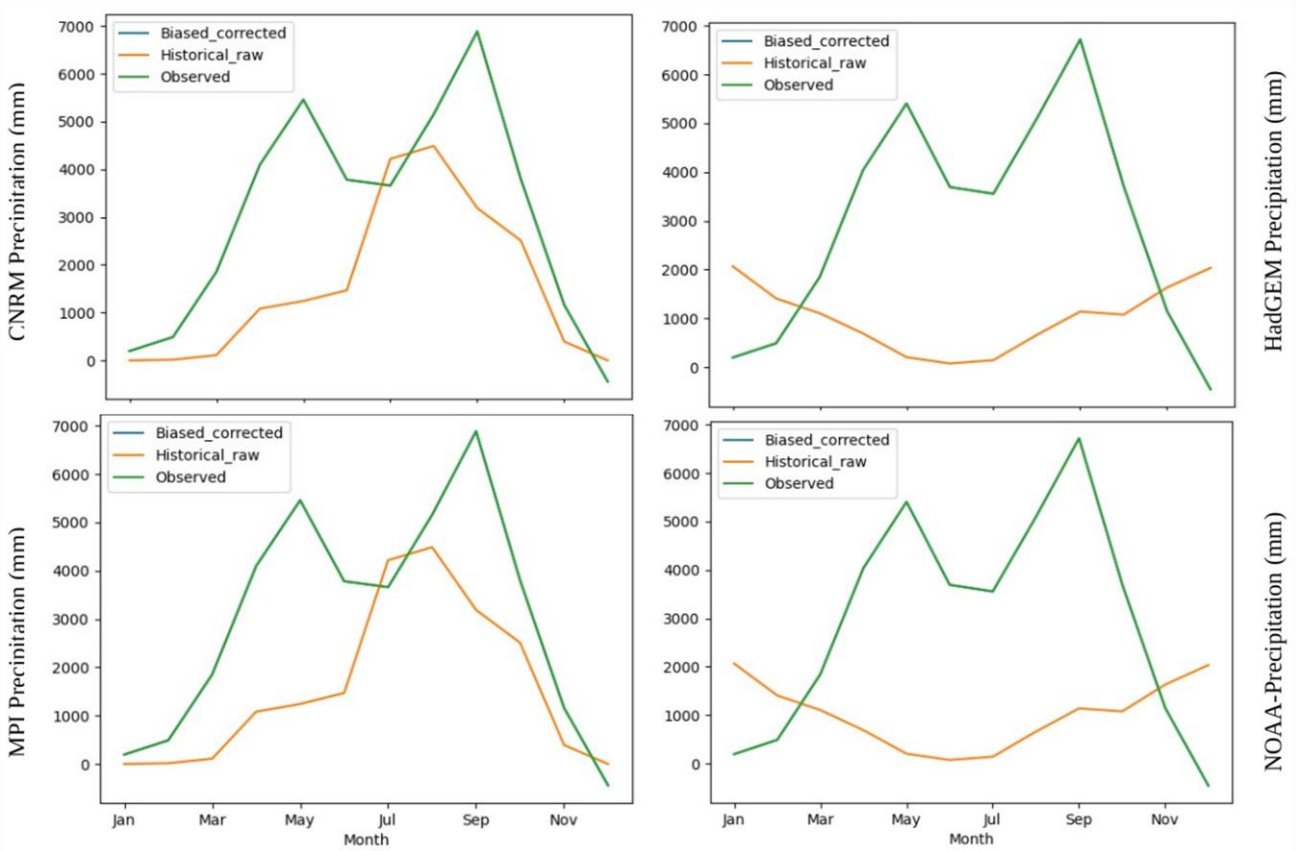

Figure 4.22. Seasonal cycle of precipitation bias correction for the four models (CNRM-CM5, HadGEM2-ES, MPI and NOAA)

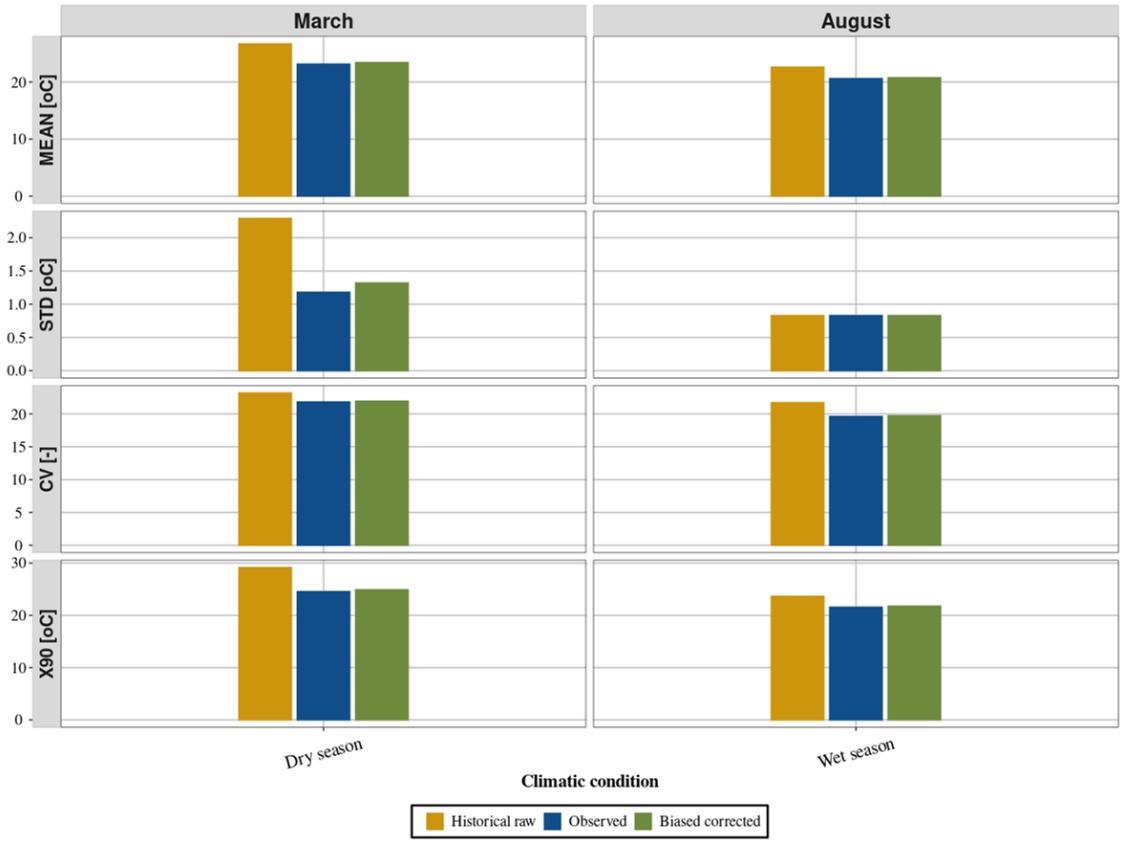

Figure 4.23. Relationship between the ensemble of raw simulation, observed and bias-corrected daily series of minimum temperature measured by mean, sta dard deviation (STD) and 90th percentile (X90) for the months of March (dry season) and August (wet season).

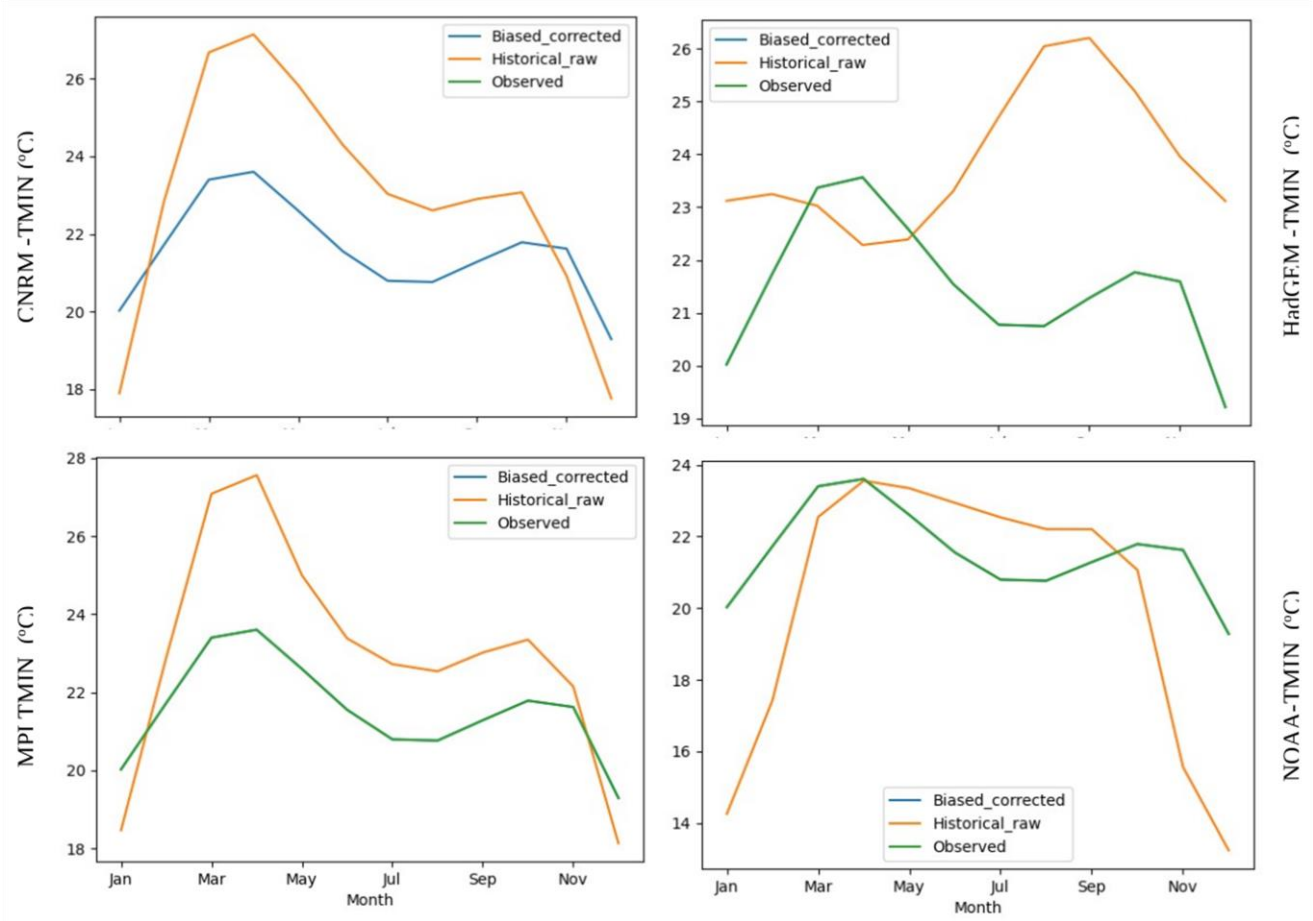

Figure 4.24. Seasonal cycle of minimum temperature bias correction for the four models (CNRM-CM5, HadGEM2-ES, MPI and NOAA)

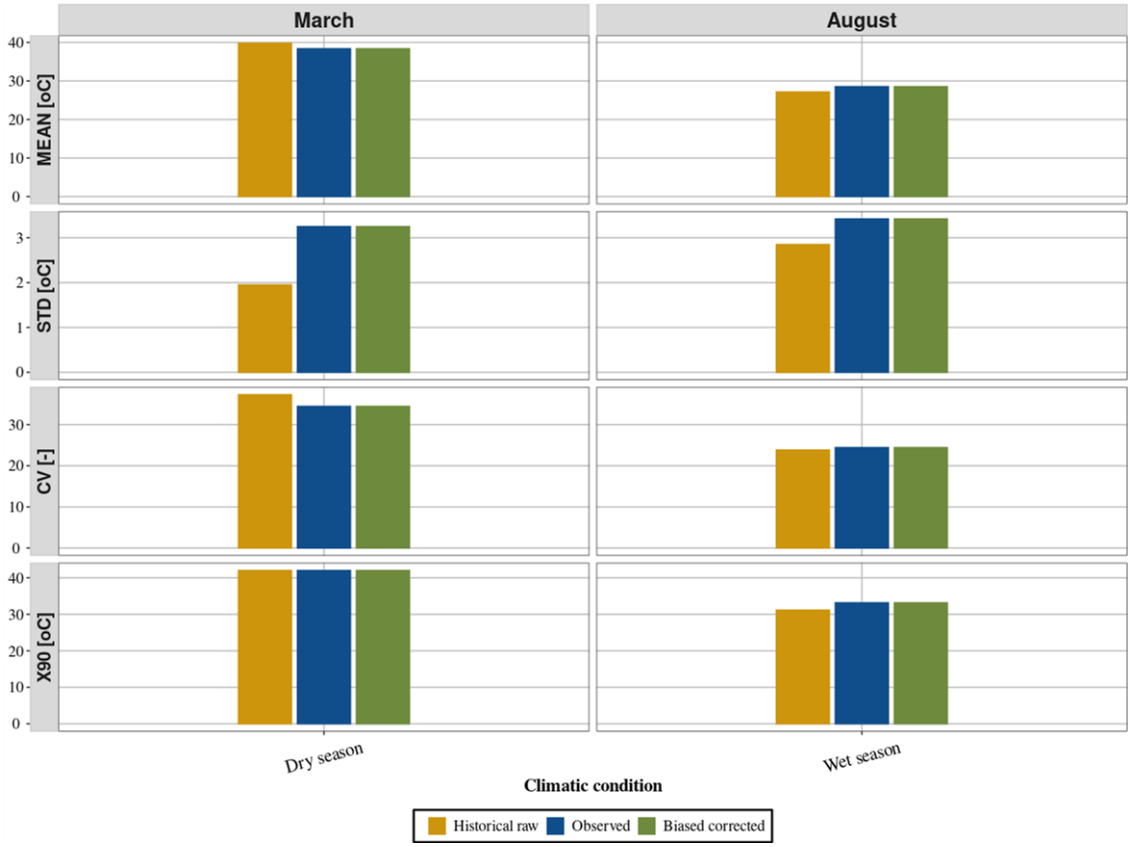

Figure 4.25. Relationship between the ensemble of raw simulation, observed and bias-corrected daily series of maximum temperature measured by mean, standard deviation (STD) and 90th percentile (X90) for the months of March (dry season) and August (wet season)

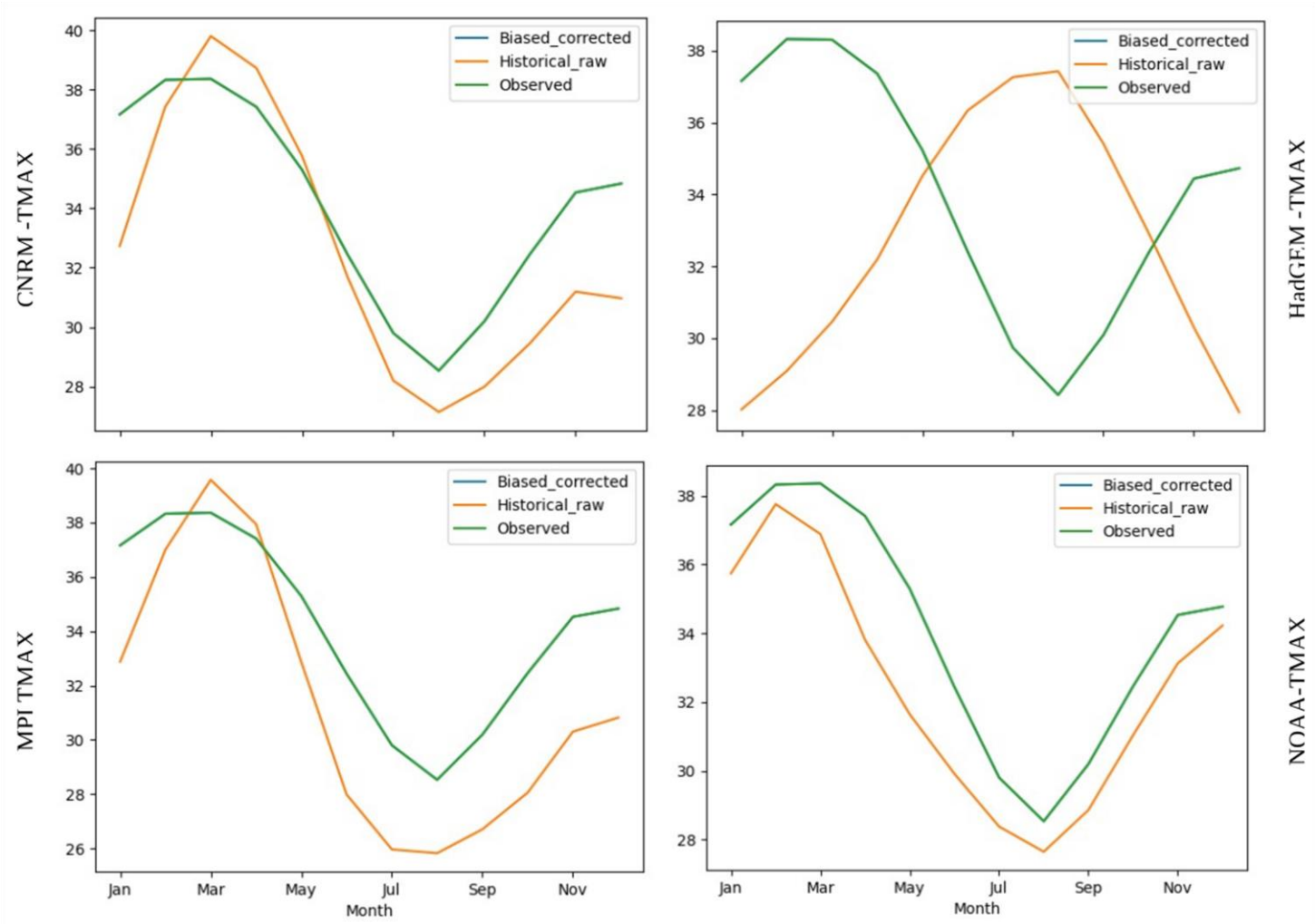

Figure 4.26. : Seasonal cycle of maximum temperature for the four model (CNRM-CM5, HadGEM2-ES, MPI and NOAA)

The comparison between the historical raw values of the GCM maximum temperature simulations and the observed data is shown in Figure 4.26. The historical raw values are for the most part lower than the observed maximum temperature values. The bias-corrected statistics based on the time series for the maximum temperature perform very well and the result is identical to the statistics based on the time series for the precipitation. Furthermore, in terms of statistical and graphical output, the bias-corrected and observed data are similar. The bias-corrected historical mean (39.8 °C) slightly overestimates the observed mean (38.36 °C) for the dry season (March), while our observed mean (28.53 °C) slightly overestimates the bias-corrected mean (27.14 °C) for the wet season.

4.2.3.3 Projected changes in the main precipitation parameters

Projected changes in annual rainfall over this century (2021 - 2100) relative to baseline (2019) under RCP4.5 and RCP8.5 emission scenarios are shown in Table 5. It seems that Bouake, Cote d'Ivoire is likely to feature increased rainfalls during the current century under both RCP 4.5 and RCP 8.5 emission scenarios. The projected change in rainfall during the century depend of the different GCMs over the study area. During the period of 2021-2100, the annual rainfall is feature to decreased by 50.95%, 58.53% and 53.32% with the models CNRM-CM5, HadGEM2-ES, and MPI respectively, while it projected to increase by 7.97% with the model NOAA compare to the baseline (2019) under the RCP 4.5 emission scenarios (Figure 4.27). The projected changes in the annual and seasonal rainfall for the periods 2021-2100 under the RCP 8.5 emission scenarios compare to the baseline are largely similar. Thus, the annual rainfall is projected to decrease by 28.77%, 30.95% and 66.29% with the model CNRM-CM5, HadGEM2-ES, and MPI respectively, while it projected to increase by 17.55% with the model NOAA under the same RCP 8.5 emission scenarios (Table 4:4).

Projection of the future climate changes is of paramount importance inasmuch as it contributes to provide useful information for adaptation planning worldwide to local scales. This study investigate the future change of climate in rice yield using CORDEX-Africa (historical and forecast dataset) ensemble simulation under the RCP 4.5 and RCP 8.5 emission scenarios. Prior of this study, the bias correction methos was apply to the dataset using the delta change method among the eight method using which give good statistical results. During the period of 2021-2100, the annual rainfall is feature to decreased with the models CNRM-CM5, HadGEM2-ES, and MPI, while it projected to increase with the model NOAA compare to the baseline (2019) under both RCP 4.5 and RCP 8.5 emission scenarios. This result is agree the founding of Ardoin-Bardin et al. (2009) ; Kouakou et al. (2012); Soro et al. (2017); Bamba et al. (2023), whose studies focus on the variability of projected climate in Cote d'Ivoire and West Africa.

Bamba et al. (2023) result project an increase of rainfall under the both RCP 4.5 and RCP 8.5 climate scenarios. Kouakou et al. (2012), using RegCM3 regional climate model show an downward of precipitation with a percentage change ranging from 2.50% to 4.90% on 2031-2040 and 2091-2100 horizon in Cote d'Ivoire. However, Soro et al. (2017) assess the future trends in monthly rainfall and temperature and its impact on surface groundwater resources using HadGEM2-ES future climate under RCP 4.5 and RCP 8.5 emission scenarios and found under the RCP 4.5 and RCP 8.5 emission scenarios, the rainfall is projected to decrease from December to April by 3% to 42% at all horizons under RCP 4.5 and by 5% to 47% under RCP 8.5. Nevertheless, seasonal rainfall in West Africa is projected to delayed and also remaining wetter by the end of the of 21st century (Serdeczny et al., 2015), but research conducted over West Africa show a good reproduction of rainfall except for HadCM3, which have real difficulty in accurately simulating rainfall (Kouakou et al., 2011). This confirmed our finding that project a

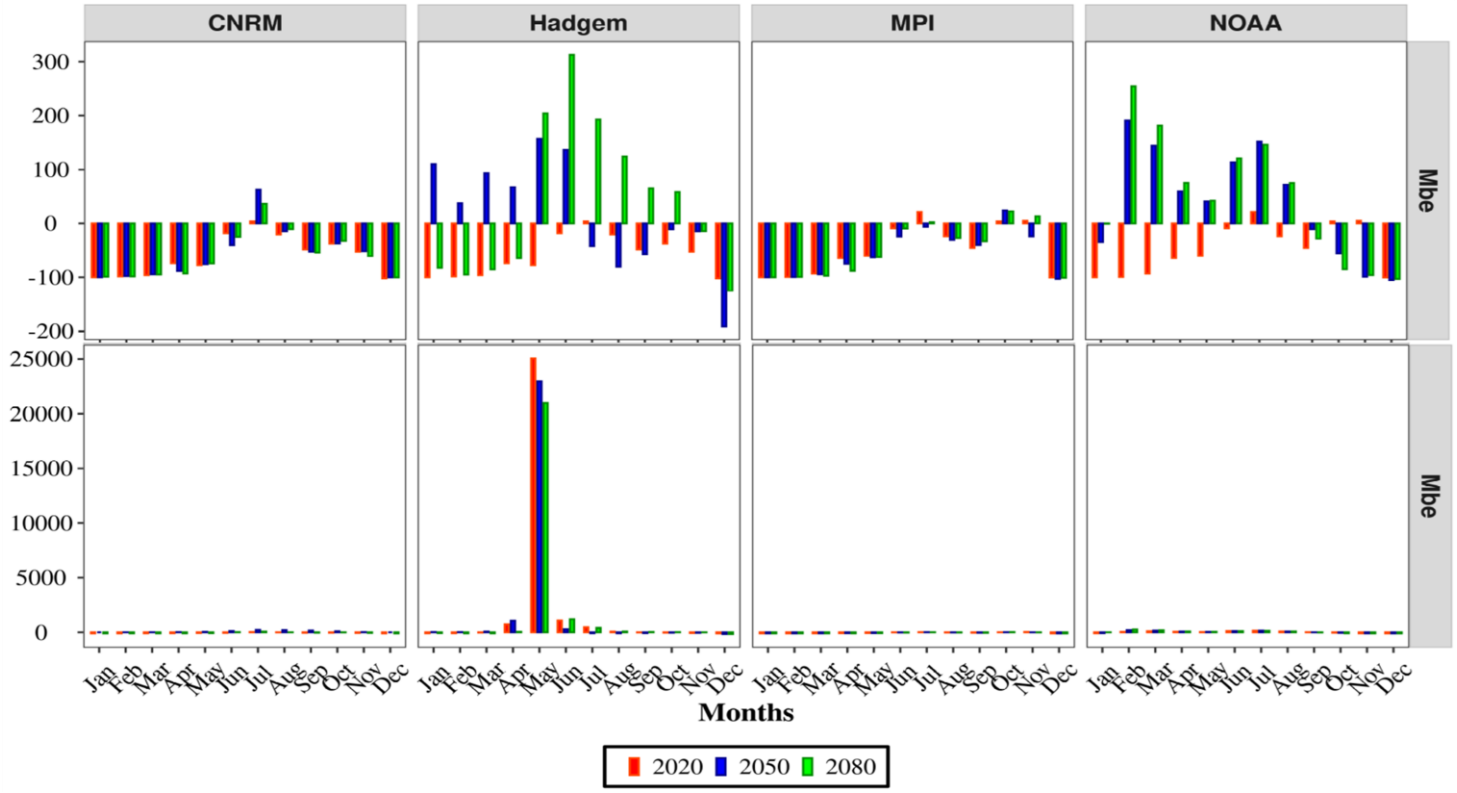

Figure 4.27. Mean monthly change of minimum temperature over the periods 2020s (2010–2040), 2050s (2041–2070) and 2080s (2071–2100) for the four GCMs under the RCP 4.5 (above) and RCP 8.5 (below) scenarios

decrease in rainfall over the study area with the three models CNRM-CM5, HadGEM2-ES, and MPI.

4.2.3.4 Projected changes in the main parameters for maximum and minimum temperature under scenarios RCP 4.5 and 8.5

In the 2021-2100 periods, the projected changes in the mean annual maximum (Tmax) and minimum (Tmin) temperature vary across both RCP 4.5 and RCP 8.5 emission scenarios as shown in Table 4:3. By 2012-2100 century, the mean annual minimum temperature will experience increase by 15,57% (3.13ºC), 15,87% (3.19ºC), 15,92% (3.20ºC) and 14,73% (2.96ºC) for the four model CNRM-CM5, HadGEM2-ES, MPI and NOAA respectively under the RCP 4.5 emission scenarios. The projected change in minimum temperature under RCP 8.5 emission scenarios compare to the baseline are largely the same (Table 4:3). Therefore, the projected annual average minimum temperature will increase throughout the study area by about 18,89% (4.31 ºC), 21,44% (4.31 ºC), 22,13% (4.45 ºC), and 17,55% (3.53 ºC) for the four GCMs respectively (Table 4:3, Figure 4.28). By 2021-2100 period century, the mean annual maximum temperature will increase by about 22,08% (6.91 ºC), 13,45% (4.21 ºC), 17,92% (5.61 ºC) and 17,92% (4.6 ºC) for the four GCMs respectively under the RCP 4.5 emission scenario, while under the RCP 8.5 emission scenarios, the mean maximum temperature will increase by 25,27% (7.91 ºC), 17,1% (5.35 ºC), 23,78% (7.44 ºC) and 20,13% (6.3 ºC) for CNRM-CM5, HadGEM2-ES, MPI and NOAA respectively (Table 4:3, Figure 4.29).

Result from our findings projected an increase in minimum and maximum temperature over the projected period 2021-2100 horizon under both RCP 4.5 and RCP 8.5 emission scenarios. This confirmed the report from ICPP which projected an increase of temperature by the future horizon. Finding from Soro et al. (2017) study show an increase

of temperature in all the month under the RCP 4.5 and RCP 8.5 and a higher crease in temperature under the RCP 8.5. Research work from Diffenbaugh and Giorgi (2012) base on climate change hotspots in the CMIP5 global climate model ensemble under both RCP 4.5 and RCP 8.5. the region will experience an increase of 1.2 in minimum temperature and a maximum temperature of about 1.7 oC by in 2025s. Work from Meehl et al. (2017); Diallo et al. (2012); Monerie et al. (2012) and Niang et al. (2014) base on change in the African monsoon using CMIP3 and CMIP5 models under climate scenarios emission in West Africa projected an increase in temperature ranging from 3 to 6 oC above the late 20th Century baseline. This confirm our finding where higher increase in minimum and maximum temperature is projected under both RCP 4.5 and RCP 8.5 in 2021-2100 Century (Table 6). The temperature is projected to increase more under RCP 8.5 than RCP 4.5 emission scenarios, and is in agreement with the finding from Ayele et al. (2016) Who has shown that the magnitude of temperature is higher for the higher emission scenarios of RCP 8.5 than for the medium–low emission scenarios of RCP 4.5.

Result from our findings projected an increase in minimum and maximum temperature over the projected period 2021-2100 horizon under both RCP 4.5 and RCP 8.5 emission scenarios. This confirmed the report from ICPP which projected an increase of temperature by the future horizon. Finding from Soro et al. (2017) study show an increase of temperature in all the month under the RCP 4.5 and RCP 8.5 and a higher crease in temperature under the RCP 8.5. Research work from Diffenbaugh and Giorgi (2012) base on climate change hotspots in the CMIP5 global climate model ensemble under both RCP 4.5 and RCP 8.5. the region will experience an increase of 1.2 in minimum temperature and a maximum temperature of about 1.7 oC by in 2025s. Work from Meehl et al. (2017); Diallo et al. (2012); Monerie et al. (2012) and Niang et al. (2014) base on change in the African monsoon using CMIP3 and CMIP5 models under climate scenarios emission in

Table 4:3. Changes (%) in precipitation, minimum and maximum temperatures during the growing season under the future climate scenarios compared to the baseline. The difference in temperature compare to the baseline is showing in parenthesis.

	RCP 4.5			RCP 8.5		
Models	Precipitation (mm)	Minimum temperature (° C)	Maximum temperature (° C)	Precipitation (mm)	Minimum temperature (° C)	Maximum temperature (° C)
CNRM-CM5	-50,95	15,57 (3.13)	22,08 (6.91)	-28,77	18,89 (4.31)	25,27 (7.91)
HadGEM 2-ES	-58,53	15,87 (3.19)	13,45 (4.21)	-30,95	21,44 (4.31)	17,1 (5.35)
MPI	-53,32	15,92 (3.20)	17,92 (5.61)	-66,29	22,13 (4.45)	23,78 (7.44)
NOAA	7,97	14,73 (2.96)	17,92 (4.6)	5,60	17,55 (3.53)	20,13 (6.3)

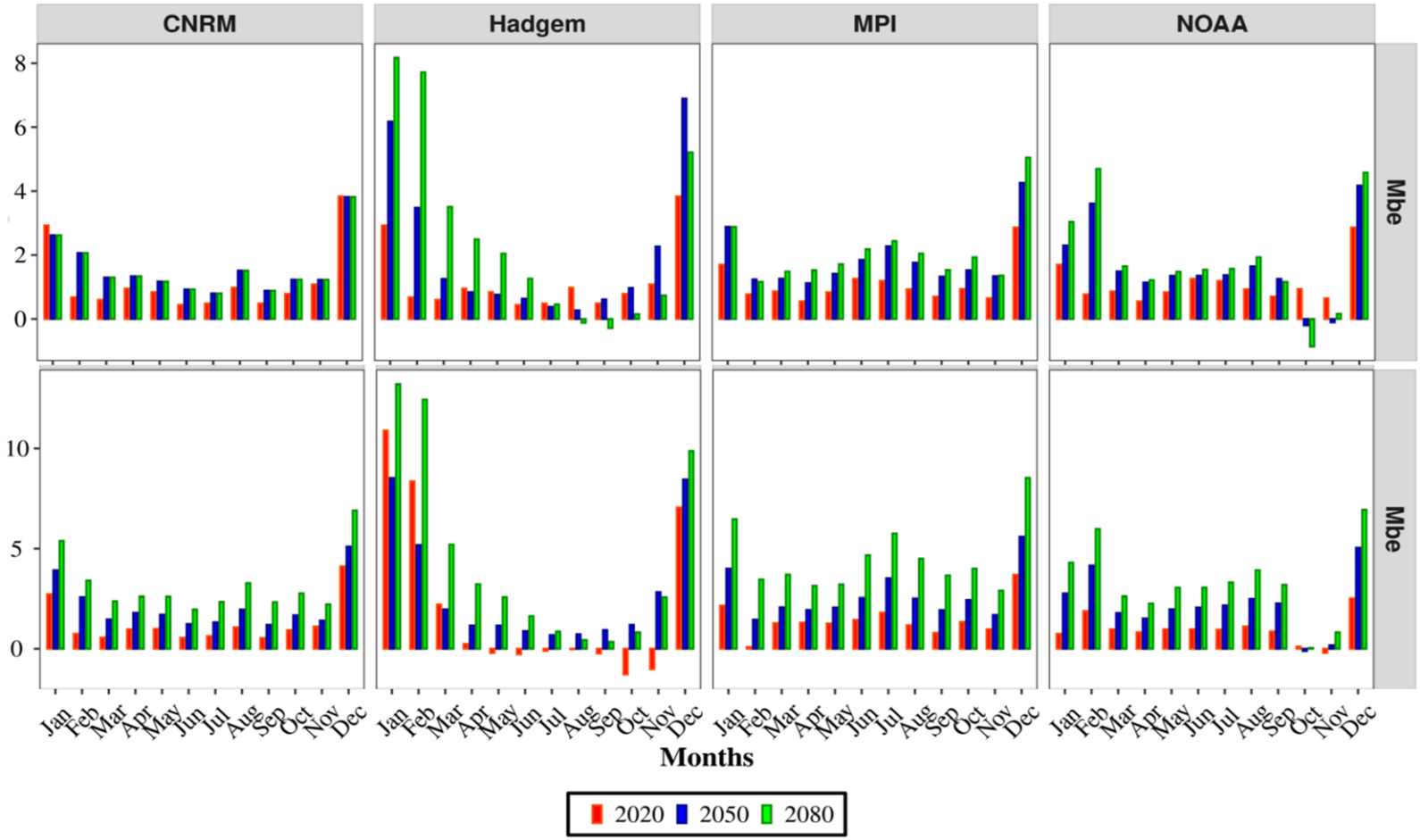

Figure 4.28. Mean monthly change of minimum temperature over the periods 2020s (2010–2040), 2050s (2041–2070) and 2080s (2071–2100) for the four GCMs under the RCP 4.5 (above) and RCP 8.5 (below) scenarios

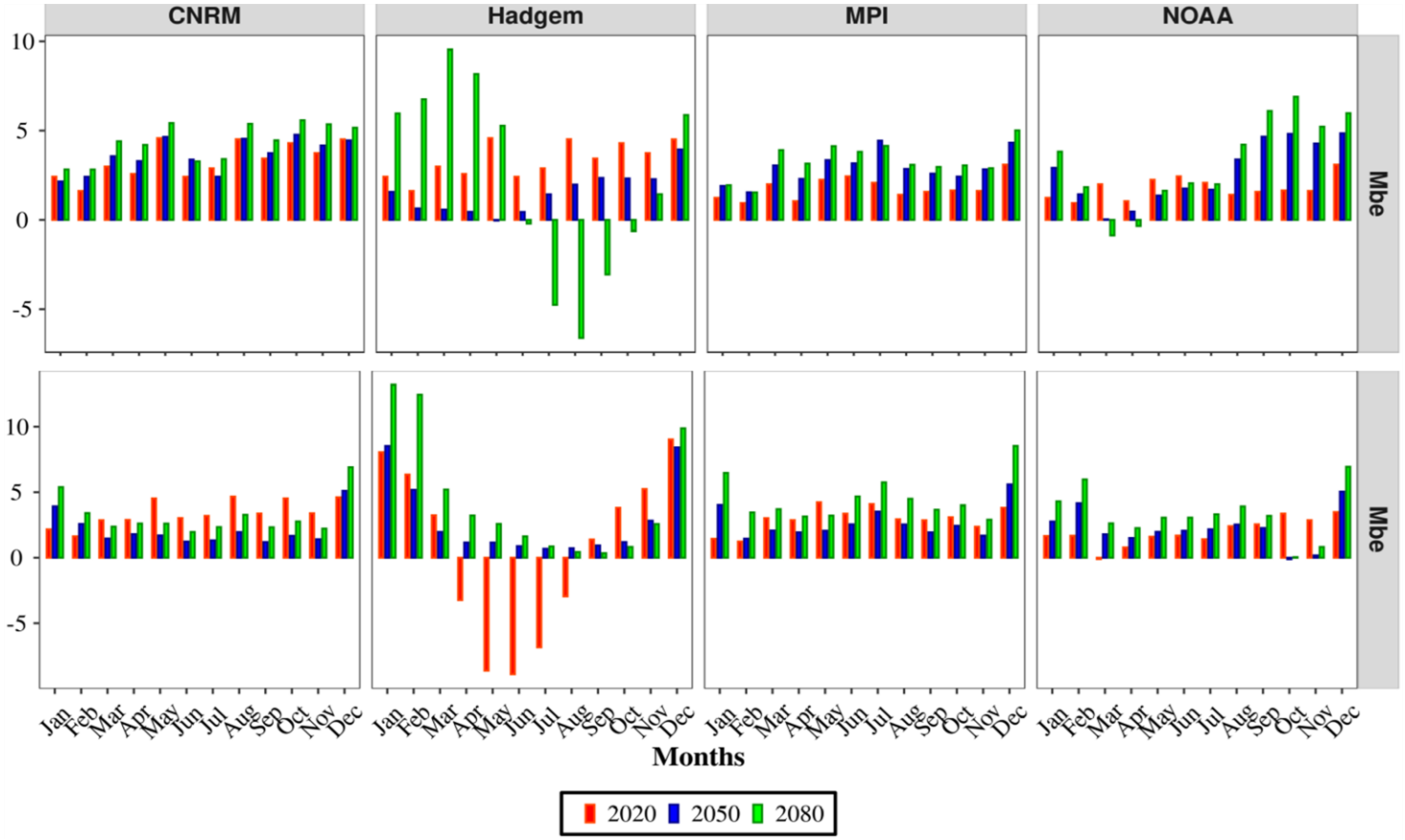

Figure 4.29. Mean monthly change of maximum temperature over the periods 2020s (2010–2040), 2050s (2041–2070) and 2080s (2071–2100) for the four GCMs under the RCP 4.5 (above) and RCP 8.5 (below) scenarios

West Africa projected an increase in temperature ranging from 3 to 6 oC above the late 20th Century baseline. This confirm our finding where higher increase in minimum and maximum temperature is projected under both RCP 4.5 and RCP 8.5 in 2021-2100 Century (Table 6). The temperature is projected to increase more under RCP 8.5 than RCP 4.5 emission scenarios, and is in agreement with the finding from Ayele et al. (2016) Who has shown that the magnitude of temperature is higher for the higher emission scenarios of RCP 8.5 than for the medium–low emission scenarios of RCP 4.5.

4.2.3.5 Climate change impacts on rice yield under RCP 4.5 and 8.5 scenarios

Under climate change projections, APSIM-Oryza predicted more rice yield with the NOAA model under both RCP 4.5 and RCP 8.5 emission scenarios in the 2050s and 2080s than the three other GCMs, CNRM-CM5, HadGEM2-ES and MPI. APSIM-Oryza projected a consistent decrease in rice yield with a relative change varying between 75% and 97% with the CNRM-CM5, HadGEM2-ES and MPI models (Table 4:4) under the RCP 4.5 and RCP 8.5 emission scenarios. The baseline (2019) average farmer rice yield was estimated to be 6.2 t/ha in Mbe and 6.01 in Lokakpli. Compared to the baseline, the APSIM-Oryza model was able to simulate a rice yield close to 4.1 t/ha and 3.2 t/ha in the 2050s and 2080s under the RCP 4.5 emission scenarios, while a rice yield of 4.1 t/ha and 3.9 t/ha was recorded in the 2050s and 2080s under the RCP 8.5 emission scenarios. For the NOAA model, which shows an increase in yield, the relative change between the projected yield and the baseline (Table 4:4) shows a decrease in rice yield of 32.8% and 47.54% in the 2050s and 2080s, respectively, under the RCP 4.5 climate scenarios. A similar decrease trend of 32.8% and 36.1% in the 2050s and 2080s, respectively, was observed under the RCP 8.5 emission scenario.

Few studies have simulated the impact of climate change on rice production in farmer trials in West Africa (Van Oort and Zwart 2018; Onyeneke 2021). Therefore, the study by Onyeneke (2021) analyses the impact of farmers' climate change adaptation decisions on rice profitability in Nigeria. Van Oort and Zwart (2018) simulated the impact of climate change on rice in irrigated and rainfed systems for four RCP climate change scenarios, by identifying the sources of yield reduction. Their results show that higher temperatures have a negative impact on yields (24% in RCP 8.5 in 2070 compared to the base year 2000). Specifically for West Africa, the authors find that wet season irrigated rice yields are projected to decrease by 21% with adaptation and increase by 7% without adaptation. Without adaptation, dry season irrigated rice yields in West Africa would decrease by 45%, with adaptation they would decrease significantly less (15%), and this decrease may be due to the high temperatures projected. This finding is consistent with our result, as temperatures are projected to increase under both RCP 4.5 and RCP 8.5 emission scenarios. Knox et al. (2012) assess the impact of climate change on crop productivity in Africa and South Asia and find a change in mean yield across Africa, but no change in rice yield. However, to mitigate the impact of climate change on farmers' rice production, some model-based approaches to scenario adaptation methods have been developed using APSIM-Oryza.

4.2.3.6 Effect of alternative management practices to mitigate climate change impact on rice yield

4.2.3.6.1 Crop establishment

The two methods of rice establishment are either direct seeding or transplanting. The baseline adoption method by farmers is rice transplanting. However, we simulate the scenarios of rice transplanting methods again as scenarios of rice direct seeding.

Table **4:4**. Percentage Changes (%) in simulated projected rice yield under the future climate scenarios compared to the baseline

RCMs	RCP 4.5		RCP 8.5	
	2021-2069	2070-2100	2021-2069	2070-2100
	Rice Yield (t/ha) and change (%)			
CNRM-CM5	1.3 (-78.69%)	1.3 (-78.69%)	1.1 (-81.97)	1.5 (-75.41%)
HadGEM2-ES	0.9 (-85.25%)	0.2 (-96.72%)	1.4 (-96.72%)	0.3 (-95.08%)
MPI	0.9 (-85.25%)	0.2 (-96.72%)	1.2 (-80.33%)	0.5 (-91.80%)
NOAA	4.1 (-32.8%)	3.2 (-47.54%)	4.1 (-32.8%)	3.9 (-36.1%)

The result shows that the average rice yield from the transplanting scenarios is higher (5.1 t/ha) than the yield from the direct seeding scenarios (4 t/ha). The difference in yield and the absolute change between direct seeding and transplanting show a reduction in rice yield of 1.7 t/ha (29.82%). This suggests to the farmers that transplanting is the method they are practising at the two sites in Bouake (Table 4:5). Although this method is good for yield improvement, it is also a popular method of planting that requires more labour, increases production costs and delays planting due to labour shortages.

Rice production is highly sensitive to the impacts of climate change, and adaptation strategies cannot be overemphasised as an important tool in climate management. However, the vulnerability of rice production to climate change has attracted the attention of researchers (Terdoo and Feola 2016; Onyeneke 2021). Rice production in sub-Saharan Africa is highly sensitive to climate change. There is therefore an urgent need to reduce the vulnerability of the rice sector to climate change. Adapting rice production to climate change is critical to increasing farmers' yields and food security. In sub-Saharan Africa, there are several local adaptation practices that farmers use to manage climate risks. Local adaptation practices include minimum tillage, drainage and consolidation, combined use of organic and inorganic fertiliser, crop diversification, improved rice varieties, use of nursery systems, use of crop protection products, diversification of income sources, and changes in planting and harvesting dates (Onyeneke 2021; Teklewold et al., 2019; Quan et al., 2019; Oselebe et al., 2016).

In this section, the six selected best alternative management practices for climate adaptation and mitigation are developed. For crop establishment, farmers used the rice transplanting method (5.7 t/ha), which is the best result compared to direct seeding (4 t/ha). However, although this method is good for yield improvement, it is also a popular method of crop establishment that requires more labour, increases production costs and

delays planting due to labour shortages. This has been studied by many authors (Johnkutty et al, 2006; Xu et al, 2019). However, direct seeding, which is recommended by many authors, suggests optimised management practices to improve the yield performance of direct seeding and limit the yield gap between direct seeding and rice transplanting (Xu et al, 2019).

4.2.3.6.2 Soil organic matter (SOM) scenarios

Table 4:5 shows the result of the different SOM application rates 15 days after transplanting. On both sites the farmers applied 114 kg N/ha at once as a baseline. The results show no improvement with the 30 kg/ha application. The change in rice yield compared to the baseline shows a decrease of 0.01 t/ha (0.20%). However, the 60 kg/ha application shows an improvement in rice yield of 0.01 t/ha (0.20%) compared to the baseline, while the 100 kg/ha application shows no change. Therefore, for the best alternative management of soil organic matter, the 60 and 100 kg/ha could be recommended to farmers to improve rice yield.

Simulation of soil organic matter scenarios in our finding show an improvement of rice with the level of 60 kg/ha. This result confirms the findings of XU et al. (2008), Iqbal et al. (2020) and Shrestha et al. (2020). Research by Shrestha et al. (2020) shows that soil organic matter provides an important amount of nitrogen to the plant, which is essential for rice growth and optimum yield and is a major component of amino acids and the building blocks of protein and chlorophyll. So far, results from Iqbal et al. (2020) show that a combination of 30% poultry manure and 70% chemical fertiliser increases rice grain yield by 11% and 15% in the early and late seasons, respectively.

Table **4:5**. Absolute difference (t/ha) and relative (%) changes in rice yield under alternative management practices compared to the farmers practices under future climate conditions.

Alternative management practices	Rice yield (t/ha)	Absolute difference (t/ha)	Change in rice yield (%)
Crop establishment			
Direct seeding	4	-1,7	-29,82
Manure application (kg/ha)			
30	5,06	-0,01	-0,20
60	5,08	0,01	0,20
100	5,07	0	0
Mulch application (Mg/ha)			
0,5	5,5	0,43	8,5
10	5,8	0,73	14,4
Seedling age (days old)			
10	4,73	-0,32	-6,3
14	4,4	-0,65	-12,9
35	5,07	0,02	0,4
Nitrogen fertilizer application (kg N/ha)			
45	3	-1,5	-33,3
90	4,1	-0,4	-8,9
120	4,8	0,3	6,7
150	4,9	0,4	8,9
180	5,1	0,6	13,3
Sowing date			
1_Feb	3,8	-1,4	-26,9
15_Feb	4,7	-0,5	-9,6
1_Mar	5,13	-0,07	-1,3
15_Mar	5,1	-0,1	-1,9
15_Apr	5,2	0	0
1_May	5,2	0	0
15_May	5,2	0	0
1_Jun	5,2	0	0

4.2.3.6.3 Scenario Mulch Management

Different levels of rice straw mulch application (5 Mg/ha, mean 5 Mg/ha mulch application and 10 Mg/ha, mean 10 Mg/ha mulch treatment) were set in the scenarios compared to the baseline of 0 Mg/ha, i.e. no rice straw mulch application. Comparing the baseline with the scenario results, rice yield increased significantly more with 0.5 and 10 Mg/ha. We observe a more significant increase with 10 Mg/ha than with 0.5 Mg/ha. The difference in rice yield and the absolute change compared to the baseline increase by 0.43 t/ha (8.5%) and 0.73 t/ha (14.4%) for 0.5 and 10 Mg/ha rice straw mulch application, respectively (Table 4:5). The baseline application of 0 Mg/ha yields 5.07 t/ha. The purpose of this study is to establish a model simulation approach by identifying the best alternative management practices to mitigate climate change. In this case of rice straw mulch, we recommend that farmers apply 0.5 and 10 Mg/ha to improve rice yield in order to mitigate the impact of climate change on rice production in Côte d'Ivoire.

The ability to APSIM-Oryza to simulate rice straw mulch management show a good result wilt an improvement of rice grain yield. The difference in rice grain yield due to rice straw mulch treatment found in our finding are similar to those from (Dosso-Yovou et al. 2016; Akhtar et al. 2018; Jabran et al. 2016). Dosso-Yovo et al. (2016) finding show that with rice straw mulch at 3 Mg/ha have increased rice grain yield and result from Akhtar et al. (2018) with 5 Mg/ha wheat straw mulch treatment had increased grain yield (7%). Similarly, result from Jabran et al. (2016) shows that water-saving rice production systems (consisting of aerobic rice and transplanted rice with intermittent irrigation) save water (18-27%) with improved water productivity, but cause rice yield loss of 22-37%. However, when mulch is applied to the system, rice yield is increased (0.18 to 0.29 kg grain). Overall, our results suggest that the 10 Mg/ha and 5 Mg/ha rice straw mulch

treatments could be used to maintain rice grain yield productivity and promote better adaptation to the effects of climate change in West Africa.

4.2.3.6.4 Scenario seedling age

Three levels of seedling age of 10, 14 and 35 days were applied in these scenarios. The result showed that seedlings at 35 days produced significantly higher rice grain yield (5.07 t/ha) compared to the other two seedlings. Transplanting rice at 35 days after sowing then gave a more promising result than transplanting at 10 and 14 days after sowing compared to the baseline. The difference in yield and the relative change from baseline show an increase of about 0.02 t/ha (0.4%) for 35-day-old seedlings and a decrease of about 0.32 t/ha (6.3%) and 0.65 t/ha (12.9%) for 10 and 14-day-old seedlings, respectively, after transplanting rice (Table 4:5). The best alternative management advice for farmers is to use 35 days old and baseline.

The seedling age scenarios were well performed, and the result of the proposed seedling age at 35 days is more promising compared to the baseline. This result is consistent with the findings of Koudjega et al. (2019), Kirttania et al. (2013), and Rahimpour et al. (2013), who found that the seedling age of rice at transplanting significantly affects panicle length. Transplanting rice at a young seedling age with soil ensures that the roots are not damaged, allowing them to adapt quickly to soil and climatic conditions, resulting in better yield growth (Uphoff, 2002). Similarly, Makarim et al. (2002) showed that rice plant components and yield can be increased by transplanting seedlings at 14 days instead of older seedlings at 21-23 days. Similarly, Ali et al. (2008) found that young seedlings have a significant effect on rice development and grain yield.

4.2.3.6.5 Scenario mineral fertilizer

Five nitrogen fertiliser rates of 45, 90, 120, 150 and 180 kg N/ha were applied and included in the model scenarios. The results show a significant increase in rice yield with 120, 150 and 180 kg N/ha nitrogen fertiliser than the other N application rates. It should be noted that as the N application rate increases, so does the rice yield. Table 4:5 show the recorded yield, the change in rice yield and the relative percentage change for the different N application rates. Compared to the baseline N application of 114 kg N/ha, the change in rice yield and the relative change increase by 0.3 t/ha (6.7%), 0.4 t/ha (8.9%) and 0.6 t/ha (13.3%) for the 120, 150 and 180 kg N/ha N application rates, while they decrease by about 1.5 (33.3%) and 0.4 t/ha (8.9%) for the 45 and 90 kg N/ha N application rates. The 120, 150 and 150 kg N/ha rates are the best alternative management of nitrogen application to mitigate the effects of climate change on the farmers' rice production system.

Several studies have assess mineral fertiliser role in rice development and yield production (Peng et al., 1999; Harrell et al., 2011). Different level of mineral fertiliser (45, 90, 120, 150, 180) have been used, setup and simulate the scenarios. The 180 kg N ha1 increases the rice grain yield by 5.1 t/ha (Table 4:5), while the baseline rice yield is 4.5 t/ha (114 kg N/ha). The results of this study agree with the findings of Djaman et al. (2018), who reported that the nitrogen application rate of 150 kg/ha was found to be the best with improved performance of the specific rice variety. Peng et al. (1999) showed a linear response of rice grain yield to nitrogen, while Harrell et al. (2011) reported a linear response of rice yield to N application below 150 kg N ha-1 and a flattening when the N application rate is higher than 150 kg N ha-1. Therefore, a N application rate of 150 kg/ha under mineral fertiliser scenarios could be recommended to improve rice yields for farmers and food security to achieve rice self-sufficiency as desired in West Africa.

4.2.3.6.6 Scenario change in sowing date

In this step, we used a cropping system model (APSIM-Oryza) to set up scenarios and compare a range of rice sowing dates (1 February to 15 June) for all selected farmers in both sites with the reference baseline using rice variety WITA9. The result suggests that changing from a short to a long rice sowing date would increase or decrease rice yield over the historical period. Rice yield would decrease from 1 February to 15 March and increase from 15 April to 15 May. The change in rice yield and the observed percentage change show a decrease of about 1.4 t/ha (26.9%), 0.5 t/ha (9.6%), 0.07 t/ha (1.3%) and 0.1 t/ha (1.9%) for 1 February, 15 February, 1 March and 15 March, respectively, compared to the baseline of 5.2 t/ha on 1 April. However, no change in rice yield was observed for the sowing dates of 1 May, 15 May and 1 June compared to the baseline (Table 4:5).

APSIM-Oryza simulation results showed that the effect of sowing date on rice grain yield varied greatly with the time of transplanting (Dharmarathna et al. 2014; Ding et al. 2020; Balwinder et al. 2014). Ding et al. (2020) analysed the impact of climate change on rice yield in China and the effects of shifting the sowing date on rice yield and irrigation water requirements, and showed that the average rice yield will decrease and that the application of the optimised sowing date will compensate for the average rice yield losses. The results of our study confirmed these earlier findings (Table 4:5). The results of Balwinder et al. (2014) showed that the long-duration varieties delayed the sowing date to late June, implying a consistency penalty on rice yield, and the subsequent shift to 15 July resulted in low yields (0-3.5 t ha-1). Rice grain yield is relatively stable over a period of transplanting dates from early May to mid-June, with a reduction in yield for transplanting after about mid-June for medium and long duration varieties (Jalota et al., 2009; Balwinder et al. 2014).

Chapter Five

5.0 Conclusion and Recommendations

5.1 Conclusion and Recommendation

During my PhD, I studied the land-atmosphere interaction and its impact on rice production in West Africa to better understand the importance of large-scale land cover types or plant functional type drivers such as vegetation (vegetation PFT, crop PFT and standard PFT) and climate interaction on condensational and convective cloudiness and rainfall. Although our study area is limited to West Africa, which is divided into four zones such as Guinean zone (rainfall > 1100 mm), Sudanian zone (rainfall range between 900 - 1100 mm), Sudano-Sahelian zone (rainfall range between 500 - 900 mm) and Sahelian zone (rainfall 250 - 500 mm). WA is also characterised by different land cover types, which can contribute significantly to climate variability. The datasets include observations from three eddy covariance stations, ERA5 land reanalysis data and GSWP version 3 used for parameterisation of the eCLM land surface model. The effect of the vegetation-atmosphere interaction over West Africa was investigated by comparing the simulation output with the observations and with ERA5 land and by expressing the lifting condensation level height (LCL).

When comparing the simulation with observations, the eCLM model performed very well when comparing the output of land surface fluxes with observation and ERA5 land. The expression of LCL from eCLM simulation output compared with the expression from observation and ERA5 land are in good agreement, showing the robustness and good performance of the model. However, the LCL height over crop land cover is larger than that over vegetation and standard land cover. We also compare the land surface fluxes with the LCL height for each different land cover. We observe that the correlation between latent heat (LH) and LCL (LH-LCL) is negative over the three land cover types, while

the relationship between sensible heat and LCL (SH-LCL) is positive over the three land cover types. LH-LCL have a mutual negative correlation, which is negatively influenced by water and energy fluxes, forming positive feedback loops and leading to a negative LH-LCL relationship. The negative correlation between LH-LCL indicates a possible influence of LH on LCL height.

We also evaluate the relationship between precipitation, LCL and energy and momentum to assess the link between LCL and convective clouds. During the dry season (October to April), we observe that the lowest atmosphere of WA has a high LCL due to low cloud cover and high aridity over the Sahel, as well as aerosol. Between May and September (rainy season), the onset and cessation of the rain cycle is observed with low levels of LCL due to high levels of convective cloud and precipitation. Due to many positive and negative feedbacks, changes in vegetation composition can have significant effects on climate, not only at regional but also at global scales. In particular, conversion of the WA vegetation PFT landscape to cropland PFT landscape can increase surface albedo (Myhre and Myhre, 2003) and reduce evapotranspiration because grasses and annual crops do not have access to as much soil water for transpiration as native vegetation/trees. The increase in albedo leads to a reduction in surface shortwave radiation (SSR) and hence surface temperatures. In a negative feedback loop, lower surface temperatures further reduce evapotranspiration, resulting in less latent cooling and more sensible heat to rewarm the surface. The LCL height is related to the cloud base height, so a high (low) LCL height is associated with more high (low) clouds, which is usually associated with less (more) moisture in the clouds, less (more) precipitation, a lower (higher) cloud albedo and more (less) solar radiation reaching the ground.

On the other hand, this study evaluated the performance of APSIM-ORYZA in simulating rice, the effects of climate change on rice yield, and how the use of alternative

management practices can mitigate the effects of climate change on rice yield. Data were collected from two years of experiments in farmers' fields in the Bouake region of central Côte d'Ivoire and used to calibrate and validate the APSIM-ORYZA model. Once validated, future bias-corrected climate data from Representation Concentration Pathways (RCPs) climate scenarios RCP4.5 and RCP 8.5 were used to assess the impact of climate change on rice yield. Seven adaptation strategies were set up to assess their potential to mitigate the impacts of climate change on rice yield. The results showed that APSIM-ORYZA simulated irrigated rice satisfactorily with R^2 values ranging from 0.8 to 1. The impact of climate change on rice yield showed that rice yield will under climate scenarios RCP 4.5 and RCP 8.5 compared to the reference rice yield. Rice yield is projected to increase under climate change when alternative management practices such as rice start mulching, alternate wetting and drying, seedling age at 35 days before transplanting, organic fertiliser application at 120 kg N ha^{-1} and rice sowing after 1 April are applied. The adoption of AWD combined with rice straw mulching, appropriate sowing dates and organic fertiliser application could be recommended to smallholder farmers to improve rice yield under climate change in the irrigated lowlands of central Côte d'Ivoire.

5.2 Limitation of the study

This research study was limited by, firstly, the issue of time to perform a spin-up to simulate the dynamics of each land cover and evaluate the lifting condensation height over the whole process. Secondly, we were not able to parameterise the model to calculate the leaf area index and evaluate the precipitation over each land cover and assess the contribution to surface runoff and the hydrological system in West Africa.

5.3 Recommendation

We recommended for future research that a simulation should be carried on the dynamic aspect of each land cover types (vegetation, crop and urban) using eCLM model to enable assessing its robustness over the West Africa. We also recommended that an evaluation should be carried through the simulation of the three land cover types dynamic the level of cloud base and assess the precipitation event over each specific land cover and identify their contribution to groundwater stock using the couple eCLM-ParFlow already available. We recommend that political decision-makers and international institutions involved in the fight against climate change to use strategies afforestation at some level as resilience with climate extreme events. We recommend for stockholder farmers and policy maker: transplanting as crop establishment, 60 and 100 kg/ha level for manure application, the amount of 0.5 and 10 Mg/ha were recommended and for mulch level application, for Nitrogen fertilizer application we recommended 120, 150 and 180 kg N/ha level and sowing date for 15 February, 1st and 15 March.

References

Abiodun, B. J., Adeyewa, Z. D., Oguntunde, P. G., Salami, A. T., & Ajayi, V. O. (2012). Modeling the impacts of reforestation on future climate in West Africa. Theoretical and Applied Climatology, 110(1–2), 77–96. https://doi.org/10.1007/s00704-012-0614-1

Adams, R. M., Hurd, B. H., Lenhart, S., & Leary, N. (1998). Effects of global climate change on agriculture: an interpretative review. Climate research, 11(1), 19-30.

Ago, E. E., Agbossou, E. K., Ozer, P., & Aubinet, M. (2016). Mesure des flux de CO2 et séquestration de carbone dans les écosystèmes terrestres ouest-africains (synthèse bibliographique). BASE, 68–82. https://doi.org/10.25518/1780-4507.12565

Ahmad, I., Ahmad, B., Boote, K., & Hoogenboom, G. (2020). Adaptation strategies for maize production under climate change for semi-arid environments. European Journal of Agronomy, 115, 126040.

Ahmed, K. F., Wang, G., Yu, M., Koo, J., & You, L. (2015). Potential impact of climate change on cereal crop yield in West Africa. Climatic Change, 133(2), 321–334. https://doi.org/10.1007/s10584-015-1462-7

Ahmed, M., Akram, M. N., Asim, M., Aslam, M., Hassan, F. ul, Higgins, S., Stöckle, C. O., & Hoogenboom, G. (2016). Calibration and validation of APSIM-Wheat and CERES-Wheat for spring wheat under rainfed conditions: Models evaluation and application. Computers and Electronics in Agriculture, 123, 384–401. https://doi.org/10.1016/j.compag.2016.03.015

Akhtar, K., Wang, W., Ren, G., Khan, A., Feng, Y., & Yang, G. (2018). Changes in soil enzymes, soil properties, and maize crop productivity under wheat straw mulching in Guanzhong, China. Soil and Tillage Research, 182, 94-102. https://doi.org/10.1016/j.still.2018.05.007

Akinsanola, A. A., Ogunjobi, K. O., Gbode, I. E., & Ajayi, V. O. (2015). Assessing the Capabilities of Three Regional Climate Models over CORDEX Africa in Simulating West African Summer Monsoon Precipitation. Advances in Meteorology, 2015, 1–13. https://doi.org/10.1155/2015/935431

Akinbile CO, Ogunmola OO, Abolude AT, Akande SO. (2020). Trends and spatial analysis of temperature and rainfall patterns on rice yields in Nigeria. Atmos Sci Lett.;21:e944. https://doi.org/10.1002/asl.944

Akponikpè, P. I., Gérard, B., Michels, K., & Bielders, C. (2010). Use of the APSIM model in long term simulation to support decision making regarding nitrogen management for pearl millet in the Sahel. European Journal of Agronomy, 32(2), 144-154. https://doi.org/10.1016/j.eja.2009.09.005

Akpoti, K., Groen, T., Dossou-Yovo, E., Kabo-bah, A. T., & Zwart, S. J. (2022). Climate change-induced reduction in agricultural land suitability of West-Africa's inland valley landscapes. Agricultural systems, 200, 103429.

Alexeeff, S. E., Nychka, D., Sain, S. R., & Tebaldi, C. (2018). Emulating mean patterns and variability of temperature across and within scenarios in anthropogenic climate change experiments. Climatic Change, 146, 319–333. https://doi.org/10.1007/s10584-016-1809-8

Ali, M. H., & Talukder, M. S. U. (2008). Increasing water productivity in crop production—A synthesis. Agricultural water management, 95(11), 1201-1213. https://doi.org/10.1016/j.agwat.2008.06.008

Amarasingha, R. P. R. K., Suriyagoda, L. D. B., Marambe, B., Gaydon, D. S., Galagedara, L. W., Punyawardena, R., Silva, G. L. L. P., Nidumolu, U., & Howden, M. (2015b). Simulation of crop and water productivity for rice (Oryza sativa L.) using APSIM under

diverse agro-climatic conditions and water management techniques in Sri Lanka. Agricultural Water Management, 160, 132–143. https://doi.org/10.1016/j.agwat.2015.07.001

Andarzian, ., Bannayan, M., Steduto, P., Mazraeh, H., Barati, M. E., Barati, M. A., & Rahnama, A. (2011). Validation and testing of the AquaCrop model under full and deficit irrigated wheat production in Iran. Agricultural Water Management, 100(1), 1-8. https://doi.org/10.1016/j.agwat.2011.08.023

Angulo, C., Rötter, R., Lock, R., Enders, A., Fronzek, S., & Ewert, F. (2013b). Implication of crop model calibration strategies for assessing regional impacts of climate change in Europe. Agricultural and Forest Meteorology, 170, 32-46.

Angulo, C., Rötter, R., Trnka, M., Pirttioja, N., Gaiser, T., Hlavinka, P., & Ewert, F. (2013a). Characteristic 'fingerprints' of crop model responses to weather input data at different spatial resolutions. European Journal of Agronomy, 49, 104-114. https://doi.org/10.1016/j.eja.2013.04.003

Archontoulis, S. V, Miguez, F. E., & Moore, K. J. (2014b). A methodology and an optimization tool to calibrate phenology of short-day species included in the APSIM PLANT model: Application to soybean. Environmental Modelling and Software, 62, 465–477. https://doi.org/10.1016/j.envsoft.2014.04.009

Archontoulis, S. V., Miguez, F. E., & Moore, K. J. (2014). Evaluating APSIM maize, soil water, soil nitrogen, manure, and soil temperature modules in the Midwestern United States. Agronomy Journal, 106(3), 1025–1040. https://doi.org/10.2134/agronj2013.0421

Ardoin-Bardin, S., Dezetter, A., Servat, E., Paturel, J. E., Mahé, G., Niel, H., & Dieulin, C. (2009). Using general circulation model outputs to assess impacts of climate change

on runoff for large hydrological catchments in West Africa. Hydrological Sciences Journal, 54(1), 77–89. https://doi.org/10.1623/hysj.54.1.77

Asseng, S., Zhu, Y., Basso, B., Wilson, T., Cammarano, D., 2014. Simulation modeling: applications in cropping systems. Enc. Agri. Food Syst., 102–112

Atreya, S. K., Adams, E. Y., Niemann, H. B., Demick-Montelara, J. E., Owen, T. C., Fulchignoni, M., ... & Wilson, E. H. (2006). Titan's methane cycle. Planetary and Space Science, 54(12), 1177-1187

Auffhammer, M., Ramanathan, V., & Vincent, J. R. (2012). Climate change, the monsoon, and rice yield in India. Climatic change, 111, 411-424.

Bado, B. V., Aw, A., & Ndiaye, M. (2010). Long-term effect of continuous cropping of irrigated rice on soil and yield trends in the Sahel of West Africa. Nutrient Cycling in Agroecosystems, 88(1), 133–141. https://doi.org/10.1007/s10705-010-9355-7

Bahri, H., Annabi, M., Cheikh M'Hamed, H., & Frija, A. (2019). Assessing the long-term impact of conservation agriculture on wheat-based systems in Tunisia using APSIM simulations under a climate change context. Science of the Total Environment, 692, 1223–1233. https://doi.org/10.1016/j.scitotenv.2019.07.307

Balasubramanian, V., Sie, M., Hijmans, R. J., & Otsuka, K. (2007). Increasing rice production in sub-Saharan Africa: challenges and opportunities. Advances in agronomy, 94, 55-133.

Balwinder-Singh, Eberbach PL, Humphreys E (2014) Simulation of the evaporation of soil water beneath a wheat crop canopy. Agri Water Manage 135:19–26

Bamba, A., Toure, N. E., Kouadio, K., Ahoua, S. A. A., Kouakou, D. V. M., Yoroba, F., M'Bo, K., Cherif, M., Kone, D., & Diedhiou, A. (2023). Contribution of Climate

Scenarios RCP4.5 and RCP8.5 to the Study of Climate Change Impacts on Cocoa Farming in Côte d'Ivoire. Atmospheric and Climate Sciences, 13(01), 84–101. https://doi.org/10.4236/acs.2023.131007

Basso, B., Liu, L., & Ritchie, J. T. (2016). A comprehensive review of the CERES-wheat,-maize and-rice models' performances. Advances in agronomy, 136, 27-132.

Bassu, S., Asseng, S., Motzo, R., Giunta, F., 2009. Optimising sowing date of durum wheat in a variable Mediterranean environment. Field Crop Res. 111 (1–2), 109–118.

Beddington, J. (2010). Food security: contributions from science to a new and greener revolution. Philosophical Transactions of the Royal Society B: Biological Sciences, 365(1537), 61-71.

Bellocchi, G., Rivington, M., Donatelli, M., & Matthews, K. (2010). Validation of biophysical models: issues and methodologies. A review. Agronomy for Sustainable Development, 30(1), 109-130. https://doi.org/10.1051/agro/2009001

Betts, A. K. (2009). Land-Surface-Atmosphere Coupling in Observations and Models: LAND-SURFACE-ATMOSPHERE COUPLING. Journal of Advances in Modeling Earth Systems, 1(3), n/a-n/a. https://doi.org/10.3894/JAMES.2009.1.4

Betts, A. K., Desjardins, R., Worth, D., & Cerkowniak, D. (2013). Impact of land use change on the diurnal cycle climate of the Canadian Prairies: LAND USE CHANGE AND DIURNAL CLIMATE. Journal of Geophysical Research: Atmospheres, 118(21), 11,996-12,011. https://doi.org/10.1002/2013JD020717

Bolton, D., 1980: The computation of equivalent potential tem- perature. Mon. Wea. Rev., 108, 1046–1053, doi:10.1175/ 1520-0493(1980)108,1046:TCOEPT.2.0.CO;2

Bonan, G. B. (2008). Forests and Climate Change: Forcings, Feedbacks, and the Climate Benefits of Forests. Science, 320(5882), 1444–1449. https://doi.org/10.1126/science.1155121

Boone, A. A., Xue, Y., De Sales, F., Comer, R. E., Hagos, S., Mahanama, S., Schiro, K., Song, G., Wang, G., Li, S., & Mechoso, C. R. (2016). The regional impact of Land-Use Land-cover Change (LULCC) over West Africa from an ensemble of global climate models under the auspices of the WAMME2 project. Climate Dynamics, 47(11),3547–3573. https://doi.org/10.1007/s00382-016-3252-y

Bouman BAM, Kropff MJ, Tuong TP, Wopereis MCS, ten Berge HFM, van L. H. (2001). ORYZA2000: modeling lowland rice. In Journal of Chemical Information and Modeling (Vol. 110, Issue 9).

Bouman, B. A. M., & Van Laar, H. H. (2006). Description and evaluation of the rice growth model ORYZA2000 under nitrogen-limited conditions. Agricultural Systems, 87(3), 249-273.

Bounoua, L., DeFries, R., Collatz, G. J., Sellers, P., & Khan, H. (2002). Effects of land cover conversion on surface climate. Climatic Change, 52, 29-64.

Brisson, N., Gary, C., Justes, E., Roche, R., Mary, B., Ripoche, D., Zimmer, D., Sierra, J., Bertuzzi, P., Burger, P., Bussière, F., Cabidoche, Y.M., Cellier, P., Debaeke, P., Gaudillère, J.P., Hénault, C., Maraux, F., Seguin, B., Sinoquet, H., 2003. An overview of the crop model STICS. Eur. J. Agron. 18 (3–4), 309–332.

C. Müller, R. D. Robertson, Projecting future crop productivity for global economic modeling. Agric. Econ. 45,37–50 (2014)

Challinor, A. J., Simelton, E. S., Fraser, E. D., Hemming, D., & Collins, M. (2010). Increased crop failure due to climate change: assessing adaptation options using models and socio-economic data for wheat in China. Environmental Research Letters, 5(3), 034012.

Challinor, A. J., Watson, J., Lobell, D. B., Howden, S. M., Smith, D. R., & Chhetri, N. (2014). A meta-analysis of crop yield under climate change and adaptation. Nature climate change, 4(4), 287-291.

Challinor, A., Wheeler, T., Garforth, C., Craufurd, P., & Kassam, A. (2007). Assessing the vulnerability of food crop systems in Africa to climate change. Climatic change, 83, 381-399.

Charney, J., Quirk, W. J., Chow, S. H. & Kornfield, J., 1977. A comparative study of the effect of albedo change on Drought in semi-arid regions. Journal of the atmospheric science, Volume 34, pp. 1366- 1386.

Charney, J., Stone, P. H. & Quirk, W. J., 1975. Drought in the Sahara: A biogiophysical feedback mechanism. Science, 187(4175), pp. 434-435.

Chase, T. N., & Pielke, R. A. (1995). Sensitivity of a general circulation model to large scale vegetation changes, The (Doctoral dissertation, Colorado State University. Libraries).

Chase, T. N., Pielke Sr., R. A., Kittel, T. G. F., Nemani, R. R., & Running, S. W. (2000a). Simulated impacts of historical land cover changes on global climate in northern winter. Climate Dynamics, 16(2–3), 93–105. https://doi.org/10.1007/s003820050007

Chase, T. N., Pielke Sr., R. A., Kittel, T. G. F., Nemani, R. R., & Running, S. W. (2000b). Simulated impacts of historical land cover changes on global climate in northern winter. Climate Dynamics, 16(2–3), 93–105. https://doi.org/10.1007/s003820050007

Chen, C., Wang, E., Yu, Q., 2010. Modelling the effects of climate variability and water management on crop water productivity and water balance in the North China Plain. Agric. Water Manage. 97 (8), 1175–1184.

Cheruy, F., Ducharne, A., Hourdin, F., Musat, I., Vignon, É., Gastineau, G., ... & Zhao, Y. (2020). Improved near-surface continental climate in IPSL-CM6A-LR by combined evolutions of atmospheric and land surface physics. Journal of Advances in Modeling Earth Systems, 12(10), e2019MS002005.

Choruma, D. J., Balkovic, J., & Odume, O. N. (2019). Calibration and validation of the EPIC model for maize production in the Eastern Cape, South Africa. Agronomy, 9(9), 494.

Chun, J. A., Li, S., Wang, Q., Lee, W. S., Lee, E. J., Horstmann, N., ... & Vang, S. (2016). Assessing rice productivity and adaptation strategies for Southeast Asia under climate change through multi-scale crop modeling. Agricultural Systems, 143, 14-21. https://doi.org/10.1016/j.agsy.2015.12.001

Claussen, M., Mysak, L., Weaver, A., Crucifix, M., Fichefet, T., Loutre, M. F., ... & Wang, Z. (2002). Earth system models of intermediate complexity: Closing the gap in the spectrum of climate system models. Climate Dynamics, 18(7), 579–586. https://doi.org/10.1007/s00382-001-0200-1

Claussen, M., Mysak, L., Weaver, A., Crucifix, M., Fichefet, T., Loutre, M. F., ... & Wang, Z. (2002). Earth system models of intermediate complexity: closing the gap in the spectrum of climate system models. Climate dynamics, 18, 579-586.

Confalonieri, R., Bregaglio, S., & Acutis, M. (2010b). A proposal of an indicator for quantifying model robustness based on the relationship between variability of errors and of explored conditions. Ecological Modelling, 221(6), 960-964. https://doi.org/10.1016/j.ecolmodel.2009.12.003

Cook, K., 1999. Generation of the African Easterly Jet and Its Role in Determining West African Precipitation. Journal of climate, Volume 12, pp. 1165-1185

Cox, P. M., Betts, R. A., Jones, C. D., Spall, S. A., & Totterdell, I. J. (2000). Acceleration of global warming due to carbon-cycle feedbacks in a coupled climate model. Nature, 408(6809), 184–187. https://doi.org/10.1038/35041539

de Noblet-Ducoudré, N., Boisier, J. P., Pitman, A., Bonan, G. B., Brovkin, V., Cruz, F., ... & Voldoire, A. (2012). Determining robust impacts of land-use-induced land cover changes on surface climate over North America and Eurasia: results from the first set of LUCID experiments. Journal of Climate, 25(9), 3261-3281

de Noblet-Ducoudré, N., Gervois, S., Ciais, P., Viovy, N., Brisson, N., Seguin, B., & Perrier, A. (2004). Coupling the Soil-Vegetation-Atmosphere-Transfer Scheme ORCHIDEE to the agronomy model STICS to study the influence of croplands on the European carbon and water budgets. Agronomie, 24(6–7), 397–407. https://doi.org/10.1051/agro:2004038

Dharmarathna, W. R. S. S., Herath, S., & Weerakoon, S. B. (2014). Changing the planting date as a climate change adaptation strategy for rice production in Kurunegala district, Sri Lanka. Sustainability science, 9(1), 103-111. https://doi.org/10.1007/s11625-012-0192-2

Diallo, I., Sylla, M. B., Giorgi, F., Gaye, A. T., & Camara, M. (2012). Multimodel GCM-RCM ensemble-based projections of temperature and precipitation over West Africa for the early 21st century. International Journal of Geophysics, 2012, 1-19.

Diffenbaugh, N.S.; Giorgi, F. Climate change hotspots in the CMIP5 global climate model ensemble. Clim. Chang. 2012, 114, 813–822.

Ding, Y., Wang, W., Zhuang, Q., & Luo, Y. (2020). Adaptation of paddy rice in China to climate change: The effects of shifting sowing date on yield and irrigation water requirement. Agricultural Water Management, 228, 105890. https://doi.org/10.1016/j.agwat.2019.105890

Dirmeyer, P. A., Wang, Z., Mbuh, M. J., & Norton, H. E. (2014). Intensified land surface control on boundary layer growth in a changing climate. Geophysical Research Letters, 41(4), 1290–1294. https://doi.org/10.1002/2013GL058826

Djaman, K., Mel, V. C., Diop, L., Sow, A., El-Namaky, R., Manneh, B., ... & Irmak, S. (2018). Effects of alternate wetting and drying irrigation regime and nitrogen fertilizer on yield and nitrogen use efficiency of irrigated rice in the Sahel. Water, 10(6), 711. https://doi.org/10.3390/w10060711

Dobermann, A., Witt, C., Dawe, D., Abdulrachman, S., Gines, H. C., Nagarajan, R., ... & Adviento, M. A. A. (2002). Site-specific nutrient management for intensive rice cropping systems in Asia. Field Crops Research, 74(1), 37-66.

Donatelli, M., Van Ittersum, M.K., Bindi, M., Porter, J.R., 2002. Modelling cropping systems-highlights of the symposium and preface to the special issues. Eur. J. Agron. 18 (1–2), 1–11.

Dosio, A., & Panitz, H. J. (2016). Climate change projections for CORDEX-Africa with COSMO-CLM regional climate model and differences with the driving global climate models. Climate Dynamics, 46(5), 1599-1625.

Dossou-Yovo, E. R., & Saito, K. (2021). Impact of management practices on weed infestation, water productivity, rice yield and grain quality in irrigated systems in Côte d'Ivoire. Field Crops Research, 270(June), 108209. https://doi.org/10.1016/j.fcr.2021.108209

Dossou-Yovo, E. R., Brüggemann, N., Ampofo, E., Igue, A. M., Jesse, N., Huat, J., & Agbossou, E. K. (2016). Combining no-tillage, rice straw mulch and nitrogen fertilizer application to increase the soil carbon balance of upland rice field in northern Benin. Soil and Tillage Research, 163, 152-159. https://doi.org/10.1016/j.still.2016.05.019

Downing, T. E., Ringius, L., Hulme, M., & Waughray, D. (1997). Adapting to climate change in Africa. Mitigation and adaptation strategies for global change, 2, 19-44.

Dunne, J. P., Horowitz, L. W., Adcroft, A. J., Ginoux, P., Held, I. M., John, J. G., ... & Zhao, M. (2020). The GFDL Earth System Model version 4.1 (GFDL-ESM 4.1): Overall coupled model description and simulation characteristics. Journal of Advances in Modeling Earth Systems, 12(11), e2019MS002015. https://doi.org/10.1029/2019MS002015

Ebrahimi-Mollabashi, E., Huth, N. I., Holzwoth, D. P., Ordóñez, R. A., Hatfield, J. L., Huber, I., Castellano, M. J., & Archontoulis, S. V. (2019). Enhancing APSIM to simulate excessive moisture effects on root growth. Field Crops Research, 236, 58–67. https://doi.org/10.1016/j.fcr.2019.03.014

Eitzinger, J., Trnka, M., Hösch, J., Z˘alud, Z., Dubrovsky´ , M., 2004. Comparison of CERES, WOFOST and SWAP models in simulating soil water content during growing season under different soil conditions. Ecol. Model. 171 (3), 223–246.

Erfanian Javadian Entezar Yazd, Amir, "Land-Atmosphere Interactions and Regional Climate in West Africa and South America" (2017). Doctoral Dissertations. 1660. https://opencommons.uconn.edu/dissertations/1660

Esham, M., & Garforth, C. (2013). Agricultural adaptation to climate change: Insights from a farming community in Sri Lanka. Mitigation and adaptation strategies for global change, 18, 535-549.

Espy, J. P. (1836). Essays on meteorology. Journal of the Franklin Institute, of the State of Pennsylvania, for the Promotion of the Mechanic Arts; Devoted to Mechanical and Physical Science, Civil Engineering, the Arts and Manufactures, and the Recording of American and Other Patent Inventions (1828-1851), 17(5), 309. , doi:10.1016/S0016-0032(36)91215-2

Eugène, K. K., Albert, G. B. T., Michel, K. A., & Alex, K. Z. (2012). Analyze of climate variability and change impacts on hydro-climate parameters: Case study of Côte d'Ivoire. ISS N, 3(2).

FAOSTAT, 2020. Food and Agriculture Data. http://www.fao.org/faostat/en/

FAOSTAT, 2022. Food and Agriculture Data. http://www.fao.org/faostat/en/

Fernando, M. E. K. K., Amerasekara, D. A. B. N., Amarasingha, R. K., Suriyagoda, L. D. B., & Marambe, B. (2015). Validation of APSIM for long duration rice varieties in different agro-climatic zones of Sri Lanka. Building Productive, Diverse and Sustainable

Landscapes. Proceedings of the 17th ASA Conference, 20-24 September. www.agronomy2015.com.au

Fitzjarrald, D. R., Acevedo, O. C., & Moore, K. E. (2001). Climatic consequences of leaf presence in the eastern United States. Journal of Climate, 14(4), 598-614.

Gaydon, D. S., Balwinder-Singh, Wang, E., Poulton, P. L., Ahmad, B., Ahmed, F., Akhter, S., Ali, I., Amarasingha, R., Chaki, A. K., Chen, C., Choudhury, B. U., Darai, R., Das, A., Hochman, Z., Horan, H., Hosang, E. Y., Kumar, P. V., Khan, A. S. M. M. R., … Roth, C. H. (2017). Evaluation of the APSIM model in cropping systems of Asia. Field Crops Research, 204, 52–75. https://doi.org/10.1016/j.fcr.2016.12.015

Gaydon, D. S., Probert, M. E., Buresh, R. J., Meinke, H., & Timsina, J. (2012a). Modelling the role of algae in rice crop nutrition and soil organic carbon maintenance. European Journal of Agronomy, 39, 35-43.

Gaydon, D. S., Probert, M. E., Buresh, R. J., Meinke, H., Suriadi, A., Dobermann, A., ... & Timsina, J. (2012b). Rice in cropping systems—Modelling transitions between flooded and non-flooded soil environments. European journal of agronomy, 39, 9-24.

Gaydon, D. S., Wang, E., Poulton, P. L., Ahmad, B., Ahmed, F., Akhter, S., ... & Roth, C. H. (2017). Evaluation of the APSIM model in cropping systems of Asia. Field Crops Research, 204, 52-75.

Giorgi, F., Jones, C., Asrar, G., 2009. Addressing climate information needs at the regional level: the CORDEX framework. Organ. Bull. 58 (July), 175–183. [Online]Available http://www.euro-cordex.net/uploads/media/Download_01.pdf

Godwin, D.C., Singh, U., 1998. Nitrogen balance and crop response to nitrogen in upland and lowland cropping systems. In: Tsuji, G., Hoogenboom, G., Thornton, P. (Eds.), Understanding Options for Agricultural Production. Springer, Netherlands, pp. 55–77.

Guidigan, M. L. G., Azihou, F., Idohou, R., Okhimamhe, A. A., Fandohan, A. B., Sinsin, B., & Adet, L. (2018). Modelling the current and future distribution of Kigelia africana under climate change in Benin, West Africa. Modeling Earth Systems and Environment, 4(3), 1225–1238. https://doi.org/10.1007/s40808-018-0491-4

Guidigan, M. L. G., Azihou, F., Idohou, R., Okhimamhe, A. A., Fandohan, A. B., Sinsin, B., & Adet, L. (2018). Modelling the current and future distribution of Kigelia africana under climate change in Benin, West Africa. Modeling Earth Systems and Environment, 4(3), 1225–1238. https://doi.org/10.1007/s40808-018-0491-4

Guidigan, M. L. G., Sanou, C. L., Ragatoa, D. S., Fafa, C. O., & Mishra, V. N. (2018). Assessing Land Use/Land Cover Dynamic and Its Impact in Benin Republic Using Land Change Model and CCI-LC Products. Earth Systems and Environment, 12. https://doi.org/10.1007/s41748-018-0083-5

Guidigan, M. L. G., Sanou, C. L., Ragatoa, D. S., Fafa, C. O., & Mishra, V. N. (2018). Assessing Land Use/Land Cover Dynamic and Its Impact in Benin Republic Using Land Change Model and CCI-LC Products. Earth Systems and Environment, 12. https://doi.org/10.1007/s41748-018-0083-5

Gupta, R., & Mishra, A. (2019). Climate change induced impact and uncertainty of rice yield of agro-ecological zones of India. Agricultural Systems, 173, 1-11.

Hammer, G. L., Chapman, S., Van Oosterom, E., & Podlich, D. W. (2005). Trait physiology and crop modelling as a framework to link phenotypic complexity to

underlying genetic systems. Australian Journal of Agricultural Research, 56(9), 947–960. https://doi.org/10.1071/AR05157

Hammer, G. L., van Oosterom, E., McLean, G., Chapman, S. C., Broad, I., Harland, P., & Muchow, R. C. (2010). Adapting APSIM to model the physiology and genetics of complex adaptive traits in field crops. Journal of experimental botany, 61(8), 2185-2202.

Harrell, D. L., Walker, T. W., Salassi, M. E., Bond, J. A., & Gerard, P. D. (2011). Modeling rice grain yield response to nitrogen fertilization for delayed-flood production. Journal of plant nutrition, 34(14), 2158-2171. https://doi.org/10.1080/01904167.2011.618575

Hatfield, J. L., & Prueger, J. H. (2015). Temperature extremes: Effect on plant growth and development. Weather and climate extremes, 10, 4-10.

Heinemann, A. B., Van Oort, P. A., Fernandes, D. S., & Maia, A. D. H. N. (2012). Sensitivity of APSIM/ORYZA model due to estimation errors in solar radiation. Bragantia, 71, 572-582.

Hewitson, B., Lennard, C., Nikulin, G., & Jones, C. (2012). CORDEX-Africa: a unique opportunity for science and capacity building. CLIVAR Exchanges, 17(3), 6-7.

Holzworth, D. P., Huth, N. I., & deVoil, P. G. (2011). Simple software processes and tests improve the reliability and usefulness of a model. Environmental modelling & software, 26(4), 510-516. https://doi.org/10.1016/j.envsoft.2010.10.014

Holzworth, D. P., Huth, N. I., deVoil, P. G., Zurcher, E. J., Herrmann, N. I., McLean, G., ... & Keating, B. A. (2014). APSIM–evolution towards a new generation of agricultural systems simulation. Environmental Modelling & Software, 62, 327-350. https://doi.org/10.1016/j.envsoft.2014.07.009

Howden, S. M., Soussana, J. F., Tubiello, F. N., Chhetri, N., Dunlop, M., & Meinke, H. (2007). Adapting agriculture to climate change. Proceedings of the national academy of sciences, 104(50), 19691-19696.

Ilori, O. W., & Ajayi, V. O. (2020). Change detection and trend analysis of future temperature and rainfall over West Africa. Earth Systems and Environment, 4, 493-512.

IPCC (2013b) Annex I: atlas of global and regional climate projections. In: Stocker TF et al (eds) Climate change 2013: the physical science basis. Contribution of Working Group I to the Fifth Assessment Report of the Intergovernmental Panel on Climate Change. Cambridge University Press, Cambridge and New York, pp1311–1394

Iqbal, A., He, L., Ali, I., Ullah, S., Khan, A., Khan, A., ... & Jiang, L. (2020). Manure combined with chemical fertilizer increases rice productivity by improving soil health, post-anthesis biomass yield, and nitrogen metabolism. Plos one, 15(10), e0238934. https://doi.org/10.1371/journal.pone.0238934

Jabran, K., Hussain, M., Fahad, S., Farooq, M., Bajwa, A. A., Alharrby, H., & Nasim, W. (2016). Economic assessment of different mulches in conventional and water-saving rice production systems. Environmental Science and Pollution Research, 23(9), 9156-9163. https://doi.org/10.1007/s11356-016-6162-y

Jalota, S. K., Singh, K. B., Chahal, G. B. S., Gupta, R. K., Chakraborty, S., Sood, A., ... & Panigrahy, S. (2009). Integrated effect of transplanting date, cultivar and irrigation on yield, water saving and water productivity of rice (Oryza sativa L.) in Indian Punjab: field and simulation study. Agricultural Water Management, 96(7), 1096-1104. https://doi.org/10.1016/j.agwat.2009.02.005

Jamieson, P. D., Porter, J. R., & Wilson, D. R. (1991). A test of the computer simulation model ARCWHEAT1 on wheat crops grown in New Zealand. Field crops research, 27(4), 337-350.

Johnkutty, I., Mathew, G., & Mathew, J. (2006). Comparison between transplanting and direct-seeding methods for crop establishment in rice. Journal of Tropical Agriculture, 40, 65-66.

Jones, C., Hughes, J. K., Bellouin, N., Hardiman, S. C., Jones, G. S., Knight, J., ... & Zerroukat, M. (2011). The HadGEM2-ES implementation of CMIP5 centennial simulations. Geoscientific Model Development, 4(3), 543-570. https://doi.org/10.5194/gmd-4-543-2011

Jones, J. W., Hoogenboom, G., Porter, C. H., Boote, K. J., Batchelor, W. D., Hunt, L. A., ... & Ritchie, J. T. (2003). The DSSAT cropping system model. European journal of agronomy, 18(3-4), 235-265.

Kamali, B., Abbaspour, K. C., Lehmann, A., Wehrli, B., & Yang, H. (2018). Uncertainty-based auto-calibration for crop yield–the EPIC+ procedure for a case study in Sub-Saharan Africa. European journal of agronomy, 93, 57-72. https://doi.org/10.1016/j.eja.2017.10.012

Katerji, N., Campi, P., & Mastrorilli, M. (2013). Productivity, evapotranspiration, and water use efficiency of corn and tomato crops simulated by AquaCrop under contrasting water stress conditions in the Mediterranean region. Agricultural Water Management, 130, 14-26. https://doi.org/10.1016/j.agwat.2013.08.005

Keating, B.A., Carberry, P.S., Hammer, G.L., Probert, M.E., Robertson, M.J., Holzworth, D., Huth, N.I., Hargreaves, J.N.G., Meinke, H., Hochman, Z., McLean, G., Verburg, K., Snow, V., Dimes, J.P., Silburn, M., Wang, E., Brown, S., Bristow, K.L., Asseng, S.,

Chapman, S., McCown, R.L., Freebairn, D.M., Smith, C.J., 2003. An overview of APSIM, a model designed for farming systems simulation. Eur. J. Agron. 18 (34), 267–288.

Khanal, U., Wilson, C., Hoang, V. N., & Lee, B. (2018). Farmers' adaptation to climate change, its determinants and impacts on rice yield in Nepal. Ecological Economics, 144, 139-147.

Kim, H. Y., Ko, J., Kang, S., & Tenhunen, J. (2013). Impacts of climate change on paddy rice yield in a temperate climate. Global change biology, 19(2), 548-562.

Kirttania, B., Sarkar, M. A. R., & Paul, S. K. (2013). Performance of transplant Aman rice as influenced by tiller seedlings and nitrogen management. Journal of the Bangladesh Agricultural University, 11(2), 249-256. http://dx.doi.org/10.3329/jbau.v11i2.19903

Knox, J., Hess, T., Daccache, A., & Wheeler, T. (2012). Climate change impacts on crop productivity in Africa and South Asia. Environmental Research Letters, 7(3), 034032. https://doi.org/10.1088/1748-9326/7/3/034032

Knox, J., Morris, J., & Hess, T. (2010). Identifying future risks to UK agricultural crop production: Putting climate change in context. Outlook on AGRICULTURE, 39(4), 249-256.

Kollias, P., Miller, M. A., Johnson, K. L., Jensen, M. P., & Troyan, D. T. (2009). Cloud, thermodynamic, and precipitation observations in West Africa during 2006. Journal of Geophysical Research, 114, D00E08. https://doi.org/10.1029/2008JD010641

Komatsu, S., Saito, K., & Sakurai, T. (2022). Changes in production, yields, and the cropped area of lowland rice over the last 20 years and factors affecting their variations in Côte d′ Ivoire. Field Crops Research, 277, 108424.

Kouakou, K.E.; Goula, B.T. A.; Kouassi, A.M. Analyze of climate variability and change impacts on hydro-climate parameters: Case study of Côte d'Ivoire. Int. J. Sci. Eng. Res. 2012, 3, 1–8.

Koudjega, K., Ablede, K. A., Lawson, I. Y. D., Abekoe, M. K., & Owusu-Bennoah, E. (2019). Assessing the Effect of Seedling Age and Time of Urea Supergranule Application on Rice Growth, Yield and Nitrogen Use efficiency. West African Journal of Applied Ecology, 27(1), 78-94.

Kurukulasuriya, P., & Mendelsohn, R. O. (2008). How will climate change shift agro-ecological zones and impact African agriculture?. World Bank Policy Research Working Paper, (4717).

Kutta, E., & Hubbart, J. A. (2023). Seasonal Lifting Condensation Level Trends: Implications of Warming and Reforestation in Appalachia's Deciduous Forest. Atmosphere, 14(1), 98.

Lawrence, M. G. (2005). The Relationship between Relative Humidity and the Dewpoint Temperature in Moist Air: A Simple Conversion and Applications. Bulletin of the American Meteorological Society, 86(2), 225–234. https://doi.org/10.1175/BAMS-86-2-225

David M. Lawrence, Rosie A. Fisher, Charles D. Koven, Keith W. Oleson, Sean C. Swenson, Gordon Bonan, Nathan Collier, Bardan Ghimire, Leo van Kampenhout, Daniel Kennedy, Erik Kluzek, Peter J. Lawrence, Fang Li, Hongyi Li, Danica Lombardozzi, William J. Riley, William J. Sacks, Mingjie Shi, Mariana Vertenstein, William R. Wieder, Chonggang Xu, Ashehad A. Ali, Andrew M. Badger, Gautam Bisht, Michiel van den Broeke, Michael A. Brunke, Sean P. Burns, Jonathan Buzan, Martyn Clark, Anthony Craig, Kyla Dahlin, Beth Drewniak, Joshua B. Fisher, Mark Flanner, Andrew M. Fox,

Pierre Gentine, Forrest Hoffman, Gretchen Keppel-Aleks, Ryan Knox, Sanjiv Kumar, Jan Lenaerts, L. Ruby Leung, William H. Lipscomb, Yaqiong Lu, Ashutosh Pandey, Jon D. Pelletier, Justin Perket, James T. Randerson, Daniel M. Ricciuto, Benjamin M. Sanderson, Andrew Slater, Zachary M. Subin, Jinyun Tang, R. Quinn Thomas, Maria Val Martin, Xubin Zeng, 2019: The Community Land Model version 5: Description of new features, benchmarking, and impact of forcing uncertainty. Journal of Advances in Modeling Earth Systems, 11, 4245-4287. https://doi-org.cuucar.idm.oclc.org/10.1029/2018MS001583

Levine, P. A., Randerson, J. T., Swenson, S. C., & Lawrence, D. M. (2016). Evaluating the strength of the land–atmosphere moisture feedback in Earth system models using satellite observations. Hydrology and Earth System Sciences, 20(12), 4837–4856. https://doi.org/10.5194/hess-20-4837-2016

Li, T., Angeles, O., Marcaida III, M., Manalo, E., Manalili, M. P., Radanielson, A., & Mohanty, S. (2017). From ORYZA2000 to ORYZA (v3): An improved simulation model for rice in drought and nitrogen-deficient environments. Agricultural and forest meteorology, 237, 246-256.

Liu, J., Liu, Z., Zhu, A. X., Shen, F., Lei, Q., & Duan, Z. (2019). Global sensitivity analysis of the APSIM-Oryza rice growth model under different environmental conditions. Science of the Total Environment, 651, 953–968. https://doi.org/10.1016/j.scitotenv.2018.09.254

Liu, L., Zhu, Y., Tang, L., Cao, W., & Wang, E. (2013). Impacts of climate changes, soil nutrients, variety types and management practices on rice yield in East China: A case study in the Taihu region. Field crops research, 149, 40-48.

Liu, X., Xu, J., Zhou, X., Wang, W., & Yang, S. (2020). Evaporative fraction and its application in estimating daily evapotranspiration of water-saving irrigated rice field. Journal of Hydrology, 584, 124317. https://doi.org/10.1016/j.jhydrol.2019.124317

Liu, Z., Hubbard, K. G., Lin, X., & Yang, X. (2013). Negative effects of climate warming on maize yield are reversed by the changing of sowing date and cultivar selection in Northeast China. Global Change Biology, n/a-n/a. https://doi.org/10.1111/gcb.12324

Loague, K., & Green, R. E. (1991). Statistical and graphical methods for evaluating solute transport models: overview and application. Journal of contaminant hydrology, 7(1-2), 51-73.

Lu, Y., & Kueppers, L. M. (2012). Surface energy partitioning over four dominant vegetation types across the United States in a coupled regional climate model (Weather Research and Forecasting Model 3–Community Land Model 3.5). Journal of Geophysical Research: Atmospheres, 117(D6).

Ma, L., Ahuja, L.R., Saseendran, S.A., Malone, R.W., Green, T.R., Nolan, B.T., Bartling, P. N.S., Flerchinger, G.N., Boote, K.J., Hoogenboom, G., 2011. A Protocol for Parameterization and Calibration of RZWQM2 in Field Research. In: Ahuja, L. R., Ma, L. (Eds.). Methods of Introducing System Models into Agricultural Research, Am Society Agron, Crop Science Society of America, Soil Science Society of America, pp. 1–64.

Ma, Y., Feng, S., Song, X., 2015. Evaluation of optimal irrigation scheduling and groundwater recharge at representative sites in the North China Plain with SWAP model and field experiments. Comput. Electr. Agric. 116, 125–136.

Makarim, A. K., Balasubramanian, V., Zaini, Z., Syamsiah, I., Diratmadja, I. G. P. A., Handoko, A., ... & Gani, A. (2002). Systems of rice intensification (SRI): evaluation of seedling age and selected components in Indonesia. Water-wise rice production, 129-139.

Mauritsen, T., Bader, J., Becker, T., Behrens, J., Bittner, M., Brokopf, R., ... & Roeckner, E. (2019). Developments in the MPI-M Earth System Model version 1.2 (MPI-ESM1. 2) and its response to increasing CO2. Journal of Advances in Modeling Earth Systems, 11(4), 998-1038. https://doi.org/10.1029/2018MS001400

Mishra, V., Cherkauer, K. A., Niyogi, D., Lei, M., Pijanowski, B. C., Ray, D. K., Bowling, L. C., & Yang, G. (2010). A regional scale assessment of land use/land cover and climatic changes on water and energy cycle in the upper Midwest United States: REGIONAL SCALE ASSESSMENT OF LAND USE/LAND COVER AND CLIMATIC CHANGES. International Journal of Climatology, 30(13), 2025–2044. https://doi.org/10.1002/joc.2095

Monerie, P. A., Fontaine, B., & Roucou, P. (2012). Expected future changes in the African monsoon between 2030 and 2070 using some CMIP3 and CMIP5 models under a medium-low RCP scenario. Journal of Geophysical Research: Atmospheres, 117(D16).

Monsi, M., Saeki, T., 2005. On the factor light in plant communities and its importance for matter production. Ann. Bot-London 95 (3), 549–567.

Nash, J. E. & Sutcliffe, J. V. (1970) River flow forecasting through conceptual models. Part I-A discussion of principles. J. Hydrol. 27(3), 282–290.

Niang, I., Ruppel, O. C., Abdrabo, M. A., Essel, A., Lennard, C., Padgham, J., et al. (2014). Africa. In: V. R. Barros, C. B. Field, D. J. Dokken, M. D. Mastrandrea, K. J. Mach, T. E. Bilir, M. Chatterjee, K. L. Ebi, Y. O. Estrada, R. C. Genova, B. Girma, E. S. Kissel, A. N. Levy, S. MacCracken, P. R. Mastrandrea & L. L. White (Eds.), Climate change 2014: Impacts, adaptation, and vulnerability. Part B: Regional aspects. Contribution of working group II to the fifth assessment report of the intergovernmental

panel on climate change (pp. 1199–1265). Cambridge, United Kingdom and New York, NY, USA: Cambridge University Press.

Nikulin, G., Jones, C., Giorgi, F., Asrar, G., Büchner, M., Cerezo-Mota, R., ... & Sushama, L. (2012). Precipitation climatology in an ensemble of CORDEX-Africa regional climate simulations. Journal of Climate, 25(18), 6057-6078.

Ochieng, J., Kirimi, L., & Mathenge, M. (2016). Effects of climate variability and change on agricultural production: The case of small scale farmers in Kenya. NJAS-Wageningen journal of life sciences, 77, 71-78.

Onyeneke, R. U., Amadi, M. U., Njoku, C. L., & Osuji, E. E. (2021). Climate change perception and uptake of climate-smart agriculture in rice production in Ebonyi State, Nigeria. Atmosphere, 12(11), 1503.

Oselebe, H. O., Nnamani, C. V., Efisue, A., Onu, D., Eze, S. O., & Ogunji, J. O. (2016). Perceptions of climate change and variabJoility, impacts and adaptation strategies by rice farmers in south east Nigeria. Our Nature, 14(1), 54-63.

Pachauri, R. K., Allen, M. R., Barros, V. R., Broome, J., Cramer, W., Christ, R., ... & van Ypserle, J. P. (2014). Climate change 2014: synthesis report. Contribution of Working Groups I, II and III to the fifth assessment report of the Intergovernmental Panel on Climate Change (p. 151). Ipcc.

Pausata, F. S., Messori, G., Yun, J., Jalihal, C. A., Bollasina, M. A., & Marchitto, T. M. (2021). The remote response of the South Asian Monsoon to reduced dust emissions and Sahara greening during the middle Holocene. Climate of the Past, 17(3), 1243-1271.

Peng, S., Cassman, K. G., Virmani, S. S., Sheehy, J., & Khush, G. S. (1999). Yield potential trends of tropical rice since the release of IR8 and the challenge of increasing

rice yield potential. Crop Science, 39(6), 1552-1559. https://doi.org/10.2135/cropsci1999.3961552x

Pielke, R. A. (2001). Influence of the spatial distribution of vegetation and soils on the prediction of cumulus Convective rainfall. Reviews of Geophysics, 39(2), 151–177. https://doi.org/10.1029/1999RG000072

Pielke, R. A., Marland, G., Betts, R. A., Chase, T. N., Eastman, J. L., Niles, J. O., Niyogi, D. dutta S., & Running, S. W. (2002). The influence of land-use change and landscape dynamics on the climate system: Relevance to climate-change policy beyond the radiative effect of greenhouse gases. Philosophical Transactions of the Royal Society of London. Series A: Mathematical, Physical and Engineering Sciences, 360(1797), 1705–1719. https://doi.org/10.1098/rsta.2002.1027

Probert, M. E., Carberry, P. S., McCown, R. L., & Turpin, J. E. (1998). Simulation of legume-cereal systems using APSIM. Australian Journal of Agricultural Research, 49(3), 317-328.

Quan, S., Li, Y., Song, J., Zhang, T., & Wang, M. (2019). Adaptation to climate change and its impacts on wheat yield: perspective of farmers in Henan of China. Sustainability, 11(7), 1928.Osel

Quansah, E., Mauder, M., Balogun, A. A., Amekudzi, L. K., Hingerl, L., Bliefernicht, J., & Kunstmann, H. (2015). Carbon dioxide fluxes from contrasting ecosystems in the Sudanian Savanna in West Africa. Carbon Balance and Management, 10(1), 1. https://doi.org/10.1186/s13021-014-0011-4

Quenum, G. M. L. D., Klutse, N. A. B., Dieng, D., Laux, P., Arnault, J., Kodja, Japhet. D., & Oguntunde, P. G. (2019). Identification of Potential Drought Areas in West Africa

Under Climate Change and Variability. Earth Systems and Environment, 3(3), 429–444. https://doi.org/10.1007/s41748-019-00133-w

Radanielson, A. M., Gaydon, D. S., Li, T., Angeles, O., & Roth, C. H. (2018). Modeling salinity effect on rice growth and grain yield with ORYZA v3 and APSIM-Oryza. European journal of agronomy, 100, 44-55.

Rahimi, J., Ago, E. E., Ayantunde, A., Berger, S., Bogaert, J., Butterbach-Bahl, K., Cappelaere, B., Demarty, J., Diouf, A. A., Falk, U., Haas, E., Hiernaux, P., Kraus, D., Roupsard, O., Scheer, C., Srivastava, A. K., Tagesson, T., & Grote, R. (2021). Modelling Gas Exchange and Biomass Production in WestAfrican Sahelian and Sudanian Ecological Zones [Preprint]. Biogeosciences. https://doi.org/10.5194/gmd-2020-417

Rahimpour, L., Daliri, M. S., & Mousavi, A. A. (2013). Effect of seedling age on yield and yield component of rice cultivars (Oryza sativa L.). Annals of Biological Research, 4(2), 72-76. http://scholarsresearchlibrary.com/AB

Rathjens, H., Bieger, K., Srinivasan, R., Chaubey, I., & Arnold, J. G. (2016). CMhyd user manual. Doc. Prep. Simulated Clim. Change Data Hydrol. Impact Study.

Ritchie, J.T., Singh, U., Godwin, D.C., Bowen, W.T., 1998. Cereal growth, development and yield. In: Tsuji, G., Hoogenboom, G., Thornton, P. (Eds.), Understanding Options for Agricultural Production. Springer, Netherlands, pp. 79–98

Romps, D. M. (2017). Exact Expression for the Lifting Condensation Level. Journal of the Atmospheric Sciences, 74(12), 3891–3900. https://doi.org/10.1175/JAS-D-17-0102.1

Rosenzweig, C., Parry, M.L., 1994. Potential impact of climate change on world food supply. Nature 367 (6459), 133–138.

Sacré Regis M, D., Mouhamed, L., Kouakou, K., Adeline, B., Arona, D., Houebagnon Saint. J, C., ... & Issiaka, S. (2020). Using the CHIRPS dataset to investigate historical changes in precipitation extremes in West Africa. climate, 8(7), 84.

Santanello Jr, J. A., Dirmeyer, P. A., Ferguson, C. R., Findell, K. L., Tawfik, A. B., Berg, A., ... & Wulfmeyer, V. (2018). Land–atmosphere interactions: The LoCo perspective. Bulletin of the American Meteorological Society, 99(6), 1253-1272.

Santanello, J. A., Peters-Lidard, C. D., & Kumar, S. V. (2011). Diagnosing the Sensitivity of Local Land–Atmosphere Coupling via the Soil Moisture–Boundary Layer Interaction. Journal of Hydrometeorology, 12(5), 766–786. https://doi.org/10.1175/JHM-D-10-05014.1

Saxton, K. E., & Rawls, W. J. (2006). Soil Water Characteristic Estimates by Texture and Organic Matter for Hydrologic Solutions. Soil Science Society of America Journal, 70(5), 1569–1578. https://doi.org/10.2136/sssaj2005.0117

Sayre, K.D., Rajaram, S., Fischer, R.A., 1997. Yield potential progress in short bread wheats in Northwest Mexico. Crop Sci. 37 (1), 36–42.

Schlenker, W., & Lobell, D. B. (2010). Robust negative impacts of climate change on African agriculture. Environmental Research Letters, 5(1), 014010.

Schwartz, M. D. (1994). Monitoring global change with phenology: the case of the spring green wave. International journal of biometeorology, 38, 18-22.

Schwartz, M. D. (1996). Examining the spring discontinuity in daily temperature ranges. Journal of Climate, 9(4), 803-808.

Schwartz, M. D., Betancourt, J. L., & Weltzin, J. F. (2012). From Caprio's lilacs to the USA national phenology network. Frontiers in Ecology and the Environment, 10(6), 324-327.

Serdeczny, O.; Adams, S.; Baarsch, F.; Coumou, D.; Robinson, A.; Hare, W.; Schaeffer, M.; Perrette, M.; Reinhardt, J. Climate change impacts in Sub-Saharan Africa: From physical changes to their social repercussions. Reg. Environ. Chang. 2015, 1–16.

Shabbir, G., Khaliq, T., Ahmad, A., & Saqib, M. (2020). Assessing the climate change impacts and adaptation strategies for rice production in Punjab, Pakistan. Environmental Science and Pollution Research, 27, 22568-22578.

Shrestha, J., Shah, K. K., & Timsina, K. P. (2020). Effects of different fertilizers on growth and productivity of rice (Oryza sativa L.): A review. International Journal of Global Science Research, 7(1), 1291-1301. 10.26540/ijgsr.v7.i1.2020.151

Slingo, J. M., Challinor, A. J., Hoskins, B. J., & Wheeler, T. R. (2005). Introduction: food crops in a changing climate. Philosophical Transactions of the Royal Society B: Biological Sciences, 360(1463), 1983-1989.

Smith, P., & Olesen, J. E. (2010). Synergies between the mitigation of, and adaptation to, climate change in agriculture. The Journal of Agricultural Science, 148(5), 543-552.

Soro, G. E., Yao, A. B., Kouame, Y. M., & Bi, T. A. G. (2017). Climate change and its impacts on water resources in the Bandama basin, Côte D'ivoire. Hydrology, 4(1), 18.

Stackpole, J. D. (1967). Numerical analysis of atmospheric soundings. Journal of Applied Meteorology (1962-1982), 464-467.

Stevanović, M., Popp, A., Lotze-Campen, H., Dietrich, J. P., Müller, C., Bonsch, M., ... & Weindl, I. (2016). The impact of high-end climate change on agricultural welfare. Science advances, 2(8), e1501452

Stevens, T., & Madani, K. (2016). Future climate impacts on maize farming and food security in Malawi. Scientific Reports, 6(1), 36241.

Sulis, M., Langensiepen, M., & Shrestha, P. (2014). Evaluating the Influence of Plant-Specific Physiological Parameterizations on the Partitioning of Land Surface Energy Fluxes Evaluating the Influence of Plant-Specific Physiological Parameterizations on the Partitioning of Land Surface Energy Fluxes. December. https://doi.org/10.1175/JHM-D-14-0153.1

Sulis, M., Langensiepen, M., Shrestha, P., Schickling, A., Simmer, C., & Kollet, S. J. (2015). Evaluating the influence of plant-specific physiological parameterizations on the partitioning of land surface energy fluxes. Journal of Hydrometeorology, 16(2), 517–533. https://doi.org/10.1175/JHM-D-14-0153.1

Sultan, B., & Gaetani, M. (2016). Agriculture in West Africa in the twenty-first century: Climate change and impacts scenarios, and potential for adaptation. Frontiers in Plant Science, 7(AUG2016), 1–20. https://doi.org/10.3389/fpls.2016.01262

Sultan, B., Defrance, D., & Iizumi, T. (2019). Evidence of crop production losses in West Africa due to historical global warming in two crop models. Scientific reports, 9(1), 12834.

Sultan, B., Guan, K., Kouressy, M., Biasutti, M., Piani, C., Hammer, G. L., McLean, G., & Lobell, D. B. (2014). Robust features of future climate change impacts on sorghum yields in West Africa. Environmental Research Letters, 9(10), 104006. https://doi.org/10.1088/1748-9326/9/10/104006

Swann, A. L. S., Longo, M., Knox, R. G., Lee, E., & Moorcroft, P. R. (2015). Future deforestation in the Amazon and consequences for South American climate. Agricultural and Forest Meteorology, 214–215, 12–24. https://doi.org/10.1016/j.agrformet.2015.07.006

Swann, A. L., Fung, I. Y., Levis, S., Bonan, G. B., & Doney, S. C. (2010). Changes in Arctic vegetation amplify high-latitude warming through the greenhouse effect. Proceedings of the National Academy of Sciences, 107(4), 1295–1300. https://doi.org/10.1073/pnas.0913846107

Teklewold, H., Mekonnen, A., & Kohlin, G. (2019). Climate change adaptation: a study of multiple climate-smart practices in the Nile Basin of Ethiopia. Climate and Development, 11(2), 180-192.

Terdoo, F., & Feola, G. (2016). The vulnerability of rice value chains in Sub-Saharan Africa: A review. Climate, 4(3), 47.

Uphoff, N., & Randriamiharisoa, R. (2002). Reducing water use in irrigated rice production with the Madagascar System of Rice Intensification (SRI). Water-wise rice production, 71-87. USDA (2022). World Rice Production 2021/2022.. Available online: http://www.worldagriculturalproduction.com/crops/rice.aspx/ (accessed on 22 March 2023)

Vaittinada Ayar, P., Vrac, M., Bastin, S., Carreau, J., Déqué, M., & Gallardo, C. (2016). Intercomparison of statistical and dynamical downscaling models under the EURO-and MED-CORDEX initiative framework: present climate evaluations. Climate dynamics, 46, 1301-1329.

Van Oort, P. A. J., Saito, K., Tanaka, A., Amovin-Assagba, E., Van Bussel, L. G. J., Van Wart, J., ... & Wopereis, M. C. S. (2015). Assessment of rice self-sufficiency in 2025 in eight African countries. Global Food Security, 5, 39-49.

Van Oort, P. A., & Zwart, S. J. (2018). Impacts of climate change on rice production in Africa and causes of simulated yield changes. Global change biology, 24(3), 1029-1045.

Vidigal, P., Romeiras, M. M., & Monteiro, F. (2019). Crops diversification and the role of orphan legumes to improve the Sub-Saharan Africa farming systems. Sustainable crop production, 45-60.

Voldoire, A., Sanchez-Gomez, E., Salas y Mélia, D., Decharme, B., Cassou, C., Sénési, S., ... & Chauvin, F. (2013). The CNRM-CM5. 1 global climate model: description and basic evaluation. Climate dynamics, 40(9), 2091-2121. https://doi.org/10.1007/s00382-011-1259-y

Wang, E., Engel, T., 2000. SPASS: a generic process-oriented crop model with versatile windows interfaces. Environ. Modell. Softw. 15 (2), 179–188.

Wang, E., Engel, T., 2002. Simulation of growth, water and nitrogen uptake of a wheat crop using the SPASS model. Environ. Modell. Softw. 17 (4), 387–402.

Wang, G., & Eltahir, E. A. B. (2000). Ecosystem dynamics and the Sahel drought. Geophysical Research Letters, 27(6), 795–798. https://doi.org/10.1029/1999GL011089

Wang, X., Williams, J. R., Gassman, P. W., Baffaut, C., Izaurralde, R. C., Jeong, J., & Kiniry, J. R. (2012). EPIC and APEX: Model use, calibration, and validation. Transactions of the ASABE, 55(4), 1447-1462.

Watts, G., Battarbee, R. W., Bloomfield, J. P., Crossman, J., Daccache, A., Durance, I., ... & Wilby, R. L. (2015). Climate change and water in the UK–past changes and future prospects. Progress in Physical Geography, 39(1), 6-28.

Wei, J., Zhao, J., Chen, H., & Liang, X. (2021). Coupling Between Land Surface Fluxes and Lifting Condensation Level: Mechanisms and Sensitivity to Model Physics Parameterizations. Journal of Geophysical Research: Atmospheres, 126(5). https://doi.org/10.1029/2020JD034313

Willmott, C. J. 1981. On the validation of models. Physical Geography 2:184–194.

Willmott, C. J. 1982. Some comments on the evaluation of model performance. Bull. Am. Meteor. Soc. 64:1309–1313.

Willmott, C.J., Ackleson, S.G., Davis, R.E., Feddema, J.J., Klink, K.M., Legates, D.R., O'Donnell, J., Rowe, C.M., (1985). Statistics for the evaluation and comparison of models. J. Geophys. Res.: Oceans 90 (C5), 8995–9005.

World Bank. (2018). Improving Transparency and Accountability in Public-Private Partnerships: Disclosure Diagnostic Report-Honduras. World Bank.

Wu, Z.-X., & Newell, R. E. (1998). Influence of sea surface temperatures on air temperatures in the tropics. Climate Dynamics, 14(4), 275–290. https://doi.org/10.1007/s003820050223

Xu, L., Li, X., Wang, X., Xiong, D., & Wang, F. (2019). Comparing the grain yields of direct-seeded and transplanted rice: a meta-analysis. Agronomy, 9(11), 767. https://doi.org/10.3390/agronomy9110767

Xu, M. G., Li, D. C., Li, J. M., Qin, D. Z., Kazuyuki, Y., & Hosen, Y. (2008). Effects of organic manure application with chemical fertilizers on nutrient absorption and yield of

rice in Hunan of Southern China. Agricultural Sciences in China, 7(10), 1245-1252. https://doi.org/10.1016/S1671-2927(08)60171-6

Xue, Y., & Shukla, J. (1993). The influence of land surface properties on Sahel climate. Part 1: desertification. Journal of climate, 6(12), 2232-2245.

Yeboah, K. A., Akpoti, K., Kabo-bah, A. T., Ofosu, E. A., Siabi, E. K., Mortey, E. M., & Okyereh, S. A. (2022). Assessing climate change projections in the Volta Basin using the CORDEX-Africa climate simulations and statistical bias-correction. Environmental Challenges, 6, 100439. https://doi.org/10.1016/j.envc.2021.100439

Yu, M., Wang, G., Parr, D., & Ahmed, K. F. (2014). Future changes of the terrestrial ecosystem based on a dynamic vegetation model driven with RCP8.5 climate projections from 19 GCMs. Climatic Change, 127(2), 257–271. https://doi.org/10.1007/s10584-014-1249-2

Yu, W., Zhou, W., Dawa, Z., Wang, J., Qian, Y., & Wang, W. (2021). Quantifying Urban Vegetation Dynamics from a Process Perspective Using Temporally Dense Landsat Imagery. Remote Sensing, 13(16), 3217.

Zhang, B., Shrestha, N. K., Daggupati, P., Rudra, R., Shukla, R., Kaur, B., & Hou, J. (2018). Quantifying the impacts of climate change on streamflow dynamics of two major rivers of the Northern Lake Erie Basin in Canada. Sustainability, 10(8), 2897. https://doi.org/10.3390/su10082897

Zhang, X., Lee, J.-H., Abawi, Y., Kim, Y., McClymont, D., & Kim, H.-D. (2007). Testing the simulation capability of APSIM-ORYZA under different levels of nitrogen fertiliser and transplanting time regimes in Korea. Australian Journal of Experimental Agriculture, 47(12), 1446. https://doi.org/10.1071/EA05363

Zheng, X., & Eltahir, E. A. B. (1998). The Role of Vegetation in the Dynamics of West African Monsoons. JOURNAL OF CLIMATE, 11.

Ziervogel, G., Nyong, A., Osman-Elasha, B., Conde, C., Cortés, S., & Downing, T. (2013). Household food security and climate change: comparisons from Nigeria, Sudan, South Africa and Mexico. Climate Change and Vulnerability, 173-197.